Università degli Studi di Sassari

PhD Course in Life Sciences and Biotechnologies

Coordinator: Prof. Daria Sanna

Proteomic Analysis of MRSA During Stress and Skin Infection: Insights and Therapeutic Targets

Department of Biomedical Sciences

A Dissertation Submitted for the Degree of Doctor of Philosophy

Supervisor **PhD candidate**

Prof. Sergio Uzzau Dina Al Nahhas

Cycle XXXVI (2021-2024)

25 June 2024

Abstract

Methicillin-resistant *Staphylococcus aureus* (MRSA) is a major public health threat due to its resistance to multiple antibiotics and ability to adapt to various stressors encountered in human infections. It is the leading cause of skin and soft tissue infections (SSTIs) worldwide. Nearly 40% of patients experience recurrent *S. aureus* skin infections within three months, and over half face recurrences within six months, often necessitating repeated antibiotic treatments and increasing the risk of resistance.

This thesis investigates MRSA's stress response mechanisms to environmental stressors, such as decreased pH, temperature, and increased salinity, which simulate conditions at wound sites. Using an *in vitro* 3D skin model and an *in vivo* mouse model, we studied bacterial responses and identified potential antimicrobial targets and treatments.

In the first study, "Comparative Proteomic Profiling of Methicillin-Resistant *Staphylococcus aureus* Under Varied Experimental Conditions," differentially expressed proteins (DEPs) were analyzed under stress conditions. We observed that decreased pH and temperature reduced bacterial growth due to impaired purine metabolism and downregulation of inosine 5'-monophosphate dehydrogenase (IMPDH), highlighting IMPDH as a promising target for novel antimicrobial drugs. Additionally, sulfur metabolism was notably affected, with reduced expression of cysteine synthase (CysK) and compensatory increases in catalase (KatA) and aldo/keto reductases. Arginine biosynthesis proteins, crucial for pH regulation, were significantly upregulated, alongside strain-specific variations in amino acid metabolism, indicating diverse adaptation strategies.

The second study, "Exploring *S. aureus* Proteome During Skin Infection: Comparative Analysis of *In Vivo* and *In Vitro* Infection Models," confirmed the essential role of arginine in MRSA virulence and adaptation. Proteins involved in betaine biosynthesis, crucial for osmotic stress management, were identified, validating our previous findings. Several proteins associated with biofilm formation, oxidative stress, and other adaptive processes were detected in the *in vivo* model, with FumC and SapS highlighted as potential targets for future therapies for skin infection.

The antimicrobial screening in the final chapter aimed to screen for compounds and extracts effective against our MRSA strains. From the compounds screening, we found paramagnetoquinones and enduracyclinones effective agents against MRSA. Additionally, screening various extracts led to the identification of three potential extracts. Purifying these extracts revealed two promising compounds, previously described, named elaiophylin and nigericin, with notable activity against MRSA.

Overall, this research enhances our understanding of MRSA's adaptive mechanisms by integrating findings from both *in vitro* and *in vivo* models. It confirms previously identified proteins as potential targets for skin infections and establishes a screening approach for discovering new compounds. These advancements contribute to combating MRSA, reducing recurrent infections, and addressing antibiotic resistance.

Foreword

This thesis, titled [*In vivo* Proteome of *Staphylococcus aureus* During Skin Infection], is based on three manuscripts written and under review during my enrolment as a PhD researcher at Porto Conte Ricerche S.r.l in Alghero, Italy, from June 2021 to June 2024. The manuscripts are titled "Comparative Proteomic Profiling of Methicillin-Resistant *Staphylococcus aureus* Under Varied Experimental Conditions", "Exploring *S. aureus* Proteome During Skin Infection: Comparative Analysis of *In Vivo* and *In Vitro* Infection Models", and “Screening of Compounds with Antimicrobial Activity Targeting Methicillin-Resistant *Staphylococcus aureus*”. It is worth noting that the first manuscript has been submitted to the Journal of Proteomics and is currently under review for publication.

This research was conducted under the supervision of Prof. Sergio Uzzau at the University of Sassari and Dr. Daniela Pagnozzi at Porto Conte Ricerche. Part of this work has been carried out at the University of Sassari (Italy), the University of Copenhagen (Denmark), and NAICONS laboratories, Milan (Italy).

The work presented here is part of the European project INNOTARGETS (Innovative Approach to Tackle Antimicrobial Resistance (Innotargets – University of Copenhagen, (ku.dk)), which aims to address antimicrobial resistance challenges. INNOTARGETS has received funding from the European Union’s Horizon 2020 research and innovation program under the Marie Sklodowska-Curie grant agreement number 956154.

The project has received funding from the European Union’s Horizon 2020 research and innovation program under the Marie Sklodowska-Curie grant agreement number 956154.

Declaration

I, the undersigned Dina Al Nahhas, declare that this dissertation is the original report on my doctoral research at the University of Sassari, it has been written by myself and has not been submitted or presented, in whole or in part, for the award of any other academic degree or diploma elsewhere.

(Dina Al Nahhas)

(2021-2024)

Acknowledgment

As an early-stage researcher, I am deeply grateful to the Marie Curie funds for making science accessible and providing invaluable experiences through secondments, workshops, conferences, and webinars over the past three years. The generous Marie Curie scholarship has made science and training accessible for young, ambitious researchers. It has taught me that great researchers are not born great; they are trained and given the opportunities to learn and express their ideas.

I extend my gratitude to my supervisors, Sergio Uzzau and Daniela Pagnozzi, for their guidance and support throughout this journey. A special acknowledgment goes to Salvatore Pisanu, whose invaluable insights and mentorship from day one have greatly impacted this work, as well as his massive daily support. I am immensely grateful to Salvatore and will always carry him in my heart. Moreover, I am thankful to Alessandro Tanca for his significant contributions to the first work and the assistance he provided.

I want to thank all my colleagues at Porto Conte Ricerche, especially Antonio Palomba for the invaluable advice and assistance he provided whenever I turned to him. He has been a great psychologist over the last year and for free. Vittorio Tedde has been an exemplary figure in the laboratory, and a great supporter, Grazia Biosa has been helpful with handling the instruments and has shown great kindness. Giulia Puggioni has been an ideal colleague and a great supporter, I look up to her. Cristina Fraumene, Angela Braca, Daniela Piras, Valentina Tonu, Manuela Sanna, Simonetta Fois, Pietro Piu, Maria Grazia, Roberto Anedda, and Roberto Capucinelli, all have provided support and camaraderie and were my family away from home. Vi voglio tanto bene!

A special thank you to Ilaria Vitangeli, whose friendship and energy have made Porto Conte a more enjoyable place. Your daily hugs and support have been a ray of sunshine in this journey.

Moreover, I am grateful for all the people who helped me in the different hosting institutions and the individuals who aided in the labs. Prof John E Olsen, Oliver Ebenhoh, Margherita Sosio, Sonia Maffioli, Bianca Paglietti, and Priscila Guerra.

I extend my gratitude to my family, especially my sister Rama, for her immense support, advice, and for always being there to listen throughout this journey. I cannot imagine these three years without her. She has been a sister, a best friend, and a mother. Rama, your love and unwavering belief in me have been my anchor. My sweet mom, as well as all my nieces and nephews, have been my little fans, giving me a great push of love and energy without even knowing it. Your innocent smiles and cheerfulness have been a source of immense joy.

I am thankful for my colleagues at the University of Sassari, especially Nader, for all the support and encouragement he gave me when I needed it. You have been my best friend in this journey. Sally Youssef, and Nicola Deiana who has also been a great supporter. I would also like to thank all my INNOTARGETS colleagues for sharing science, joy, and support over the years, especially Yibing Ma, Sandra Wellner, and Hettie Chapman.

Last but not least, my supportive, loving friends around the world: Tony Chahine, his support in the last month was particularly precious and unforgettable. Yara Azzawi, Maico Lechner, Maurine Fucito, Maurice Mager, Mohamad Itani, Andrea Gentile, Gaia Strepparola, Sarah Jarade, Ingrid Saade, Chilperic Armel, Martha Salamero, Paula,

Emily, Tim, Dora, Maria Diab, Leen Ghazal, Reham Attar, Dima Akkach, Tuleen Ridai, Warde Geha, Lana Jaafari, and Christelle.

It was not an easy journey; however, with love and support, I was able to get through the difficult times.

List of Figures

Figure 1. Description of skin layers and the position of *S. aureus* on the skin surface (https://mindthegraph.com/).....24

Figure 2. Growth curves of MRSA ST398 strain (**A**) and MRSA JE2 strain (**B**) in EC1 (blue), EC2 (orange) and EC3 (green). Each curve is obtained from the mean of the three replicates at each point.....45

Figure 3. Histograms illustrating the total number of proteins quantified in ST398 and USA300 JE2 strains grown under EC1 (blue), EC2 (orange), and EC3 (green). Every bar represents the average deviation standard obtained from three biological replicates. The asterisk (*) indicates the statistically significant differences (p-value ≤0.05) obtained after applying the t-test. 47

Figure 4. PCA plot of all samples analyzed in this study. Samples belonging to the JE2 strain are represented by a circle, while those belonging to the ST398 strain are represented by a square. Blue, orange, and green colors mark EC1, EC2, and EC3, respectively.....48

Figure 5. Proteins with significantly differential expression between EC2 and EC1 in strain ST398. The binary logarithm of the abundance ratio is plotted on the y-axis, while the abbreviated protein names are plotted on the x-axis. DEPs with higher abundance in EC2 are colored in orange, while those with higher abundance in EC1 are colored in black. logAR: Abundance Ratio (log2). Arg and Pro for arginine and proline, ADI for arginine deiminase. K+ for potassium. Val, Leu, Ile for valine, leucine and isoleucine, Pur for purine, and Sul for sulfur. 51

Figure 6. Proteins with significantly differential expression between EC3 and EC1 in strain ST398. The binary logarithm of the abundance ratio is plotted on the y-axis, while the abbreviated protein names are plotted on the x-axis. DEPs with higher abundance in EC3 are colored in green, while those with higher abundance in EC1 are colored in black. logAR: Abundance Ratio (log2). Arg for arginine, K+ for potassium, GSH for glutathione, Val, Leu, Ile for valine, leucine, and isoleucine, Pur for purine, and Sul for sulfur.....53

Figure 7. Proteins with significantly differential expression between EC2 and EC1 in strain JE2. The binary logarithm of the abundance ratio is plotted on the y-axis, while the abbreviated protein names are plotted on the x-axis. DEPs with higher abundance in EC2 are colored in orange, while those with higher abundance in EC1 are colored in black. logAR: Abundance Ratio (log2). Arg and Pro for arginine and proline, Arg for arginine, Lys for lysine, His for histidine, Pur for purine, Sul for sulfur, Cys and Met for cysteine, and methionine.....55

Figure 8. Proteins with significantly differential expression between EC3 and EC1 in strain JE2. The binary logarithm of the abundance ratio is plotted on the y-axis, while the abbreviated protein names are plotted on the x-axis. DEPs with higher abundance in EC3 are colored in green, while those with higher abundance in EC1 are colored in black. logAR: Abundance Ratio (log2). Arg for arginine, Arg and Pro for arginine and proline, His for histidine, Lys for lysine, K+ for potassium, Pur for purine, and Sul for sulfur. 58

Figure 9. The Venn diagrams show the overlap between DEPs increased **(A)** or decreased **(B)** in EC2 or EC3 compared to EC1**.**.....59

Figure 10. *Workflow of the in vivo infection experiments (https://www.biorender.com).*.....80

Figure 11. Mean body weight of mice with standard deviation during the infection period. Each dot represents the average body weight, calculated from six biological replicates per group, expressed in grams (g) on days 0, 2, and 4. 88

Figure 12. Bacterial counts at the termination of experiments at day 2 (G1, G3, and G5) and day 4 (G2, G4, G6) from the in vivo infection model **(A)** and the in vitro infection model **(B).** The scatter plots display bacterial counts for each tissue and the vertical line indicates the mean CFU value. 89

Figure 13. The number of bacteria proteins shared and not shared between ST398 and JE2 during mice infection of the skin (A). The proteins with average normalized abundance showed higher expression in ST398 than in JE2 (B). Bar graphs showing the number of proteins according to COG categories during in vivo mice infections with ST398 and JE2 (C). 92

Figure 14. Bar graphs showing the average normalized abundance of proteins with significant differences between 2dpi and 4dpi and expressed in both ST398 (A) and JE2 (B). 93

Figure 15. Column chart showing the total proteins during the infection in ST398 (green) and JE2 (red) clustered into orthologous groups with their description on the right **(A).** Bar graph showing the total proteins involved in different pathways during skin infection in ST398 **(B)** and JE2 in **(C).** The significance notation (*** $p<0.001$ and ns for non-significant). Pur for purine, Val, Leu, Ile for valine, leucine, and isoleucine, His for histidine, and Arg for arginine. 96

Figure 16. Venn diagram shows the comparison of DEPs with increased expression during infection with ST398 and JE2 (A). Heat map reporting the normalized abundance of the shared DEPs, expressed as a scaling factor based on Log10 average normalized abundance between samples. The lower abundances are in green, and the highest abundances are in red (B). Characteristic proteins for the infection expressed by ST398 (C) and JE2 strain (D). The rectangles represent specific functions of the DEPs associated with virulence (pink), host adherence capability (yellow), and capable of immune evasion (blue). 99

Figure 17. Venn diagrams show the comparison of DEPs with decreased expression in the skin model infections with ST398 and JE2 **(A)**. A Heat map of the shared DEPs demonstrated in Log10 average normalized abundance scaling from lower abundances (green) to highest abundances (red) **(B).**. 100

Figure 18. Workflow followed for extract screening. 117

Figure 19. Scatter plots showing the percentage inhibition of ST398 (**A**) and JE2 (**B**) strains obtained from the screening of known compounds. In green, compounds with an inhibitory activity equal to or greater than 70% are reported. 119

Figure 20. Scatter plots showing the percentage inhibition of ST398 strain (**A**) and JE2 strain (**B**) obtained from the screening of extracts from Streptomyces. In green and orange dots, extracts with an inhibitory activity equal to or greater than 70% are reported. Specifically, green dots represent extracts with activity in common between the two strains, and orange dots, extracts with activity detected only on a single strain. 122

Figure 21. Scatter plots showing the percentage inhibition of ST398 strain (**A**) and JE2 strain (**B**) obtained from the screening of extracts from rare actinomycetes. In green and orange dots, extracts with an inhibitory activity equal to or greater than 70% are reported. Specifically, green dots represent extracts with activity in common between the two strains, and orange dots, extracts with activity detected only in a single strain. 123

Figure 22. Scatter plots showing the percentage inhibition of ST398 strain (**A**) and JE2 strain (**B**) of the subfractions obtained through fractionation in the HPLC system. D6 subfractions are shown in the orange box**,** H6 subfractions are in the green box, and D8 subfractions are in the red box**.**..... 124

Figure 23. Fragmentation mass spectrum of nigericin displayed by m/z ratio and relative abundance. . 126

Figure 24. Fragmentation mass spectrum of elaiophylin displayed by m/z ratio and relative abundance. 126

List of Tables

Table 1. Proteins overexpressed under EC2 in both ST398 and JE2 strains. 59

Table 2. Proteins overexpressed under EC3 in both ST398 and JE2 strains. 60

Table 3. Proteins under expressed under EC2 in both ST398 and JE2 strains. 60

Table 4. Proteins under expressed under EC3 in both ST398 and JE2 strains. 60

Table 5. Proteins detected in ST398 and JE2 strains during skin infection. 93

Table 6. Antibiotics and compounds used for drug screening, positions A1, F1, H1, G3, and E5 are empty. 114

List of Supplementary Tables

ST 1. DEPs increasing in EC2 shared in ST398 and JE2. 69

ST 2. DEPs increasing in EC3 shared in ST398 and JE2. 70

ST 3. DEPs decreasing in EC2 shared in ST398 and JE2. 71

ST 4. DEPs decreasing in EC3 shared in ST398 and JE2. 72

ST 5. Average inhibition percentage of known compounds on MRSA strains ST398 and JE2 (4 biological replicates). 131

ST 6. Serial dilutions (checkup points) of the 11 hits from the streptomyces plate, initially identified for inhibiting both ST398 and JE2 strains, represented by the full extract and its serial dilutions. 134

ST 7. Serial dilutions (checkpoints) of the 8 hits from the rare actinomycetes plate, initially identified for inhibiting both ST398 and JE2 strains, represented by the full extract and its serial dilutions. 134

ST 8. Serial dilutions (checkpoints) of the six fractions from each active selected extract, were tested against ST398 and JE2 strains. 135

List of Supplementary Figures

Figure S1. Venn diagram showing the number of total shared and unique proteins in three different ECs in ST398 (**A**) and JE2 (**B**). 69

Table of Contents

Chapter 1: Introduction 18

Chapter 2: Comparative Proteomic Profiling of Methicillin-Resistant Staphylococcus aureus Under Varied Experimental Conditions 34

Abstract 34

1. Introduction 38

2. Materials and Methods 41

2.1 Bacterial strains and growth conditions 41

2.2 Bacterial protein extraction 41

2.3 Protein digestion by filter-aided sample preparation (FASP) 42

2.4 LC-MS/MS analysis, data processing, and statistical analysis 42

3. Results 45

3.1. MRSA growth in different experimental conditions 45

3.2. Identification metrics and multivariate statistics 46

3.3. Proteins significantly associated with different growth conditions in the ST398 strain 48

3.3.1. EC2 vs EC1 48

3.3.2. EC3 vs EC1 51

3.4. Proteins significantly associated with different growth conditions in the JE2 strain 54

3.4.1. EC2 vs EC1 54

3.4.2. EC3 vs EC1 56

3.5. Shared features between the strains and the ECs 58

4. Discussion and Conclusion 60

5. Supplementary Data_1 69

Chapter 3: Exploring S. aureus Proteome During Skin Infection: Comparative Analysis of In Vivo and In Vitro Infection Models 74

Abstract 74

1. Introduction 76

2. Materials and Methods 78

2.1. Bacterial strains and culture 78

2.2. *In vivo mice model for human wound infection and bacterial clearance* 78

2.3. Protein extraction 80

2.4. TMT10plex labeling for protein quantification 81

2.5. *In vitro* 3D skin infection model 82

2.6. Protein extraction and quantification from 3D skin model 83

2.7. Shotgun proteomics and statistical analysis 84

3. Results 87

3.1. Mice infection model 87

3.1.2. Infection observation and development 87

3.1.3. Bacterial clearance 88

3.1.4. Protein expression and identification 90

3.2. *In vitro* skin model 94

3.2.2. Bacterial responses: Pathway analysis 94

3.2.3. Bacterial responses – Identification of Differentially Expressed Proteins (DEPs) 96

4. Discussion and Conclusion 101

Chapter 4: Screening of Compounds with Antimicrobial Activity Targeting Methicillin-Resistant Staphylococcus aureus 108

Abstract 108

1. Introduction 110

2. Materials and Methods 112
2.1. Compound and Extract Acquisition 112
2.2. Strains and bacterial growth 112
2.3. Screening compounds of known activity 113
2.4. Screening extracts of unknown activity and molecules purification 115
3. Results 118
3.1. Evaluation of the inhibition percentage of the tested compounds 118
3.2. Evaluation of the inhibition percentage of the extracts and molecule purification 119
3.3. Identification of compounds by mass spectrometry analysis 125
4. Discussion and Conclusion 127
5. Supplementary Data_3 131
Chapter 5: Discussion, Conclusions, and Future Perspectives 136
References 140

List of abbreviations

ACME	Arginine Catabolic Mobile Element
ACN	Acetonitrile
AD	Atopic Dermatitis
ADI	Arginine Deiminase
AIDS	Acquired Immune Deficiency Syndrome
AKRs	Aldo-Keto Reductases
AR	Abundance Ratio
ATP	Adenosine Triphosphate
CA-MHB	Cation Adjusted- Mueller Hinton Broth
CA-MRSA	Community Associated - methicillin-resistant *Staphylococcus aureus*
CDC	Centers for Disease Controls
CFU	Colony Forming Unit
COGs	Cluster Orthologous Groups
DEP	Differentially Expressed Protein
DPI	Days Post Infection
DTT	Dithiothreitol
EC	Experimental Condition
FASP	Filter-Aided Sample Preparation
FDR	False Discovery Rate
Fnbp	Fibronectin-Binding Protein
GSH	Glutathione
GSM	Genome-Scale Model
HA-MRSA	Hospital Acquired - Methicillin-Resistant *Staphylococcus aureus*
HCD	Higher Energy Collisional Dissociation
HPLC	High-Performance Liquid Chromatography
HRMS	High Resolution Mass Spectrometry
IAA	Iodoacetamide

ICAT	Isotope-Coded Affinity Tag
ITRAQ	Isobaric tags for relative and absolute quantitation
KEGG	Kyoto Encyclopedia of Genes and Genomes
LA-MRSA	Life Stock Associated- Methicillin-Resistant *Staphylococcus aureus*
LC	Liquid Chromatography
LFQ	Label-Free Quantification
MHB	Mueller Hinton Broth
MIC	Minimum Inhibition Concentration
MRSA	methicillin-resistant *Staphylococcus aureus*
MS	Mass Spectrometry
MSCRAMMs	Microbial Surface Components that Recognize Adhesive Matrix Molecules
MudPIT	Multidimensional Protein Identification Technology
NETs	Neutrophil Extracellular Traps
PBP	Penicillin Binding Protein
PBS	Phosphate Buffer Saline
PCA	Principal Component Analysis
PD	Proteome Discoverer
PVL	Panton Valentine Leucocidins
RNS	Reactive Nitrogen Species
ROS	Reactive Oxygen Species
RPF	Rabbit Plasma Fibrinogen
S. aureus	*Staphylococcus aureus*
SCCmec	Staphylococcal Cassette Chromosome mec
SCV	Small Colony Variant
SDS	Sodium Dodecyl Sulfate
SILAC	Stable Isotope Labeling by Amino Acids in Cell Culture
SSTIs	Skin and Soft Tissues Infections
ST	Sequence Type

ST	Supplementary Table
TEAB	Tetraethylammonium Bromide
TMT	Tandem Mass Tags
TSA	Tryptic Soy Agar
TSB	Tryptic Soy Broth
VRSA	Vancomycin-Resistant *Staphylococcus aureus*
WHO	World Health Organization

Chapter 1: Introduction

Staphylococcus aureus

Staphylococcus aureus is a Gram-positive bacterium. It is a non-motile, coagulase-positive, and under the microscope, it appears as grape-like clusters. It can grow in both aerobic and anaerobic environments (facultative) (Kloos and Bannerman, 1994). It was first described in 1880 by Alexander Ogston, who confirmed the bacterium's role in wound infections during a conference. Adding to the knowledge from his senior colleagues, Louis Pasteur, and Joseph Lister, Ogston first observed pus from 88 abscesses using the microscope and it was when he first described *Staphylococcus aureus's* spherical shape and noticed the golden yellow colonies (Classics in infectious diseases. "On abscesses". Alexander Ogston (1844-1929)., 1984). *S. aureus* was introduced to the world as a pathogenic organism. Since then, it has been a focus of microbiological research due to its dual role as both a commensal (normal skin flora) and a pathogen. It thrives in various environments, including human skin (primary reservoir) and mucous membranes, and is responsible for about 30% of nasal colonization in the population (Franklin D. Lowy, 1998),(Martins Costa et al., 2013). It causes a range of diseases including Skin and Soft Tissue Infections (SSTIs) (e.g., cellulitis, impetigo, furuncles, folliculitis, and others), osteomyelitis, endocarditis, bacteremia, severe pneumonia, and toxic shock syndrome (Tong et al., 2015a).

The discovery of penicillin

For many years, treatment was mainly done by topically applying carbolic acid (phenol), which was originally introduced by Lister and further advocated by Ogston, as a standard antiseptic method (Myles and Datta, 2012). In 1928, Alexander Fleming, a bacteriologist, coincidentally discovered that his *Staphylococcus aureus* Petri dishes were contaminated (Swann, 1983). The contamination was due to the fungus *Penicillium notatum.* He noticed that this contamination had influenced the growth of *S. aureus* and has further proved that penicillin was able to inhibit the bacterium growth *in vitro* (Aminov, 2010). Nevertheless, he was not able to isolate it, later on, by the mid-1940s, a sufficient amount of penicillin was accessible at the Sir William Dunn School of Pathology in Oxford. Researchers, including Norman Heatley and colleagues, conducted an experiment using mice. This study yielded crucial data demonstrating the *in vivo* effect of penicillin (Normal Heatley and Norman George, 2004),(Cranston D and Sidebottom E, 2016). This highlighted the beginning of the antimicrobial era in the management of *Staphylococcus aureus* infections.

The start of the resistance era

Unfortunately, only shortly after penicillin was introduced, clinical strains of *S. aureus* acquired resistance (Barber and Rozwadowska-Dowzenko, 1948). The development of resistance occurred due to the acquisition of β-lactamase (also known as penicillinase). Strains producing penicillinase diffused rapidly in both communities and hospitals (MUNCH-PETERSEN and BOUNDY, 1962),(Blair and Carr, 1960). In 1959, methicillin was introduced as a treatment for infections caused by penicillin-resistant *S. aureus*. However, by 1961, reports emerged from the United Kingdom of *S. aureus* isolates that had

developed resistance to beta-lactam antibiotics including methicillin, leading to what we now know as methicillin-resistant *S. aureus* (MRSA) ("Celbenin" - resistant Staphylococci, n.d.). The genetic basis of methicillin resistance is attributed to a mobile gene cassette, the staphylococcal cassette chromosome mec (SCCmec) (Katayama et al., 2000). Within the cassette, lies the *mecA* gene, which is responsible for resistance to β-lactams, including methicillin. It encodes penicillin-binding protein (PBP) 2a, which is involved in peptidoglycan synthesis and cross-linking in the bacterial cell wall. Unlike the native PBP encoded in the core genome of *S. aureus*, PBP2a has a lower binding affinity for β-lactam antibiotics. The combination of reduced penicillin-binding affinity and increased PBP2a production leads to observed resistance to β-lactam antibiotics (Hartman and Tomasz, 1984a; Matthews and Tomasz, 1990).

During the early 1960s, MRSA was detected in Europe, particularly in the UK and Denmark, where the strains were isolated. These events marked the emergence of the initial epidemic of MRSA clone (ERIKSEN and ERICHSEN, 1964). However, in the late 1970s, hospitals in the United States began reporting outbreaks of infections caused by MRSA strains. By the mid-1980s, these infections had become endemic (Crossley et al., 1979). MRSA was first described to cause hospital outbreaks, known as healthcare-associated MRSA (HA-MRSA) (Chambers and DeLeo, 2009). A significant shift in MRSA epidemiology occurred when it was found in people with no prior healthcare exposure, termed community-associated MRSA (CA-MRSA). This was notably observed among Indigenous populations in Australia (Faoagali et al., 1992), as well as in otherwise healthy individuals, including children, in the United States during the 1990s (Fridkin et al., 2005). While in the mid-2000s, it has also been linked to exposure to livestock, known as livestock-associated MRSA (LA-MRSA) (Voss et al., 2005).

In a recent study, Larsen et al. (Larsen et al., 2022) offered a compelling explanation for the emergence and propagation of MRSA, focusing on the impact of horizontal gene transfer and environmental antibiotic pressure. Their findings highlighted the capacity of MRSA strains to evolve and spread across various species and ecosystems, highlighting the necessity of a One Health approach that acknowledges the interconnected health of humans, animals, and the environment.

The One Health approach, which integrates human, animal, and environmental health sectors, is essential for controlling MRSA spread. Strategies to reduce antibiotic use, including stricter regulations on prescriptions and promoting alternative treatments, are crucial in limiting the development of resistant strains. According to the Centers for Disease Controls in the United States (CDC), the mortality rate associated with MRSA infection surpassed that of acquired immune deficiency syndrome (AIDS), Parkinson's disease, and homicide combined (Lessa et al., 2012).

Antibiotics

The control of MSRA infections has benefited from the discovery and design of novel antibiotics using a limited number of chemical compounds and their derivatives. Vancomycin, a glycopeptide antibiotic, was discovered in late 1950. Three decades later, vancomycin became the preferred treatment for MRSA infections (Levine, n.d.). Vancomycin targets the cell wall by binding to the d-ala-d-ala residues in newly synthesized UDP-MurNAc-pentapeptides, effectively blocking the assembly of peptidoglycan (J. C. J. Barna and D. H. Williams, 1984). The first case of vancomycin-resistant *S. aureus* (VRSA) was reported in 2002 in a 40-year-old woman from Michigan. The resistance mechanism to vancomycin in *S. aureus* involves the *vanA* operon capable

of encoding an enzyme that binds D-alanine-D-lactate (D-Ala-D-Lac) instead of D-alanine-D-alanine (D-Ala-D-Ala) during peptidoglycan synthesis. It is essential to underline that, following this substitution, the bacterial cell's sensitivity to vancomycin and glycopeptide antibiotics significantly decreases due to the loss of the binding site (Arthur et al., 1996). The development of new antibiotics has been essential ever since. Some antibiotics evolved from glycopeptides as vancomycin to lipoglycopeptides like telavancin, oritavancin, and dalbavancin. They incorporate lipophilic side chains, which extend their half-life and enable interactions with cell membranes. Meanwhile, the heptapeptide core within them inhibits key reactions involved in cell wall synthesis, specifically trans glycosylation and transpeptidation (Cornaglia and Rossolini, 2009). Dalbavancin primarily hinders the final steps of peptidoglycan synthesis by interfering with transglycosylase activity. In contrast, oritavancin and telavancin attach to the bacterial membrane via their lipophilic side chains, leading to membrane disruption and subsequent cell lysis (Françoise Van Bambeke, 2015). All those antibiotics work on the cell wall, while some other discovered antibiotics inhibit protein synthesis (translation), such as macrolides, tetracyclines, lacosamide, linezolid, aminoglycosides, etc. For example, aminoglycosides, including gentamicin, disrupt protein synthesis by binding to the A-site of the 16S rRNA within the 30S subunit of the bacterial ribosome. This interaction results in inaccurate recognition between codons and anticodons, ultimately reducing the fidelity of translation and producing mistranslated proteins (Kotra et al., 2000). Linezolid, an oxazolidinone antibiotic approved in 2000, is commonly used to treat nosocomial pneumonia and skin and soft tissue infections caused by MRSA and MSSA (Mendes et al., 2014). Its mechanism of action involves binding to the bacterial ribosome's 23S rRNA,

thereby preventing proper placement of aminoacyl-tRNA in the peptidyl transferase center and ultimately blocking protein synthesis (Leach et al., 2007; Mendes et al., 2014). Other antibiotics work on RNA synthesis (transcription), such as rifamycin (CALVORI et al., 1965), DNA replication, like quinolones (Drlica, 1999), or folic acid biosynthesis like trimethoprim (Hitchings, 1973). Nevertheless, in the rapid race of antibiotic discovery, just four classes of these compounds—cephalosporins, macrolides, penicillin's, and quinolones—make up a significant 73% of all antibiotics introduced between 1981 and 2005 (Fischbach and Walsh, 2009). The bacterium can develop antibiotic resistance through drug treatment, constantly evolving through mutations.

S. aureus adaptation to the host and skin immune responses

S. aureus adaptability extends not only to antibiotics but also to the host environment during infections. The molecular mechanisms of adaptation during infections include *S. aureus's* ability to incorporate foreign DNA through mobile genetic elements. However, this process is primarily significant during the colonization phase (Golubchik et al., 2013). *S. aureus* manifests adaptive mutations in essential genes related to pathogenesis. In addition, it employs phenotype-switching arising from chromosomal rearrangements (Proctor et al., 1984). *S. aureus* colonization of the host usually begins with attachment to the surface of host cells, facilitated by microbial surface components that recognize adhesive matrix molecules (MSCRAMMs). *S. aureus* possesses surface proteins—fibronectin-binding proteins A (FnbpA) and B (FnbpB) that bind to fibronectin and fibrinogen; those genes are found to be correlated with invasive diseases facilitating *S. aureus* internalization into the host cell (Guérillot et al., 2019). Additionally, *S. aureus*

FnbpB assists in evading neutrophil extracellular traps (NETs) by neutralizing the lethal activity of histones. During infection, in particular skin infection, the host senses *S. aureus* peptidoglycan and lipoproteins, triggering an immune response that recruits B cells, T cells, NK cells, and macrophages **(Figure 1)** (Liu, 2009).

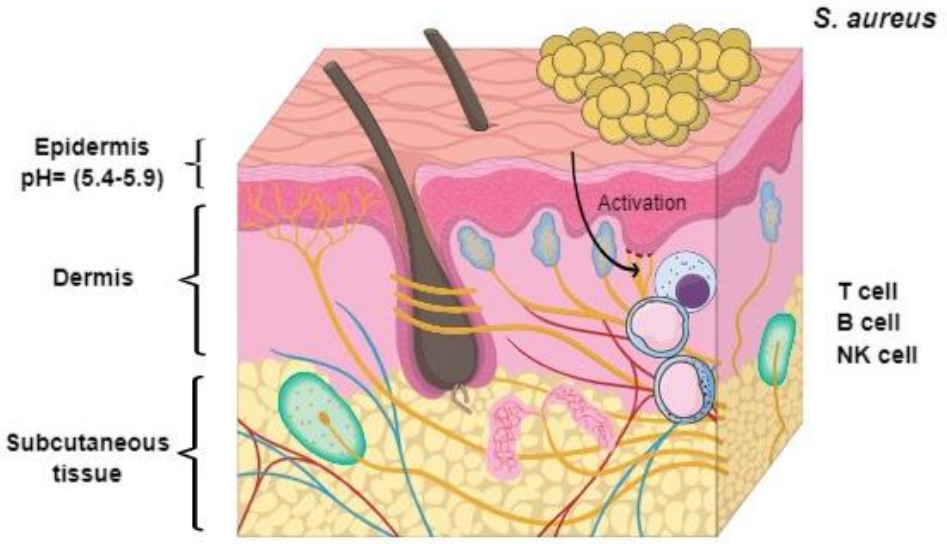

Figure 1. *Description of skin layers and the position of S. aureus on the skin surface (https://mindthegraph.com/)*.

Subsequently, staphylococci produce an extracellular matrix composed of polysaccharides, proteins, and extracellular DNA. This three-dimensional structure also inhibits the effect of NETs on the bacteria growing within the biofilm. Lastly, the bacteria within the biofilm generate planktonic cells that spread and establish new infection sites within the host (Schilcher and Horswill, 2020; Speziale and Pietrocola, 2021). Besides biofilm formation, *S. aureus* can adapt by adjusting its metabolism, leading to Small Colony Variant formation (SCV). They are characterized by their slow growth rate, small colony size, reduced hemolysis, and virulence, they develop either from the biofilm or in host cells (von Eiff et al., 2001; Tuchscherr et al., 2020). Understanding its adaptive responses to infection is essential to identify novel targets. One of the main infections caused by

S. aureus is SSTIs. Their incidence rate is estimated at 24.6 per 1000 person-years (ELLIS SIMONSEN et al., 2006). During infection, *S. aureus* must navigate and adapt to the unique environment of the skin, where it encounters various challenges, including acidity and temperature. The acidity of the skin surface is influenced by organic and fatty acids secreted by the host, as well as the metabolic by-products of the skin's microbiota (Proksch, 2018). Skin temperature typically ranges from 32℃ to 35℃ (Benedict et al., 1919). In many bacterial species, acidic conditions are linked to the suppression of virulence (Lund et al., 2014). Understanding how *S. aureus* adapts to the skin and overcomes these natural defenses is crucial for developing effective treatments, highlighting the need for innovative research approaches to decipher these complex interactions. As the battle against *S. aureus* continues, our understanding of its adaptation strategies to the hostile environment of the human skin has been significantly advanced by proteomics. The improvement and development of proteomics technologies have transformed our ability to comprehend these complex adaptation strategies, revealing the intricate molecular dialogue between *S. aureus* and the human skin. This leap in understanding has provided insights into the bacterium's resilience and versatility but has also opened new avenues for targeted therapeutic interventions.

Proteomics

Proteomics focuses on studying the interactions, functions, compositions, and structures of proteins, and their roles in cellular activities to better understand the organisms and their specific biological systems. Unlike genomics, which primarily deals with DNA and genes, proteomics offers a deeper understanding of an organism's structure and function

by examining its protein landscape (Wilkins et al., 1996). However, it can be more complicated due to the alteration of protein expression across different times and environmental conditions (Holman et al., 2013).

Proteomics progresses toward high-throughput analysis

Initially, proteomics included mainly gel-based techniques such as one-dimensional (1D) gel electrophoresis and two-dimensional gel electrophoresis (2-DE) (Vercauteren et al., 2004). In addition, 2-DE was modified to include two-dimensional difference gel electrophoresis (2D-DIGE), allowing the proteomes of 2-3 biological samples to be analyzed simultaneously on the same gel (Klose et al., 2002). Subsequently, owing to the limitations of these methods, proteomics has evolved resulting in the development of shotgun proteomics. Shotgun proteomics is similar to shotgun sequencing, where DNA is fragmented, sequenced in small sections, and then recombined in silico to reconstruct the entire DNA sequence of an organism. In a typical shotgun proteomic workflow, a complex protein mixture is digested into smaller peptides using proteases like trypsin. These peptides are then separated using at least a two-dimensional chromatography system. Following separation, the peptides are automatically introduced into a tandem mass spectrometer, where they are analyzed. The resulting tandem mass spectrometry data are then processed by advanced computational systems. The field of large-scale shotgun proteomics gained significant traction with the development of multidimensional protein identification technology (MudPIT) (Link et al., 1999; Washburn et al., 2001; Wolters et al., 2001). Shotgun proteomics has two methods for quantification: label-free quantification (LFQ) or labeling techniques-based quantification. LFQ offers a

straightforward approach for large-scale analysis of biological samples. Unlike label-based methods, in LFQ, the samples to be compared are injected independently into the mass spectrometer (MS) (Kito and Ito, 2008; Kalra et al., 2013).

On the other hand, Label-based quantitation involves comparing samples by labeling them with different mass tags, enabling detection through specific changes in mass. This comparative method typically uses chemically similar labels that differ isotopically (Domon and Aebersold, 2010). Labeling techniques include stable isotope labeling with amino acids in cell culture (SILAC) (Ong et al., 2002), isotope-coded affinity tag (ICAT), isobaric tagging for absolute and relative quantitation (iTRAQ) (Ross et al., 2004), and Tandem Mass Tags (TMT) (Thompson et al., 2003a). The effectiveness of labeling techniques lies in their ability to quantify a wide range of proteins, enhancing the interpretability of proteomics results. Employing labeling techniques such as TMT, allows thousands of proteins of lower abundance to be identified for quantifying relative protein abundances (Thompson et al., 2003b). Over the past decade, proteomics has been categorized into protein expression mapping and protein interaction mapping (Yoithapprabhunath et al., 2015).

Proteomics top applications

Proteomics is a powerful technique with applications in various fields, including microbial infections and host-pathogen interactions, using methods like 2-D gel-based and gel-free approaches combined with MALDI-TOF-LC-MS/MS. This analysis provides crucial insights into pathogen virulence and resistance, aiding in the understanding of infections and the development of anti-microbial strategies (Cheng et al., 2016).

The elucidation of antibiotic resistance mechanisms for diagnostic responses (Pérez-Llarena and Bou, 2016), molecular mechanisms of diseases (Pankow et al., 2019), and biomarker and drug discovery (Amiri-Dashatan et al., 2018).

Research on skin infection

Advancements in research on skin infections have included the use of this powerful tool to elucidate bacterial pathogenesis, such as studying the bacterial proteomics associated with atopic dermatitis (AD) and the microbiota of AD. Proteins that are responsible for pathogenesis have been identified from different bacterial communities, including *S. aureus*, such as enolase, glyceraldehyde-3-phosphate dehydrogenase, and the chaperone proteins DnaK and HtpG (Kandil et al., 2020). There has also been progress in understanding how *S. aureus* adapts to skin infections and colonization (Gehrke et al., 2023). As discussed, skin characteristics, including lower pH and temperature, might influence bacterial adaptation. It was found that SigB, an alternative sigma factor, plays a crucial role in regulating responses to stress. When environmental stress signals (such as heat, osmotic stress, and pH changes) are detected, sensor proteins activate SigB, which leads to the upregulation of about 200 genes, that allow the bacterium to adapt to stress (Georgiou and Segatori, 2005). It is usually active in the skin's atypical pH and heightened osmolarity, which are the skin's usual conditions (Costa and Horswill, 2022). Given that *S. aureus* is adversely affected by low pH levels, the bacteria need to counteract acidity to successfully inhabit the skin. The bacterium typically reduces acid production and increases arginine deiminase and urease protein bioactivity (Bore et al., 2007; Costa and Horswill, 2022),(Rode et al., 2010a). Studies have revealed that *in vivo*,

S. aureus utilizes urea-derived ammonia to counteract acidic pH levels, thereby aiding its survival and role in causing disease (Zhou et al., 2019a). Additionally, research has shown that the arginine deiminase (Arc) enzyme, encoded within the arginine catabolic mobile element (ACME) found in the prevalent ST8 USA300 clone, plays a crucial role in *S. aureus* adaptation to the skin. Arc facilitates ammonia production by breaking down arginine, which not only inhibits nitric oxide formation but also triggers polyamine synthesis. Moreover, the presence of the spermidine N-acetyltransferase SpeG, also encoded in ACME, provides resistance against polyamines generated as a consequence of Arc-mediated arginine catabolism. Thus, the presence of ACME within this clone emerges as a pivotal factor enabling adaptation to the skin environment (Joshi et al., 2011).

Different models of skin infections

Studying skin infections varies from *in vitro* predictions to *in vivo* experiments. A pivotal approach was initially attempted to characterize the skin infection conditions to mimic them *in vitro,* as a solid foundation to understand how the bacteria adapts and reacts to environmental stressors (Alreshidi et al., 2016). However, the power of this approach was undermined by the choice of the conditions measured and to be mimicked. On the other hand, an effective animal model system must be clinically relevant, ethically justifiable, and practical, ensuring dependable and consistently reproducible outcomes (Zak and O'Reilly, 1991). Using mice as a model organism for investigating skin wound infections has been pivotal in advancing our comprehension of host-pathogen interactions and wound healing processes. The genetic proximity of mice to humans allows for meaningful extrapolation of findings to clinical scenarios (Li and Auwerx, 2020). Furthermore,

supplementing findings with a 3D skin model could enhance our understanding of host-bacterial interactions. Unlike current 2D models, 3D models can simulate physiological wounds and offer a more accurate assessment of disease progression by better replicating the skin's three-dimensional structure and complexity (Randall et al., 2018).

By integrating advanced proteomic techniques with robust *in vitro* and *in vivo* models, and screening for compounds that could potentially inhibit MRSA, this work aims to bridge the gap in our understanding of *S. aureus* skin infections. The focus is on two important strains of MRSA, including ST398 (LA-MRSA), a predominant zoonotic strain isolated from pigs and cows, that also causes infections in humans, sometimes leading to severe outcomes, including death (Goerge et al., 2017; Abreu et al., 2019). Numerous studies, including those conducted on dairy farms, have reported the transfer of LA-MRSA from animals to humans (Cuny et al., 2015; Locatelli et al., 2017), highlighting the importance of this strain in understanding transmitted infections. The other strain, JE2, is a plasmid-cured variant of CA-MRSA, USA300 (Fey et al., 2013a). The strain is of great importance because it has been identified as a primary cause of SSTIs in various communities (King et al., 2006a). Its rapid spread and high virulence are attributed to specific genetic characteristics, such as the presence of Panton-Valentine Leukocidin (PVL) and the ACME. These factors contribute to the strain's ability to cause severe infections and survive in harsh environments like the skin, making it a significant public health concern and an important strain for research (Tenover et al., 2006; David et al., 2013).

This thesis explores the bacterium's adaptation at the proteomic level under various experimental conditions and infection models, with a particular emphasis on shifts in protein expression during infection and the potential for inhibiting its growth.

The findings of this work are expected to significantly advance the development of novel therapeutic strategies, offering promising solutions to the critical challenge of antimicrobial resistance in MRSA skin infections.

Objectives of the studies

- The first study, 'Comparative Proteomic Profiling of Methicillin-Resistant *Staphylococcus aureus* Under Varied Experimental Conditions,' this study evaluates the proteomes of *S. aureus* under different environmental stressors (such as pH, temperature, and salinity) to understand the bacterium's adaptive mechanisms in human wound sites. This study aims to identify stress-responsive proteins and enhance our understanding of *S. aureus* adaptation to challenging conditions such as those on the wound site, ultimately identifying potential targets for new therapeutic strategies.
- The second study, 'Exploring *S. aureus* Proteome During Skin Infection: Comparative Analysis of *In Vivo* and *In Vitro* Infection Models', aims to bridge the gap between experimental conditions and real-world infections by comparing the proteome of *S. aureus* in both *in vivo* (using a mouse model) and *in vitro* (using a 3D skin model). This dual approach aims to robustly identify key *S. aureus* proteins involved in skin infections, contributing to the design of targeted therapies. By combining the controlled conditions of *in vitro* experiments with the complexity of *in vivo* systems, the study enhances its relevance to human disease.
- The third study, 'Screening of Compounds with Antimicrobial Activity Targeting Methicillin-Resistant *Staphylococcus aureus*', addresses the critical need for new antimicrobials against MRSA, which poses a major public health challenge due to its resistance to many existing antibiotics. This study aims to test known antimicrobial compounds and purify molecules from extracts to expand the arsenal against MRSA. The focus on discovering and suggesting potential new therapeutic

molecules highlights a practical, application-oriented research goal essential for translating laboratory findings into clinical treatments.

Chapter 2: Comparative Proteomic Profiling of Methicillin-Resistant Staphylococcus aureus Under Varied Experimental Conditions

Dina Al Nahhas[1,2*], Salvatore Pisanu[1], Alessandro Tanca[3], Bianca Paglietti[2], Antonella Santona[2], Sergio Uzzau[2,3], Daniela Pagnozzi[1]

[1] Porto Conte Ricerche S.r.l, Tramariglio, Alghero (SS), Italy.
[2] Department of Biomedical Sciences, University of Sassari, Sassari, Italy.
[3] Unit of Microbiology and Virology, University Hospital of Sassari, Sassari, Italy

Corresponding author: nahhas@portocontericerche.it

Abstract

Understanding the response of methicillin-resistant *Staphylococcus aureus* (MRSA) to environmental stressors is crucial for elucidating their adaptive mechanisms and identifying potential therapeutic targets. This study employed a shotgun proteomic approach to analyze and compare the protein profiles of MRSA strains ST398 and JE2 under different experimental conditions (ECs). These conditions aimed to mimic wound site stress, modifying parameters such as pH, temperature, and salinity as follows: EC1 (control, 37°C, pH=7), EC2 (35°C, pH=6), and EC3 (35°C, pH=6 and 5% NaCl).

Bacterial proteins were extracted and trypsin-digested using a filter-aided sample preparation (FASP) approach to obtain peptide mixtures, which were subsequently analyzed via liquid chromatography coupled with high-resolution tandem mass spectrometry. Raw data were analyzed using Proteome Discoverer software for protein identification and differential analysis, employing label-free quantification (LFQ) based on the intensity of precursor ions as an abundance parameter. A mean of 3444±123 proteins per sample was identified across the tested ECs. Qualitative and quantitative differences in protein expression were observed both between strains ST398 and JE2 and between the tested ECs. Notably, several of the proteins exhibiting a significant increase in

abundance under EC2 and EC3 in both strains were involved in arginine biosynthesis. In contrast, a group of proteins involved in sulfur and purine metabolism showed a decrease in expression in the same conditions in both strains. The decrease in sulfur metabolism, marked by reduced levels of cysteine synthase (CysK) and cysteine desulfurase (Csd), was compensated by increased expression of catalase (KatA), along with a rise in alkyl hydroperoxide reductase (AhpC) in ST398 for both EC2 and EC3 and an increased expression of proteins involved in glutathione metabolism in EC3, indicating an adaptive oxidative stress response.

This study identifies specific proteins and related pathways actively involved in the complex adaptive response of MRSA strains to changes in pH, salinity, and temperature.

Keywords: MRSA, shotgun proteomics, experimental conditions, environmental stress.

Significance of the study

Life-threatening methicillin-resistant *Staphylococcus aureus (*MRSA) infections remain a major concern worldwide. *S. aureus* dynamically adapts to host environmental cues, such as pH, nutrients, and reactive oxygen species, modulating its pathogenesis and growth in response to stress. Our findings provide evidence of strain-specific proteomic responses to these conditions, highlighting distinct pathways that are significantly increasing or decreasing in response to environmental changes. Therefore, this study adds up to the previous knowledge by exploring the proteome variation of two MRSA strains grown in experimental conditions mimicking the wound skin infection site. Such insights are crucial for the development of targeted treatments and highlight the importance of considering strain variability in MRSA management strategies.

Highlights:

- ST398 and JE2 MRSA exhibit partly different proteomic profiles when exposed to the same stress conditions.
- The arginine biosynthesis pathway has shown an increase in EC2 and EC3 in both strains.
- In EC2, proteins involved in sulfur metabolism, specifically cysteine synthase (CysK) and cysteine desulfurase (Csd), are diminished in both strains. This reduction is compensated by an increase in catalase protein (KatA) under both conditions to help maintain redox balance.
- An increase in glutathione (GSH) metabolism is observed in ST398 during EC3. Additionally, alkyl hydroperoxide reductase (AhpC) levels have increased in ST398 strain during both EC2 and EC3.

- Proteins involved in purine metabolism showed decreased expression levels in both EC2 and EC3 across both strains.

1. Introduction

Staphylococcus aureus (S. aureus) is a Gram-positive opportunistic bacterium commonly isolated on the skin and in the nasal cavity of many healthy individuals (Otto, 2010). It can cause a range of infections, from local skin and soft tissue infections (SSTIs) like wound infections, abscesses, and cellulitis to more severe conditions such as endocarditis, pneumonia, sepsis, and toxic shock syndrome (Tong et al., 2015b). Its pathogenicity is influenced by numerous virulence factors and its adaptability to environmental changes including pH, oxygen, CO2, and temperature during host infections (Pal et al., 2020).

S. aureus is a significant cause of hospital-acquired infections, especially in critically ill patients, and community-acquired *S. aureus* is a leading cause of SSTI admissions in emergency wards (Frazee et al., 2005). It adapts to environmental variations, altering protein expression and metabolite release (Choueiry et al., 2022). Methicillin-resistant strains (MRSA) emerged soon after methicillin was introduced in 1961 (Livermore, 2000), and their prevalence is now a major concern due to rapid transmission, treatment challenges, and higher mortality rates.

Bacterial pathogens encounter various environmental conditions depending on the infection route, timing, and site. For instance, the mean temperature of healthy human skin is usually 2–4°C lower than the body's core temperature, depending on the surroundings and location of the wound (Lenhardt and Sessler, 2006a). The skin is characterized by a slight acid pH ranging from 4 to 6 (Ehrhardt Proksch, 2018), while the infected wound site changes in pH value, depending on the infection phase. Typically, pH ranges from 5.7 to 7.6 in the early phase of infection, followed by a gradual increase toward alkaline values ranging from 7.5 to 8.9 in the chronic phase of infection. NaCl

concentrations can also increase in response to trauma (Schneider et al., 2007; Alreshidi et al., 2016). Additionally, bacteria usually contribute to generating tissue hypoxia due to their increased replication at the infection site (Hajdamowicz et al., 2019).

Understanding metabolic adaptation is crucial for identifying new therapeutic targets to combat antibiotic-resistant pathogens (Lee et al., 2013; Shoaib et al., 2023). Proteomic approaches are essential for studying microbial protein expression during environmental changes to understand metabolic pathways and antibiotic resistance mechanisms (Bo Peng et al., 2019),(Tsakou et al., 2020).

In this study, we investigated the protein expression of two MRSA strains under three experimental conditions (ECs) to simulate the variations in pH, temperature, and NaCl concentration expected during a wound infection. One strain is Livestock-Associated (LA-MRSA) ST398, which colonizes the nasal cavity of pigs and has also been reported in other animals and used in the food industry. It poses a risk for farmers and people in direct contact with animals, such as veterinarians (Kadlec et al., 2012; Pete Kinross1, 2017). The other strain is Community Associated (CA-MRSA), JE2 strain (USA300 isolate), one of the major causes of SSTI and the main cause of CA infections in the USA (King et al., 2006b).

The selected ECs mimic the stress conditions occurring on the skin during infection with *S. aureus*. These ECs were named experimental condition 1 (EC1), characterized by pH 7 at 37°C and considered as a control condition; experimental condition 2 (EC2), characterized by pH 6 at 35°C, and experimental condition 3 (EC3), characterized by pH 6 at 35°C with 5% NaCl added to the medium. The comparative analysis of bacterial proteomes under these diverse *in vitro* exposures provided evidence of metabolic

reshaping and highlighted strain-specific and environmental-specific variations in critical bacterial functions.

2. Materials and Methods

2.1 Bacterial strains and growth conditions

MRSA strains, ST398 (van Rijen et al., 2008), and JE2 (Fey et al., 2013b), were obtained from the Department of Veterinary and Animal Sciences at the University of Copenhagen, Denmark.

In vitro growth of the bacteria was performed in different ECs as follows: EC1 (control condition) was carried out in tryptic soy broth (TSB) at pH 7 at 37°C; EC2 in TSB at pH 6 at 35°C, and EC3 in TSB at pH 6 with 5% NaCl at 35°C. Each condition was done by growing both strains in 3 replicates and growth curves were reported by taking the mean of the three replicates. In brief, a total of 2-3 colonies of each strain were inoculated in 8 mL of TSB in a 50 mL tube and shaken at 120 RPM overnight in an incubator. Then, subcultures were prepared after 18 hours by 1:66 dilution, starting at optical density (OD_{600} of 0.05) and measuring OD_{600} every 30 minutes using a UV-Vis spectrophotometer (SHIMADZU), until reaching mid-log phase at OD_{600} of 0.5. Subsequently, after reaching 10^7 colony-forming units per mL (CFU/mL), bacteria were harvested, pelleted by centrifugation, and washed 3 times with cold PBS (Phosphate buffer saline). Bacterial counts were verified after doing 6 serial dilutions in PBS when harvesting. Subsequently, the diluted samples were plated on tryptic soy agar (TSA). Bacterial colonies were counted after overnight incubation.

2.2 Bacterial protein extraction

Proteins were extracted following a previously established protocol (Tanca et al., 2014). In brief, bacterial pellets were dissolved in lysis buffer containing 2% sodium dodecyl sulfate (SDS), 20 mM Tris-HCl (pH 8.8), and 100 mM dithiothreitol (DTT), followed by agitation

in a Thermomixer (Eppendorf, Hamburg, Germany) at 600 rpm for 20 minutes at 95°C. To disrupt the extracellular bacterial wall, mechanical force was applied using a TissueLyser LT mechanical homogenizer (Qiagen). This process involved bead beating for 10 minutes at 30 cycles/s, combined with three freeze-thaw cycles, followed by a 15-minute sonication step. Finally, samples were centrifuged at 12,000 g for 12 minutes at 4°C to separate the bacterial proteins in the supernatant, which was then stored at -80°C for later use.

2.3 Protein digestion by filter-aided sample preparation (FASP)

Protein extracts underwent reduction with dithiothreitol (DTT), alkylation with iodoacetamide (IAA), and digestion with trypsin, according to the FASP protocol to obtain peptide mixtures for mass spectrometry analysis, as previously described in (Pisanu et al., 2015). Following digestion, the peptide mixtures were collected, dried, and resuspended in 0.2% formic acid. Peptide concentrations were determined using a Nanodrop 2000 spectrophotometer (Thermo Fisher Scientific, San Jose, CA, USA), employing a HeLa protein digest standard (Thermo Fisher Scientific) to obtain a calibration curve.

2.4 LC-MS/MS analysis, data processing, and statistical analysis

Peptide mixtures were analyzed in mass spectrometry using a Q-Exactive mass spectrometer coupled with an UltiMate 3000 RSLCnanoLC system (Thermo Scientific, San Jose, CA, USA). For each sample, 4 µg of peptide mixture was concentrated and washed in a trap-column (Acclaim PepMap C18, 75 µm × 2 cm nanoViper, 3 µm, 100 Å, Thermo Scientific) and then fractionated on a C18 RP column (Acclaim PepMap RSLC C18, 75 µm × 50 cm nanoViper, 2 µm, 100 Å, Thermo Scientific) using a linear gradient of 245 minutes from 5 to 37.5% eluent B (0.1% formic acid in 80% acetonitrile) in eluent

A (0.1% formic acid) (Addis et al., 2022). Spectra fragmentation was obtained by Higher Energy Collision Dissociation (HCD), with nitrogen as the collision gas. MS raw files were subjected to database searching using Proteome Discoverer software (version 2.4, Thermo Scientific), with SEQUEST-HT as a search engine. Protein identifications were obtained using the following settings; database: *Staphylococcus aureus* strain ST398 and strain JE2 (8614 sequences retrieved from UniProt Knowledgebase (UniProtKB), 2022_05 release), enzyme: trypsin, with two missed cleavages allowed; precursor mass tolerance: 10 ppm; MS/MS tolerance: 0.02 Da; charge states: +2, +3, and +4; cysteine carbamidomethylation as static modification; methionine oxidation and acetylation (Acetyl), loss of Methionine (Met-loss) and loss of Methionine + Acetylation (Met-loss+Acetyl) on N-Terminus as dynamic modifications. Validation of identification significance was carried out using Percolator, setting a false discovery rate (FDR) threshold of 1%. A Consensus step was performed to compare two conditions at a time (EC1 *vs* EC2 and EC1 *vs* EC3), considering three biological replicates per condition. A standard consensus workflow was set on Proteome Discoverer 2.4 to evaluate label-free precursor ion quantification. The relative quantification of peptides across different samples was performed using the peak area under the curve of detected peptide ions. This quantification was obtained by setting the “Minora feature detector node” in the processing workflow (Peak Feature Detection: min. trace length, 5; max. ΔRT of isotope pattern multiplets [min], 0.2; and Feature to ID Linking: PSM Confidence at least, high) to detect features in individual raw data files and map them to PSMs and the “Feature Mapper node” in the consensus workflow (Chromatographic Alignment: RT alignment, true; Tuning, coarse; RT shift [min], 10; mass tolerance, 10 ppm; and Feature Linking and

Mapping: RT tolerance [min], 0; mass tolerance, 0 ppm; min. S/N threshold, 5) to find the most abundant features. Using the results from the Minora algorithm, the features were then aligned to have the same retention time across all sample files. The abundance ratio (AR) between the two groups compared was log_2-transformed (LogAR) and differential proteins were evaluated using the t-test (background-based) and adjusting the p-value by Benjamini-Hochberg correction. Proteins were considered significantly differential if they had an abundance ratio of less than, or equal to −1.5 and greater than, or equal to +1.5 ($-1.5 \leq Log_2\ AR \geq +1.5$) with an adjusted p-value ≤0.05 (Shah et al., 2019). PSM filter was set to greater than or equal to 2.

Venn diagrams were created by a web tool denominated InteractiVenn (https://www.interactivenn.net/), and principal component analysis (PCA) was conducted using the Perseus bioinformatics tool, which utilized the normalized abundance data of all proteins identified via Proteome Discoverer analysis. The normalization was based on all peptides found in each sample. Then we chose to concentrate on DEPs that showed a higher average abundance in a specific direction of the comparison and were involved in relevant metabolic pathways or biological processes.

3. Results

3.1. MRSA growth in different experimental conditions

Growth curves for MRSA strains ST398 and JE2 under different ECs are seen in **Figure 2A** and **Figure 2B**, respectively. ST398 achieved a mid-exponential phase OD_{600} of 0.5 at approximately 130, 200, and 260 minutes in EC1 (37°C, pH=7), EC2 (35°C, pH=6), and EC3 (35°C, pH=6 and 5% NaCl), respectively. In contrast, the JE2 strain exhibited a prolonged duration to reach a mid-exponential phase, with an OD_{600} of 0.55, taking 150 minutes in EC1, and extending to 180 and 300 minutes in EC2 and EC3, respectively. These observations indicate that the growth of both MRSA strains is partly influenced by the altered pH and temperature, and by the presence of NaCl in TSB. Additionally, the data reveal slight growth discrepancies between the strains under these conditions.

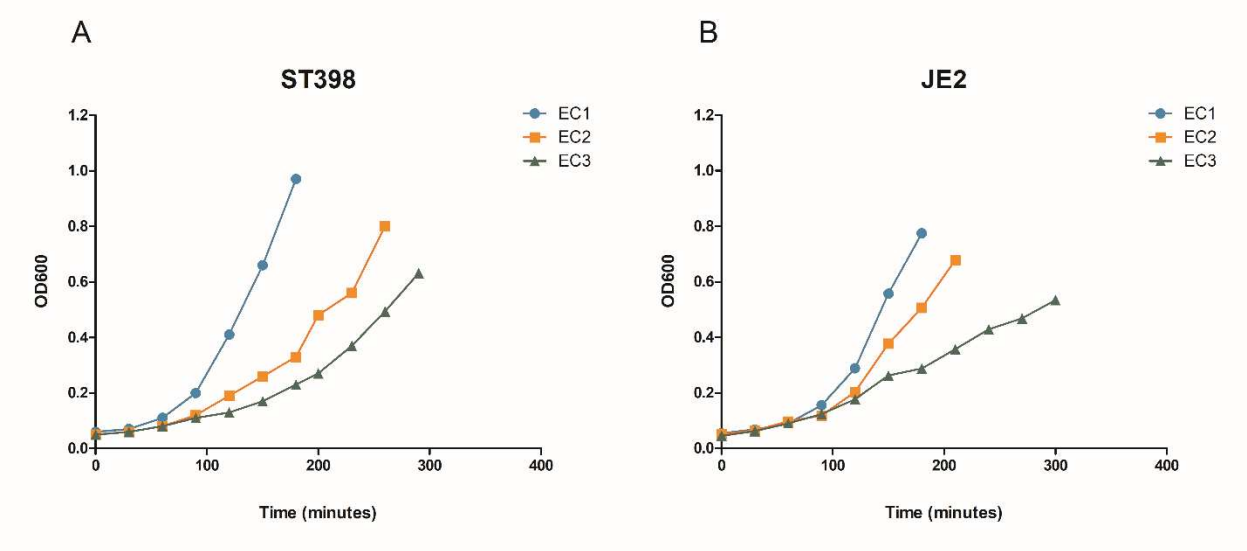

Figure 2. *Growth curves of MRSA ST398 strain (**A**) and MRSA JE2 strain (**B**) in EC1 (blue), EC2 (orange) and EC3 (green). Each curve is obtained from the mean of the three replicates at each point.*

3.2. Identification metrics and multivariate statistics

To characterize the bacterial cell proteome of MRSA ST398 and JE2 strains, their peptide mixtures were separated by long-gradient liquid chromatography, analyzed by a Q-Exactive mass spectrometer, and identified by a tandem mass spectrometry database search engine, SEQUEST-HT, included in the Proteome Discoverer (PD) software. The identifications were obtained by applying an FDR significance threshold of 1%. PD allowed the identification of fairly similar numbers of proteins in the two strains, with 2579 ± 81, 2371 ± 62, and 2197 ± 298 ST398 proteins in EC1, EC2, and EC3 respectively, and 2679 ± 31, 2442 ± 126, and 2785 ± 30 JE2 proteins in EC1, EC2, and EC3, respectively, as shown in **Figure S1** (Supplementary Data).

Analysis of both strains showed a significant difference between the number of proteins obtained in EC1 *vs* EC2 (**Figure 3**). In contrast, no statistical difference emerged from the comparison between EC1 and EC3, most likely due to the higher variability between the EC3 samples analyzed.

A high number of shared proteins between the three different growth conditions was observed in both ST398 and JE2 strains, as illustrated in **Figure S1** (Supplementary Data). Unique proteins (i.e., proteins that were exclusively expressed in one condition, in all three biological replicates) ranged between 4.6% for EC1-grown ST398 and 1.4% for EC1-grown JE2.

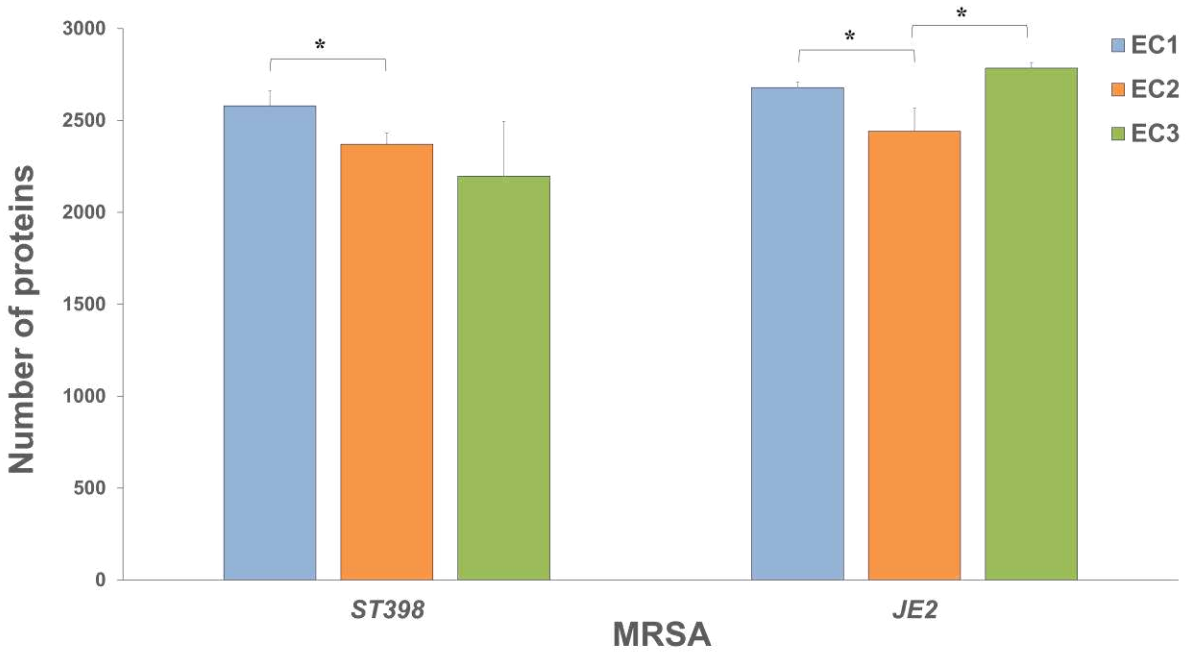

Figure 3. *Histograms illustrating the total number of proteins quantified in ST398 and USA300 JE2 strains grown under EC1 (blue), EC2 (orange), and EC3 (green). Every bar represents the average deviation standard obtained from three biological replicates. The asterisk (*) indicates the statistically significant differences (p-value ≤0.05) obtained after applying the t-test.*

The normalized abundances of the proteins quantified by PD were used to perform multivariate statistics utilizing principal component analysis (PCA). This analysis was carried out to evaluate whether the samples could be discriminated according to the growth conditions based on their proteome profile. **Figure 4.** shows a clear separation between the two strains associated with the first component, accompanied by a further clustering based on the three ECs associated with the second component.

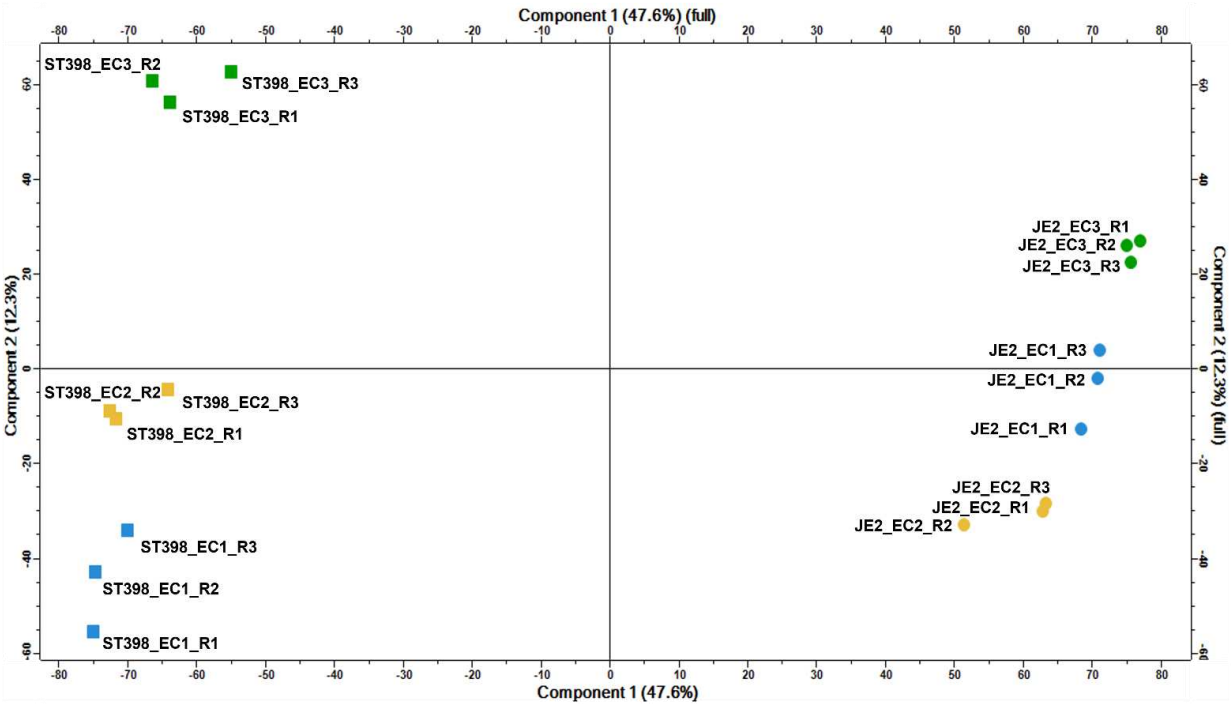

Figure 4. *PCA plot of all samples analyzed in this study. Samples belonging to the JE2 strain are represented by a circle, while those belonging to the ST398 strain are represented by a square. Blue, orange, and green colors mark EC1, EC2, and EC3, respectively.*

3.3. Proteins significantly associated with different growth conditions in the ST398 strain

3.3.1. EC2 vs EC1

Protein abundance data were further parsed to perform differential analysis between the different ECs, focusing initially on the ST398 strain. Comparing EC2 to EC1, we identified 570 differentially expressed proteins (DEPs), of which 256 exhibited a significantly higher abundance and 314 had a significantly lower abundance under EC2 than EC1. We then clustered these DEPs based on the biological processes and metabolic pathways to which they belong, with the aim of understanding their roles in each growth condition.

As shown in **Figure 5**, we identified 24 DEPs involved in amino acid metabolism. Some of them with significantly higher abundance under EC2 compared to EC1 included two

DEPs involved in arginine and proline metabolism namely pyrroline-5-carboxylate reductase (ProC) and 1-pyrroline-5-carboxylate dehydrogenase (RocA). Additionally, we identified two DEPs that are part of the arginine deiminase (ADI) pathway: arginine repressor (ArcR) and arginine deiminase (ArcA). Conversely, six DEPs showed significantly lower expression in EC2 compared to EC1 involved in valine, leucine, and isoleucine metabolism: dihydroxy-acid dehydratase (IlvD), acetolactate synthase (IlvH), isoleucine--tRNA ligase (IleS), 3-isopropylmalate dehydrogenase (LeuB), 3-isopropylmalate dehydratase large subunit (LeuC), and 3-isopropylmalate dehydratase small subunit (LeuD).

Ten DEPs significantly increased their abundance in EC2 compared to EC1 that belong to ABC transporters, including ABC transporter substrate-binding protein (PsaA_2), Betaine/proline/choline family ABC transporter ATP-binding protein (GAY51_09330), Lipoprotein (MetQ), SWIM zinc finger family protein (NWMN_1289), Zinc ABC transporter ATP-binding protein (BSZ10_06550), Iron chelate uptake ABC transporter family permease subunit (E3A28_00695), permease protein (NikB), Nickel import system ATP-binding proteins (NikD and NikE), and Zinc ABC transporter substrate-binding lipoprotein (ZinT). The TrkH family potassium uptake protein (G0V76_11885) was also increased in EC2.

The decreasing DEPs also included seven proteins playing crucial roles in the *de novo* synthesis of purines, particularly of inosine monophosphate (IMP), an essential precursor in purine metabolism: N5-carboxyaminoimidazole ribonucleotide mutase (PurE), phosphoribosyl formyl glycinamidine synthase subunit (PurS), amidophosphoribosyl transferase (PurF), phosphoribosyl formyl glycinamidine cyclo-ligase (PurM),

phosphoribosyl aminoimidazole-succino carboxamide synthase (PurC), N5-carboxyaminoimidazole ribonucleotide synthase (PurK), and bifunctional purine biosynthesis protein (PurH). Five DEPs involved in sulfur metabolism were also decreased, including sulfur carrier protein (FdhD), cysteine desulfurase (Csd), iron-sulfur cluster repair protein (CsdA), cysteine-tRNA ligase (CsyS), and cysteine synthase (CysK).

Finally, we observed three DEPs with increased expression in EC2 that could not be mapped to any specific pathway, namely catalase (KatA), alkyl hydroperoxide reductase protein C (AhpC), both of which compensatory play roles in peroxide stress resistance (Cosgrove et al., 2007), and Aldo/keto reductase family protein (YdhF) which plays relevant roles in redox balance and homeostasis.

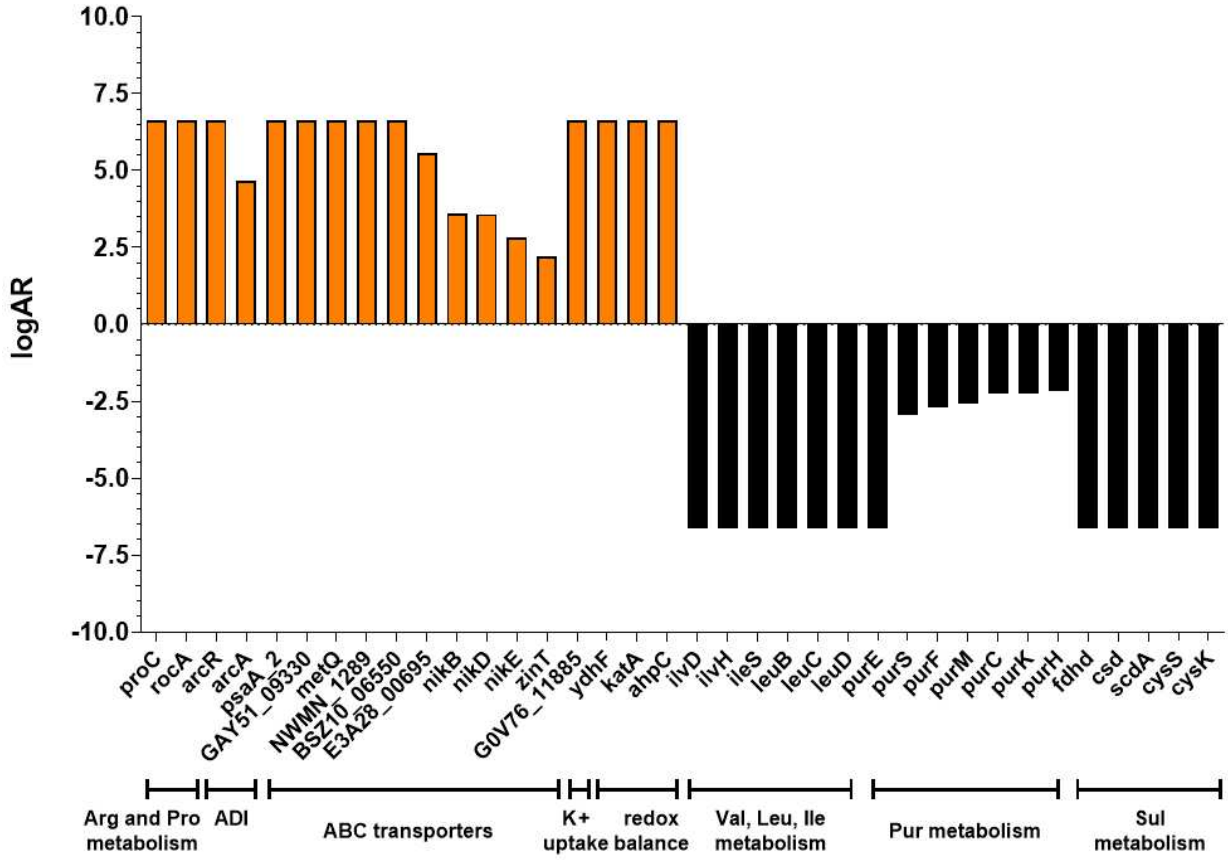

Figure 5. *Proteins with significantly differential expression between EC2 and EC1 in strain ST398. The binary logarithm of the abundance ratio is plotted on the y-axis, while the abbreviated protein names are plotted on the x-axis. DEPs with higher abundance in EC2 are colored in orange, while those with higher abundance in EC1 are colored in black. logAR: Abundance Ratio (log2). Arg and Pro for arginine and proline, ADI for arginine deiminase. K+ for potassium. Val, Leu, Ile for valine, leucine and isoleucine, Pur for purine, and Sul for sulfur.*

3.3.2. EC3 vs EC1

Comparing EC3 to EC1, we found 625 DEPs, of which 418 exhibited a significantly higher abundance and 207 exhibited a significantly lower abundance under EC3 compared to EC1. As in the previous comparison, we clustered the DEPs into biological processes and metabolic pathways. Accordingly, we identified some similarities to the previous comparison, as shown in **Figure 6**. We found two DEPs, involved in valine, leucine, and isoleucine metabolism, that were significantly decreasing in EC3 compared to EC1, consistently with EC2: 3-isopropyl malate dehydratase large subunit (LeuC) and 3-

isopropyl malate dehydratase small subunit (LeuD). We found two DEPs, involved in valine, leucine, and isoleucine metabolism, that were significantly decreasing in EC3 compared to EC1, consistently with EC2: 3-isopropyl malate dehydratase large subunit (LeuC) and 3-isopropyl malate dehydratase small subunit (LeuD). We also detected DEPs involved in ABC transporters, including ABC transporter substrate-binding protein (PsaA_2), peptide ABC transporter, peptide-binding protein (SAUSA300_0073), iron citrate ABC transporter substrate-binding protein (FecB), lantibiotic protection ABC transporter ATP-binding subunit (EpiF), and nickel ABC transporter, nickel/metallophore periplasmic binding protein (CntA). Only the first protein was shared between EC2 and EC3. Similarly to EC2, catalase (katA) was also increasing in this condition, aldo/keto reductase (YdhF), besides another protein that plays the same role, namely aldo/keto reductase hypothetical protein (SAOUHSC_01907).

Moreover, we found three significantly increasing DEPs in EC3 compared to EC1 involved in arginine biosynthesis: arginine deiminase (ArcA), ornithine carbamoyl transferase (ArgF), and carbamoyl phosphate synthase small subunit (CarA). Additionally, we identified a protein involved in potassium transportation, namely K+-transporting ATPase, C subunit (KdpC), and three DEPs involved in glutathione metabolism (GSH): isocitrate dehydrogenase [NADP] (Icd), 6-phosphogluconate dehydrogenase (GndA), and glucose-6-phosphate 1-dehydrogenase (Zwf_2). Five DEPs associated with lipid metabolism were also found: lipase 2 (Lip2), heptaprenylglyceryl phosphate synthase (PcrB), lipoteichoic acid-specific glycosyltransferase (YfhO), cardiolipin synthase (Cls), and aldehyde dehydrogenase (AldA).

On the other hand, we noted decreasing DEPs, some of which are shared with EC2. Six DEPs are involved in purine metabolism: GMP reductase (GMPR), xanthine phosphoribosyl transferase (Xpt), phosphoribosyl amine--glycine ligase (PurD), nucleoside diphosphate kinase (Ndk_2), hypoxanthine phosphoribosyl transferase (Hpt), and (p)ppGpp synthetase II (RelA). Finally, four decreasing DEPs are involved in sulfur metabolism, three of which were also recorded in EC2: cysteine desulfurase (Csd), cysteine synthase (CysK), sulfur carrier protein (FdhD), and cysteine protease staphopain A (ScpA).

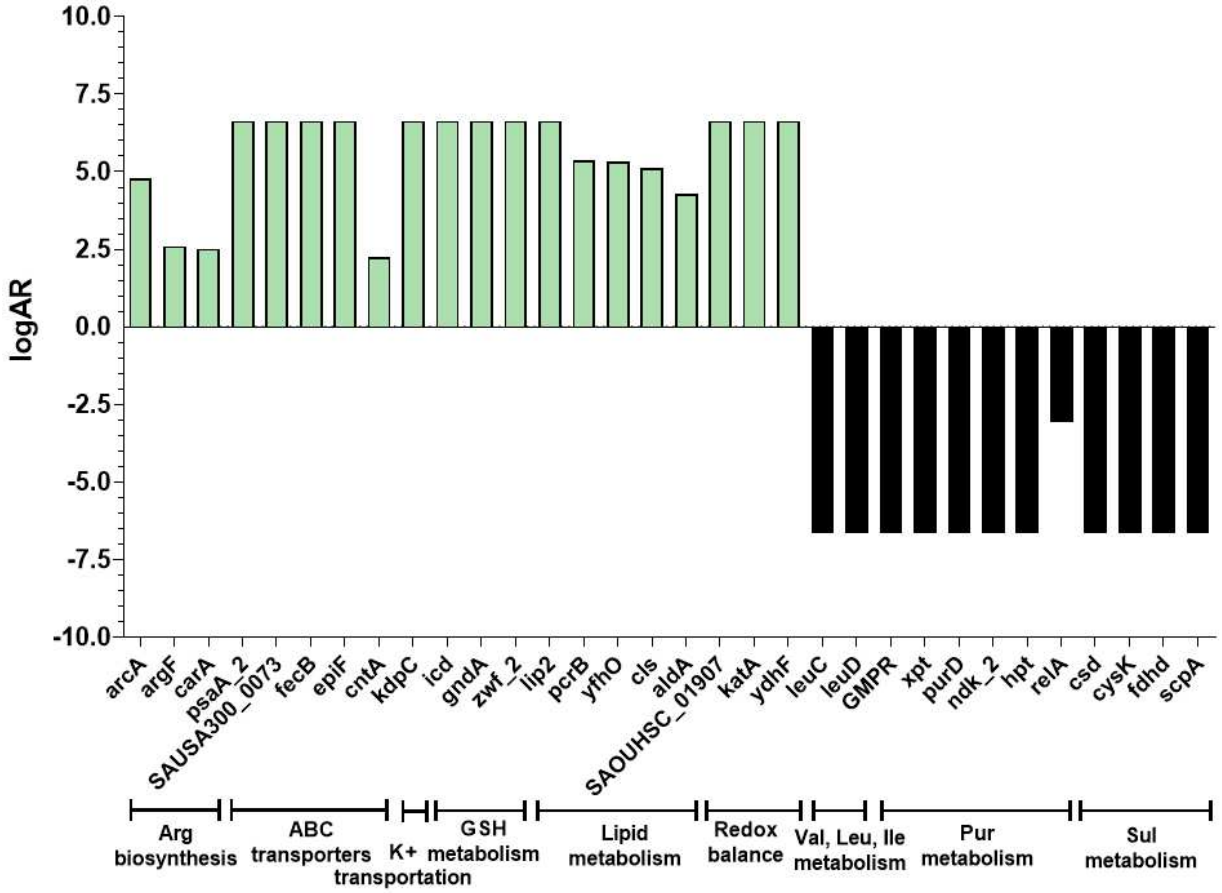

Figure 6. *Proteins with significantly differential expression between EC3 and EC1 in strain ST398. The binary logarithm of the abundance ratio is plotted on the y-axis, while the abbreviated protein names are plotted on the x-axis. DEPs with higher abundance in EC3 are colored in green, while those with higher abundance in EC1 are colored in black. logAR: Abundance Ratio (log2). Arg for arginine, K+ for potassium, GSH for glutathione, Val, Leu, Ile for valine, leucine, and isoleucine, Pur for purine, and Sul for sulfur.*

3.4. Proteins significantly associated with different growth conditions in the JE2 strain

3.4.1. EC2 vs EC1

Comparing EC2 to EC1, we identified a total of 488 DEPs, with 180 exhibiting significantly higher abundance and 308 significantly lower abundance in EC2 compared to EC1**.** **Figure 7.** shows a selection of DEPs that belong to several relevant biological processes and metabolic pathways.

DEPs involved in amino acid metabolism showed an increase in arginine and proline metabolism, including two DEPs, namely pyrroline-5-carboxylate reductase (ProC) and aldehyde dehydrogenase (Aldh). Several DEPs were involved in arginine biosynthesis, namely arginine deiminase (ArcA) and seven urease subunits (UreEABCGFD). Lysine biosynthesis was involved with three DEPs: 4-hydroxy-tetrahydrodipicolinate reductase (DapB), 2,3,4,5-tetrahydropyridine-2,6-dicarboxylate N-acetyltransferase (DapD), and aspartokinase (LysC). We found one DEP, histidinol phosphate aminotransferase (HisG), playing a role in histidine metabolism. We also observed an increase in catalase protein (KatA) and aldo/keto reductase protein (YdhF). Moreover, five DEPs involved in ABC transporters, including glycine betaine ABC transport system (ProV), ABC transporter ATP-binding protein (MsbA_1), ABC transporter substrate-binding protein (Opp5A), betaine/proline/choline family ABC transporter ATP-binding protein (OpuCB), and betaine-carnitine-choline ABC transporter (OpuCC).

On the other hand, cysteine and methionine metabolism was decreasing, encompassing the following seven DEPs: cysteine metabolism repressor (CymR), cysteine synthase (CysK), purine nucleoside phosphorylase (YlmD), D-3-phosphoglycerate dehydrogenase

(SerA), cystathionine gamma-synthase (MccB), peptide methionine sulfoxide reductase (MsrB), and probable cysteine desulfurase (Csd). Moreover, we found eight decreasing DEPs involved in purine metabolism, including inosine-5-monophosphate dehydrogenase (GuaB_5), N5-carboxyaminoimidazole ribonucleotide mutase (PurE), phosphoribosyl amine--glycine ligase (PurD), phosphoribosyl formyl glycinamidine synthase subunit (PurQ), phosphoribosyl formyl glycinamidine synthase subunit (PurS), phosphoribosyl glycinamide formyl transferase (PurN), purine nucleoside phosphorylase (YlmD), and bifunctional purine biosynthesis protein (PurH). In addition, four DEPs involved in sulfur metabolism were decreasing: cysteine synthase (CysK), assimilatory sulfite reductase (NADPH) flavoprotein subunit (CysJ), probable cysteine desulfurase (Csd), and oligo ribonuclease (NrnA).

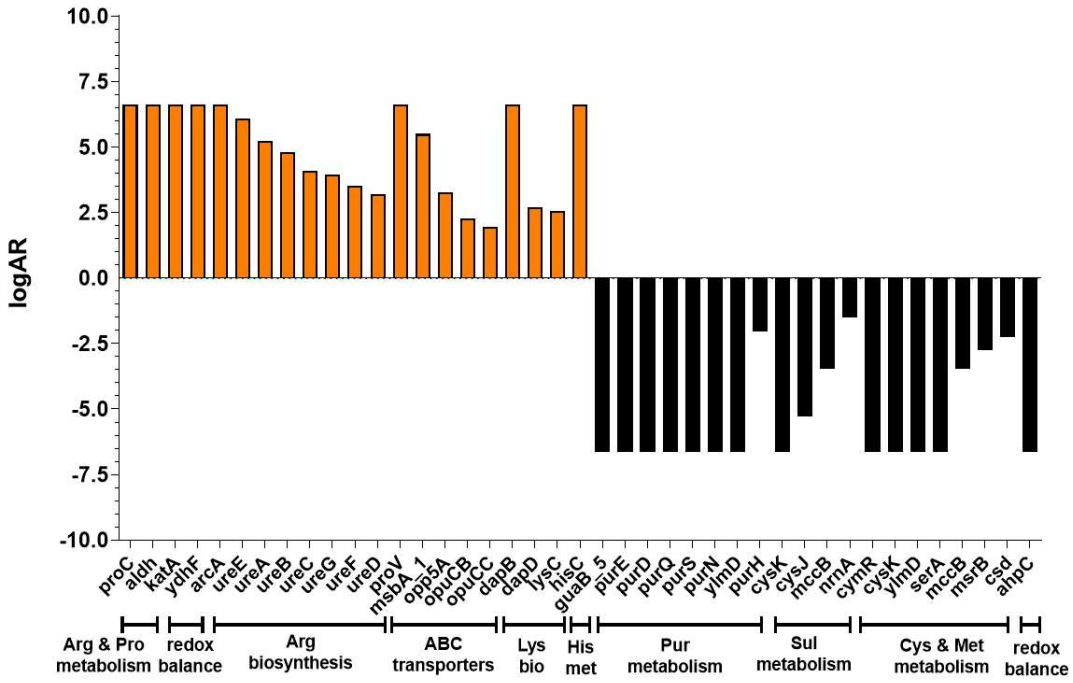

Figure 7. *Proteins with significantly differential expression between EC2 and EC1 in strain JE2. The binary logarithm of the abundance ratio is plotted on the y-axis, while the abbreviated protein names are plotted on the x-axis. DEPs with higher abundance in EC2 are colored in orange, while those with higher abundance in EC1 are colored in black. logAR: Abundance Ratio (log2). Arg and Pro for arginine and proline, Arg for arginine, Lys for lysine, His for histidine, Pur for purine, Sul for sulfur, Cys and Met for cysteine, and methionine.*

3.4.2. EC3 vs EC1

Comparing EC3 to EC1, we identified a total of 359 DEPs. Of these, 220 had significantly higher abundance, and 139 had significantly lower abundance in EC3 compared to EC1. A selection of DEPs related to relevant biological processes and metabolic pathways is shown in **Figure 8**. Similar to EC2, we found DEPs significantly increasing compared to EC1 involved in arginine biosynthesis, encompassing nine DEPs: ornithine carbamoyl transferase (ArcB), six urease accessory proteins (UreECGABF), arginine succinate synthase (ArgG), and arginine succinate lyase (ArgH). Five increasing DEPs involved in histidine metabolism were also identified, including histidinol-phosphate aminotransferase (HisC), imidazole glycerol-phosphate dehydratase (HisB), histidinol dehydrogenase (HisD), 1-(5-phosphoribosyl)-5-[(5-phosphoribosyl amino) methylidene amino] imidazole-4-carboxamide isomerase (HisA), and imidazole glycerol phosphate synthase subunit (HisH). The first DEP was shared with EC2. We also found the same two increasing DEPs involved in L-lysine biosynthesis as those identified in EC2: 2,3,4,5-tetrahydropyridine-2,6-dicarboxylate N-acetyltransferase (DapD) and 4-hydroxy-tetrahydrodipicolinate reductase (DapB). Additionally, five increasing DEPs functioned as ABC transporters, including ABC transporter ATP-binding protein (SAUSA300_1852), ABC transporter permease subunit (Opp3B), peptide ABC transporter ATP-binding protein (SAUSA300_2465), ABC transporter ATP-binding protein (NikD), and ABC transporter substrate-binding protein (Opp5A). Four increasing DEPs were identified as potassium-transporting ATPase potassium-binding subunits (KdpCBEA), playing a role in potassium transportation. Similarly to EC2, we also identified the catalase protein

(KatA) as differentially expressed in EC3 compared to EC1 besides aldo/keto reductase protein (SAOUHSC_01907).

Furthermore, similar to EC2, decreasing DEPs associated with biological processes were involved in purine and sulfur metabolism. Purine metabolism included three DEPs: LPXTG-motif protein cell wall anchor domain protein (HMPREF3211_02100), N5-carboxy aminoimidazole ribonucleotide synthase (PurK), and phosphoribosyl amine--glycine ligase (PurD). Two decreasing DEPs were involved in sulfur metabolism: beta-cyano-L-alanine synthase (CysK_1) and DoxX protein (BN1321_170040). It is worth noting that CysK_1 plays a dual role in the metabolism of both cysteine and methionine, and sulfur. Finally, similar to our findings in EC2, we also identified alkyl hydroperoxide reductase subunit F (AhpC).

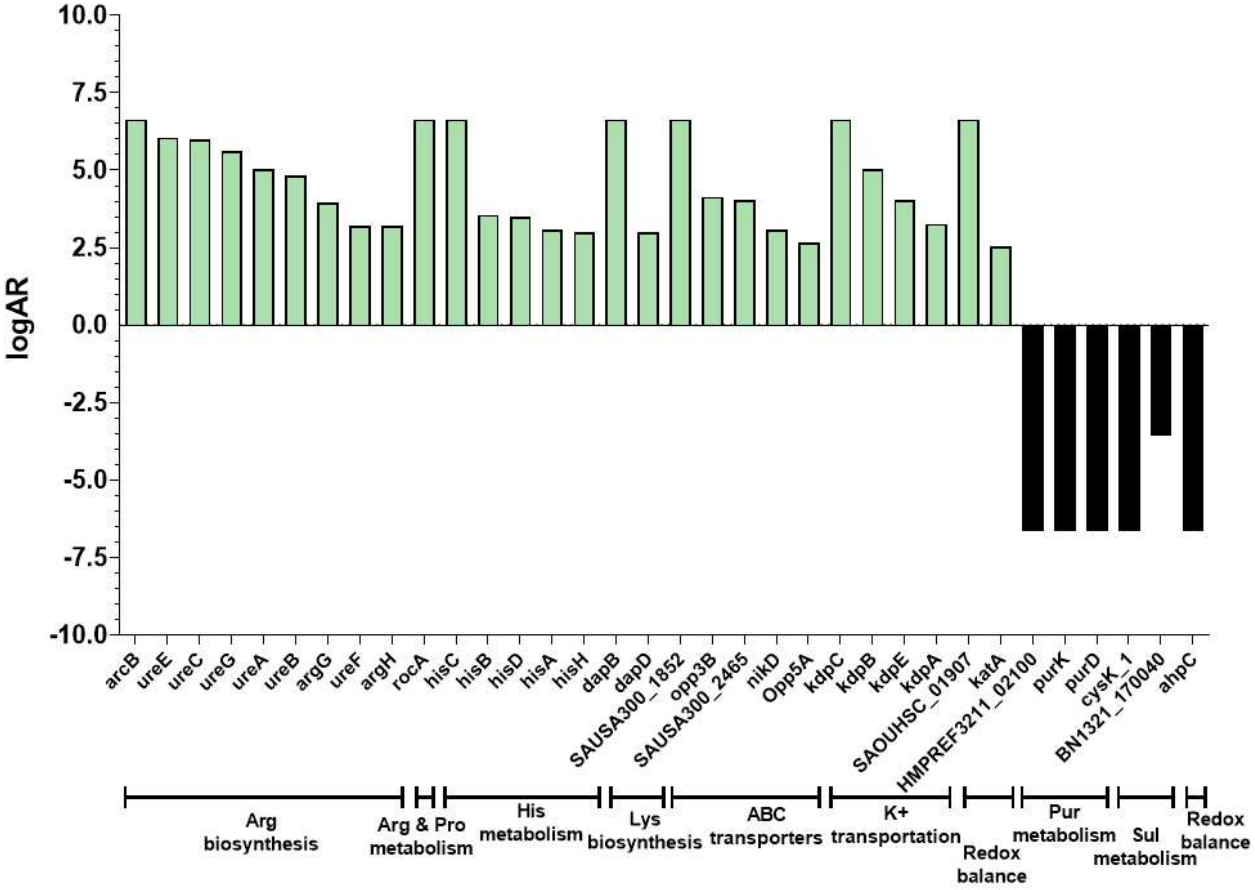

Figure 8. *Proteins with significantly differential expression between EC3 and EC1 in strain JE2. The binary logarithm of the abundance ratio is plotted on the y-axis, while the abbreviated protein names are plotted on the x-axis. DEPs with higher abundance in EC3 are colored in green, while those with higher abundance in EC1 are colored in black. logAR: Abundance Ratio (log2). Arg for arginine, Arg and Pro for arginine and proline, His for histidine, Lys for lysine, K+ for potassium, Pur for purine, and Sul for sulfur.*

3.5. Shared features between the strains and the ECs

The outputs of the differential analysis were further investigated to identify which DEPs were shared between conditions and/or strains or unique to one of them. As shown in **Figure 9A.** and detailed in **Tables ST1** and **ST2**, the number of DEPs more abundant in EC2 compared to EC1 for both strains was 25, while those more abundant in EC3 compared to EC1 for both strains were 20. Moreover, 9 DEPs were uniquely more abundant in EC2 for both strains, and another 8 DEPs were uniquely more abundant in EC3 for both strains; those with known functions are listed in **Tables 1** and **2**. DEPs

increasing in abundance under both conditions in both strains included catalase (KatA), chaperone protein (DnaK), and coproheme decarboxylase (CdhC).

Additionally, the analysis identified several proteins commonly downregulated in both strains. Specifically, 57 DEPs were less abundant in EC2 compared to EC1 and 41 were less abundant in EC3 compared to EC1, as shown in **Figure 9B.** and detailed in **Table ST3** and **ST4**. Among these, 21 DEPs were uniquely less abundant in EC2 and for both strains, while 12 DEPs were uniquely less abundant in EC3 for both strains; those with known functions are listed in **Tables 3** and **4**.

Interestingly, alkyl hydroperoxide reductase (AhpC) exhibited opposite trends in the two strains (increasing in ST398 and decreasing in JE2) under both EC2 and EC3.

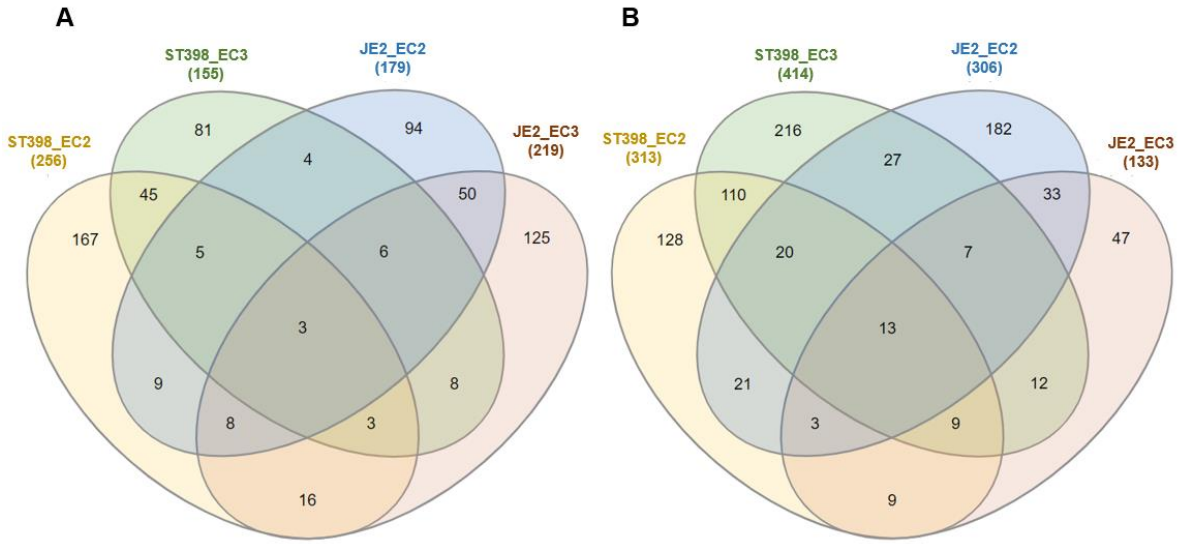

Figure 9. *The Venn diagrams show the overlap between DEPs increased* ***(A)*** *or decreased* ***(B)*** *in EC2 or EC3 compared to EC1.*

Table 1. *Proteins overexpressed under EC2 in both ST398 and JE2 strains.*

Protein Name	Gene Name	LogAR[1] (ST398)	LogAR[1] (JE2)
Arginine repressor	*arcR*	6.64	2.57
Pyrroline-5-carboxylate reductase	*proC*	6.64	6.64
Glutamate synthase [NADPH] large subunit	*gltB_2*	6.64	6.64
Iron-regulated surface determinant protein H	*harA*	2.99	2.39
Similar to xylitol dehydrogenase	*SAI7S6_1001930*	4.22	6.64

Catalase	*katA*	6.64	6.64
Aldo/keto reductase family protein	*ydfH*	6.64	6.64
Iron-sulfur cluster regulator	*IscR*	6.64	6.64

[1] LogAR: logarithm of the abundance ratio.

***Table 2**. Proteins overexpressed under EC3 in both ST398 and JE2 strains.*

Protein Name	Gene Name	LogAR[1] (ST398)	LogAR[1] (JE2)
Acylphosphatase	*ST398NM01_1406*	3.69	3.03
Fructose-bisphosphate aldolase class 1	*fda*	4.18	2.83
Aldo/keto reductase	*SAOUHSC_01907*	6.64	6.64
Amidase domain-containing protein	*G0Y40_03125*	6.64	6.64
DNA polymerase beta	*polX*	6.64	6.64
DNA topoisomerase 4 subunit A	*parC*	6.64	6.64
Catalase	*katA*	2.53	6.64
K+-transporting ATPase	*kdpC*	6.64	6.64
Oxygen-dependent choline dehydrogenase	*betA*	6.64	6.64

[1] LogAR: logarithm of the abundance ratio.

***Table 3**. Proteins under expressed under EC2 in both ST398 and JE2 strains.*

Protein Name	Gene Name	LogAR[1] (ST398)	LogAR[1] (JE2)
Phosphoribosyl formyl glycinamidine synthase subunit	*purS*	-6.64	-6.64
Bifunctional purine biosynthesis protein	*purH*	-2.15	-2.04
N5-carboxyaminoimidazole ribonucleotide mutase	*purE*	-6.64	-6.64
Inosine-5-monophosphate dehydrogenase A	*guaB_5*	-6.64	-6.64
N-acetyltransferase domain-containing protein	*paiA*	-3.87	-6.64

[1] LogAR: logarithm of the abundance ratio.

***Table 4.** Proteins under expressed under EC3 in both ST398 and JE2 strains.*

Protein Name	Gene Name	LogAR[1] (ST398)	LogAR[1] (JE2)
AraC family transcriptional regulator	*A6762_03215*	-6.64	-2.56
Heat shock protein 60 family co-chaperone	*groES*	-6.64	-6.64
Serine-aspartate repeat-containing protein	*SAGV69_02059*	-6.64	-6.64
VWFA domain	*BSZ10_04415*	-6.64	-6.64
YozE_SAM_like domain-containing protein	*A6762_04255*	-6.64	-6.64
Triosephosphate isomerase	*tpi*	-4.58	-6.64
Acetyl-CoA carboxylase biotin carboxyl carrier protein subunit	*SAEG_02002*	-2.81	-6.64
D-alanyl carrier protein	*dltC*	-3.83	-1.89

[1] LogAR: logarithm of the abundance ratio.

4. Discussion and Conclusion

The persistent threat of *S. aureus* infections remains a critical public health issue, stemming from the bacterium's ability to adapt its metabolism to fit the environmental condition, during commensalism, colonization, and deep tissue infections (Wood et al.,

2013). Metabolic changes are also expected to be strain-dependent, yet few studies have been conducted recently to tackle this issue (Choueiry et al., 2022). Previous research has employed proteomic approaches to investigate these adaptations, either by testing the effects of different antibiotic levels (Liu et al., 2016) or by comparing clinical strains of MRSA (Philip Nikolic, 2023). In this study, we characterized the proteomic profile of two different MRSA strains subjected to experimental conditions mimicking the stressful environment faced by *S. aureus* during skin infection. When *S. aureus* translocates across the epithelial barrier, its growth rate is limited by the host's innate immunity. However, self-limiting bacterial growth also represents a successful response to the new environment, facilitating the evasion from immune response and antibiotic treatment (Wood et al., 2013). Our data confirmed a reduced growth rate of MRSA strains ST398 and JE2 when exposed to a lowered pH, and increased salinity, especially by their combination, as previously reported (Rode et al., 2010b).

In the tested ECs, a slight decrease in the pH and temperature was meant to mimic the "acid mantle" of healthy human skin" (Lenhardt and Sessler, 2006b; Costa and Horswill, 2022). These represent typical environmental stressors that pathogens like *S. aureus* encounter. Adding NaCl to EC2 enabled the examination of how an additional factor affects bacterial metabolism. This condition simulates the skin's environment more closely, providing insights into how *S. aureus* adapts its metabolic processes in response to increased salinity on top of acidic conditions (YASMINE BELKAID and JULIA A. SEGRE, 2014). Further, *S. aureus* is recognized to possess the ability to deal with osmotic pressure and to adapt to salinity stress by orchestrating a complex metabolic shift, including biofilm formation (Julia M Ross and Marten, 2015). Consistently, our ECs led to a reduction of bacterial growth

rate and reassortment of several metabolic pathways. Among these, purine metabolism was affected by both conditions in both strains. Specifically, we observed the reduction of several functions required for *de novo* biosynthesis of IMP that, in turn, is the substrate of the growth rate-limiting enzyme inosine 5′-monophosphate dehydrogenase (IMPDH), being required to expand the cell guanine nucleotide pool and providing an interesting target for novel antimicrobial drugs (Juvale et al., 2019). These data suggest a rapid metabolic shift to actively slow down bacterial replication acting on key limiting pathways. Previous studies have agreed that in acidic pH and skin infection, the purine biosynthesis pathway usually increases (Walker and Miller, 2020). Contrary to these findings, our study observed a decrease in the purine metabolism pathway, suggesting a potential link between reduced purine metabolism and enhanced survival. Interestingly, our finding agrees with a previous study that has seen reduced levels of PurE, PurQ, and PurK proteins when *S. aureus* was exposed to mupirocin, an antibiotic used to treat skin infection, which induced a stress response and led to the inactivation of purine proteins (Reiß et al., 2012). These observations also align with another study that noted a reduction in the purine metabolism pathway in *S. aureus* when challenged with antimicrobials (Ren et al., 2022), favoring other pathways that could be more essential for stress adaptation.

The other pathway decreased in both strains under ECs was sulfur metabolism. This pathway plays a critical role in maintaining proper oxidation states of cellular thiols. Noteworthy, oxidative damage is a hallmark of the host's innate response to *S. aureus* infection.

Furthermore, we observed a decrease in DEPs associated with cysteine and methionine metabolism in JE2 under EC3. This decrease included DEPs directly or indirectly linked

to this pathway, such as D-3-phosphoglycerate dehydrogenase (SerA). Although SerA is primarily involved in L-serine biosynthesis, it's important to note that serine serves as a precursor for cysteine, thus SerA indirectly influences cysteine metabolism (Caballero Cerbon et al., 2024). We believe that this decrease was compensated by proteins that contribute to homeostasis. Specifically, catalase (KatA), significantly increased in EC2 in both strains. The catalase enzyme plays a pivotal role in conferring resistance against hydrogen peroxide (H2O2), it is the primary scavenger for high levels of (H2O2) (Horsburgh et al., 2001; Gaupp et al., 2012). Another protein found was aldo/keto reductase protein (YdhF). Aldo-keto reductases (AKRs) are a large superfamily of enzymes that rely on NADPH to function as oxidoreductases. They are known for their ability to stereo-specifically reduce various aromatic and aliphatic aldehydes and ketones (Lapthorn et al., 2013). Their role in *S. aureus* is not well studied, as their activity does not directly contribute to redox balance, however, they can play a role in detoxification contributing to the cell redox balance (Ellis, 2002).

We also found alkyl hydroperoxide reductase (AhpC) increasing in ST398 which belongs to the peroxiredoxin enzyme family, known for neutralizing hydrogen peroxide, organic peroxides, and peroxynitrite, thereby protecting cells from oxidative damage (Poole, 2005). Catalase (KatA), and alkyl hydroperoxide reductase (AhpC) enzymes, both are proven to have a compensatory role in peroxide stress resistance and are also required for nasal colonization (Cosgrove et al., 2007). An interesting finding was that (AhpC) was decreased in JE2 in EC2 and EC3 proving different strains' adaptive response to stress conditions, specifically, oxidative stress, and that KatA is more protective than AhpC. Complementary to redox homeostasis, ST398 strain showed a concurrent increase of protein functions

related to glutathione metabolism (GSH) under acidic pH and high salinity (EC3). Glutathione is a low molecular weight thiol, essential for the homeostasis of intracellular redox in bacteria (Ku and Gan, 2019). Glutathione metabolism is usually used by bacteria for cell protection from different sources of physiological stress such as reactive oxygen species (ROS) and reactive nitrogen species (RNS) besides acid and osmotic stress (Lluis Masip and George Georgiou, 2006; Lushchak, 2012). This suggests that the EC3 mimics *in-vivo* conditions with active production of ROS and RNS with increased glutathione levels serving to neutralize these potentially damaging molecules and protect cellular components.

We also noticed an increase in DEPs related to arginine and proline metabolism in both strains under EC2 represented by pyrroline-5-carboxylate (ProC), a key degradation product of proline that serves as a precursor for the synthesis of arginine, proline, and glutamate (Jeong et al., 2022). An increase in the arginine biosynthesis pathway in both EC2 in ST398 was represented by arginine deiminase, highlighting the importance of arginine for both *S. aureus* growth (Audretsch et al., 2021), and the intracellular pH homeostasis to fight acid shock (Guan and Liu, 2020). Arginine deiminase (ArcA) is involved in the synthesis of NH_3, leading to an increase in NH_4^+ levels. This elevation acts as a buffering power, moderating both intra- and extracellular pH levels during acidic challenges, as described by Cotter P. et al (Cotter and Hill, 2003). Moreover, bacteria can utilize arginine as a source of energy when grown in oxygen-competent conditions which was the case when the bacteria were grown with limited oxygen space (Makhlin et al., 2007). In the JE2 strain, DEPs significantly increasing associated with arginine biosynthesis pathway have involved the urease complex. They function synergistically

with arginine to neutralize the medium. This observation is consistent with other studies (Bäckhed et al., 2012; Zhou et al., 2019b; Walker and Miller, 2020). They have shown that both urease and arginine deiminase activities are increased under acidic conditions, generating ammonia to buffer the medium. Specifically, urease catalyzes the conversion of urea into ammonia and carbon dioxide through a reaction dependent on nickel cations, thus acting as a key agent in medium neutralization (Bore et al., 2007). Proving the importance of arginine for bacterial metabolism during stress adaptation.

Increased levels in DEPs belonging to different transporting systems were also noticed, especially, ABC transporters. It included proteins associated with ion transports such as nickel, zinc, iron, and members of the betaine/proline/choline family. These transport systems are crucial for linking ATP hydrolysis to the translocation of substrates across the membrane. These components also facilitate nutrient uptake crucial for bacterial survival and pathogenesis or act as osmoprotectants. For instance, the proteins we identified, nickel, zinc, and iron transporters, are vital for several biological functions, including resistance to oxidative stress and as structural components of proteins, highlighting their importance in pathogenicity as demonstrated in previous studies (Akhtar and Turner, 2022a). Conversely, the transport proteins associated with betaine, proline, and choline are primarily implicated as osmoprotectants. Their elevated expression in conditions of slightly acidic pH suggests an adaptive mechanism to maintain cellular integrity against environmental stress (Akhtar and Turner, 2022b),(Bore et al., 2007). Meanwhile, the increased proteins identified within the JE2 strain, especially in EC2, are primarily involved in the betaine/carnitine/choline/proline metabolic pathway. Among these proteins, OpuC stands out as a critical component. OpuC is recognized for its role

as a primary osmoprotectant, facilitating the uptake of osmolytes such as glycine, betaine, and carnitine. These osmolytes play a vital role in the cell's response to osmotic stress, helping to maintain fluid balance and protect cellular structures. Furthermore, the involvement of OpuC may extend beyond osmoprotection, potentially contributing to the pathogenicity of the organism (kiran-et-al-2018-opuc-an-abc-transporter-that-is-associated-with-staphylococcus-aureus-pathogenesis, n.d.). This trend suggests a strategic shift in JE2, favoring the expression of osmoprotectant-associated transporters over those involved in iron transport, essential for bacterial viability. This response indicates the strain's adaptation to osmotic stress, aligning with the slightly acidic pH adjustments in the experimental condition. Furthermore, increased levels of DEPs involved in potassium-transporting ATPase due to potassium limitation, such as those seen increasing in EC3 in JE2, and one potassium uptake protein was also found increasing in ST398 in EC3. Potassium transport is vital for chemiosmotic homeostasis, thus, when the pH is acidic, the upregulation of potassium uptake becomes crucial to maintain its range under pH stress (Gries et al., 2016; Yang et al., 2020). This suggests that the osmotic and pH imbalance caused a potassium limitation within the cell, which was compensated by increasing potassium transport to achieve that balance again.

Moreover, DEPs increased levels involved in the histidine metabolism pathway were also observed especially in JE2 in EC3. Histidine is usually used by gram-positive bacteria as a carbon and nitrogen source (Kimhi and Magasanik, 1970). This is also crucial for gene regulation, structural organization, and RNA processing, in addition to its significance in maintaining cell wall integrity. Thus, the increase of histidine metabolism is a sensor of cell wall damage, which agrees with the salt addition experimental condition (Alifano et al.,

1996; Feng et al., 2022b). It was also confirmed in a previous study that histidine levels increase to ensure pH homeostasis (Loi et al., 2023), confirming its role in our studied conditions. Also, it was seen previously that histidine is not utilized until proline and arginine are limited or depleted (Halsey et al., 2017), which explains our previous evidence of increased arginine biosynthesis.

Also, we observed an increased metabolic shift in ST398 in EC3 when compared to the control condition. such as lipid metabolism, involving several key genes, such as Lip2, PcrB, YfhO, Cls, and A6762_10755. Specifically, cardiolipin (Cls), a phospholipid known for its presence in the bacterial cell membrane and its role in eukaryotic mitochondria, emerges as critical for the survival of *S. aureus* under prolonged salinity stress. It is thought to facilitate the formation of the L-variant form of *S. aureus*, a cell wall-deficient state that aids in bacterial persistence during infection and survival under stress conditions (Xu et al., 2020), highlighting cardiolipin's role in enhancing bacterial resilience to salinity stress, though not essential for growth under such conditions (Tsai et al., 2011; Calderón-Rivera et al., 2023). Another gene comprised in this pathway is N-acetyltransferase (YfhO), which is implicated in the glycosylation of lipoteichoic acid (LTA) and plays a role in the bacterial stress response (Rismondo et al., 2018; Sivapragasam and Grove, 2019; Pinilla et al., 2021). Phospholipids also compromise an important role of maintaining cell size and shape during growth as well as the lipid role in bacterial envelope during stress (Sivapragasam and Grove, 2019).

To our knowledge, this study is the first to compare the differences between the proteomes of two MRSA strains under identical conditions and to evaluate the variations of their proteomes and the specific metabolic pathways associated with them. Our

findings contribute to understanding mechanisms involved in stress conditions that could mimic the stress experienced at the wound site and suggest new targets for combating antimicrobial resistance.

5. Supplementary Data_1

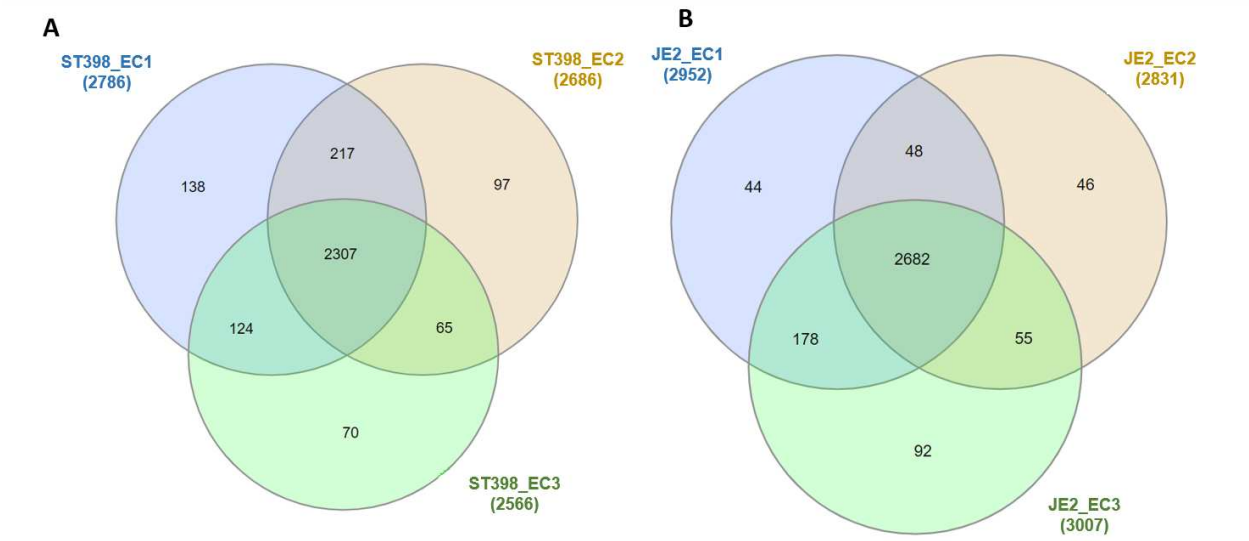

Figure S1. *The Venn diagram shows the number of total shared and unique proteins in three different ECs in ST398 (**A**) and JE2 (**B**).*

ST 1. *DEPs increasing in EC2 shared in ST398 and JE2.*

Gene name	Description	AbundancelogAR in JE2	Abundance logAR in ST398
arcA	Arginine deiminase	6.64	4.66
arcR	HTH-type transcriptional regulator	2.57	6.64
argF	Ornithine carbamoyltransferase	2.29	3.46
chdC	Coproheme decarboxylase	6.64	6.64
dnaK	Chaperone protein	6.64	3.54
dnaX	DNA polymerase III subunit gamma/tau	6.64	6.64
ftsZ	Cell division protein FtsZ	6.64	6.64
G0Y31_12115	Beta-channel forming cytolysin	2.68	6.64
katA	Catase	6.64	6.64
gltB_2	Glutamate synthase	6.64	6.64
gltS	Soldium/glutamate simporter	6.64	4.17
harA	Iron-regulated surface determinant protein H	2.39	2.99
iscR_1	Iron-sulfur cluster regulator IscR	6.64	6.64
ligA	DNA ligase	6.64	6.64

Gene name	Description	AbundancelogAR in JE2	Abundance logAR in ST398
lukF-PV	Panton-Valentine leukocidin F	2.23	3.03
M013TW_0192	Lysostaphin	6.64	6.64
metG	Methionine--tRNA ligase	6.64	6.64
proC	Pyrroline-5-carboxylate reductase	6.64	6.64
proS	Proline--tRNA ligase	2.89	6.64
rep	Replication protein Rep	6.64	4.48
chdC	Coproheme decarboxylase	6.64	6.64
SAI7S6_1001930	Similar to xylitol dehydrogenase	4.22	6.64
SATG_00573	Uncharacterized protein	6.64	6.64
ureC	Urease subunit alpha	4.09	1.73
ydhF	Aldo/keto reductase family protein	6.64	6.64

ST 2. *DEPs increasing in EC3 shared in ST398 and JE2.*

Gene name	Description	Abundance logAR in JE2	Abundance logAR in ST398
betA	Choline dehydrogenase	6.64	6.64
chdC	Coproheme decarboxylase	6.64	6.64
mdtH	MFS transporter	6.64	6.64
dnaK	Chaperone protein	6.64	6.64
fda	Fructose-bisphosphate aldolase, involved in glycolysis.	2.83	4.18
G0Y40_03125	Amidase domain-containing protein	4.45	6.64
G6Y24_14705	FAD-dependent oxidoreductase (Fragment)	3.77	6.64
gpmA	2,3-bisphosphoglycerate-dependent phosphoglycerate mutase	4.32	4.59
groEL	Chaperonin GroEL	6.64	6.64
infB	Translation initiation factor IF-2	6.64	5
SAOUHSC_01907	Aldo/keto reductase	6.64	6.64
katA	Catalase	2.53	6.64
kdpC	K+-transporting ATPase, C subunit.	6.64	6.64
parC	DNA topoisomerase 4 subunit A	6.64	6.64

Gene name	Description	Abundance logAR in JE2	Abundance logAR in ST398
polX	DNA polymerase beta	6.64	6.64
rplW	50S ribosomal protein L23	6.36	6.64
rpoB	DNA-directed RNA polymerase subunit beta	6.64	6.64
tuf	Elongation factor Tu	6.64	6.64
ST398NM01_1406	Acylphosphatase	3.03	3.69
asd	Aspartate-semialdehyde dehydrogenase	3.85	6.64

ST 3. *DEPs decreasing in EC2 shared in ST398 and JE2.*

Gene name	Description	Abundance logAR in JE2	Abundance logAR inST398
V070_00321	Uncharacterized protein	-6.64	-6.64
ST398NM01_2174	Putative cytosolic protein	-6.64	-6.64
HMPREF0776_2045	Uncharacterized protein	-6.64	-6.64
mnhF	Na(+)/H(+) antiporter subunit F1	-6.64	-6.64
SACOL0289	Uncharacterized protein	-6.64	-6.64
rplT	50S ribosomal protein L20	-6.64	-6.64
thrS	Threonine--tRNA ligase	-6.64	-6.64
BSZ10_09265	Methyltransferase	-6.64	-6.64
tpiA	Triosephosphate isomerase	-6.64	-3.57
C7P97_13505	DUF1541 domain-containing protein	-6.64	-6.64
guaB_5	Inosine-5-monophosphate dehydrogenase	-6.64	-6.64
G0X69_01540	DUF910 family protein	-6.64	-6.64
purE	N5-carboxyaminoimidazole ribonucleotide mutase	-6.64	-6.64
SATG_02286	DUF2529 domain-containing protein	-6.64	-3.21
SCAG_02492	HTH hxlR-type domain-containing protein	-6.64	-6.64
KMZ21_05445	Pseudouridine synthase	-6.64	-2.67
nasF	Uroporphyrinogen-III C-methyltransferase	-4.22	-6.64
paiA	N-acetyltransferase domain-containing protein	-3.87	-6.64
purS	phosphoribosyl formyl glycinamidine synthase subunit	-6.64	-6.64
rlmN	Probable dual-specificity RNA methyltransferase RlmN	-2.35	-1.78
purH	bifunctional purine biosynthesis protein	-5.04	-6.64
ST398NM01_0423	Ribosomal-protein-serine acetyltransferase	-6.64	-6.64
dnaK	Chaperone protein DnaK (Fragment)	-6.64	-6.64
SAMEA70245418_02317	MTH538 TIR-like domain (DUF1863)	-6.64	-6.64
purD	Phosphoribosylamine--glycine ligase	-6.64	-6.64
BN1321_270024	DUF4352 domain-containing protein	-6.64	-2.11
BSZ10_03410	Oligoendopeptidase F	-6.64	-6.64
gyrA	DNA gyrase subunit A	-6.64	-6.64
clfB	Clumping factor B (Fragment)	-6.64	-3.53

Gene name	Description	Abundance logAR in JE2	Abundance logAR inST398
rep	Rep protein	-6.64	-6.64
E25	Dihydrolipoamide dehydrogenase E2 subunit	-6.64	-6.64
pta	Phosphate acetyl transferase (Fragment)	-6.64	-6.64
sodA	Superoxide dismutase	-6.64	-6.64
spa	Immunoglobulin G binding protein A	-3.99	-3.59
nirD	Nitrite reductase small subunit	-2.94	-1.5
Psma5	Proteasome subunit alpha type-5	-2.92	-6.64
rpsA	30S ribosomal protein S1	-2.54	-6.64
tuf	Elongation factor Tu (Fragment)	-6.64	-6.64
prfC	Peptide chain release factor 3	-6.64	-6.64
nuoF	NADH dehydrogenase I, F subunit	-6.64	-2.85
rpsJ	30S ribosomal protein S10	-6.64	-6.64
ileS	Isoleucine--tRNA ligase	-6.64	-2.28
CSC87_18215	AA_TRNA_LIGASE_II_ALA domain-containing protein	-6.64	-6.64
pyk	Pyruvate kinase	-6.64	-6.64
tkt_3	Transketolase	-6.64	-2.54
argS	Arginine--tRNA ligase	-6.64	-4.09
kdpE	DNA-binding response regulator	-6.64	-6.64
M013TW_0722	Siderophore ABC transporter substrate-binding protein	-6.64	-2.78
E4U00_09490	3-hydroxy-3-methylglutaryl coenzyme A reductase	-6.64	-2.7
cysK	Cysteine synthase	-6.64	-6.64
gpmI	2,3-bisphosphoglycerate-independent phosphoglycerate mutase	-6.64	-6.64
KRH48_13600	Uncharacterized protein	-6.64	-6.64
csd	Probable cysteine desulfurase	-6.64	-2.26
gap	Glyceraldehyde-3-phosphate dehydrogenase	-6.64	-3.16
KQU62_03965	DUF420 domain-containing protein	-4.63	-6.64
CV021_07320	FAA hydrolase family protein	-4.38	-3.92
ST398NM01_1435	Multidrug resistance protein B	-2.92	-3.14

ST 4. *DEPs decreasing in EC3 shared in ST398 and JE2.*

Gene name	Description	Abundance logAR in JE2	Abundance logAR in ST398
purD	Phosphoribosyl amine--glycine ligase	-6.64	-6.64
BN1321_270024	DUF4352 domain-containing protein	-6.64	-2.61
BSZ10_03410	Oligoendopeptidase F	-6.64	-6.64
gyrA	DNA gyrase subunit A	-6.64	-6.64
clfB	Clumping factor B	-6.64	-3.49
rep	rep	-6.64	-6.64
E25	Dihydrolipoamide dehydrogenase E2 subunit	-6.64	-6.64
pta	Phosphate acetyltransferase	-6.64	-3.91
sodA	Superoxide dismutase	-6.64	-6.64

Gene name	Description	Abundance logAR in JE2	Abundance logAR in ST398
spa	Immunoglobulin G binding protein A	-6.64	-6.2
nirD	Nitrite reductase small subunit	-3.54	-2.02
Psma5	Proteasome subunit alpha type-5	-3.31	-6.64
rpsA	30S ribosomal protein S1	-2.02	-6.64
NCTC10702_00545	Acid phosphatase	-6.64	-6.64
TMSFP482_01390	Amidohydrolase	-6.64	-6.64
GO782_16045	CHAP domain-containing protein	-6.64	-6.64
C7P97_05670	Cna B-type domain-containing protein	-6.64	-6.64
SDAG_01495	dUTPase	-6.64	-6.64
A6762_04230	Uncharacterized protein	-6.64	-3.25
SAXG_00611	HTH-type transcriptional regulator sarS	-2.3	-2.66
A6762_03215	AraC family transcriptional regulator	-6.64	-2.56
groES_2	Heat shock protein 60 family co-chaperone GroES	-6.64	-6.64
SAGV69_02059	Serine-aspartate repeat-containing protein E	-6.64	-6.64
KXJ66_04195	Uncharacterized protein	-6.64	-1.92
BSZ10_04415	VWFA domain-containing protein	-6.64	-6.64
G0Y58_03690	XkdX family protein	-6.64	-6.64
A6762_04255	YozE_SAM_like domain-containing protein	-6.64	-6.64
tpi	Triosephosphate isomerase (Fragment)	-4.58	-6.64
dltC	D-alanyl carrier protein	-3.83	-6.64
SAEG_02002	Acetyl-CoA carboxylase biotin carboxyl carrier protein subunit	-2.81	-6.64
SAKOR_01003	Uncharacterized protein	-2.36	-6.64
esaC_3	DUF4176 domain-containing protein	-2.26	-2.03
NCTC6133_01109	Peptidyl-prolyl cis-trans isomerase	-6.64	-6.64
rpoB	DNA-directed RNA polymerase	-6.64	-6.64
CSC87_16340	ABC transporter ATP-binding protein (Fragment)	-6.64	-6.64
sbi	Immunoglobulin-binding protein	-6.64	-4.91
scpB	Segregation and condensation protein B	-2.46	-6.64
lipM	Octanoyltransferase	-6.64	-6.64
SAZG_01902	NreA	-6.64	-6.64
BN1321_170040	DoxX	-6.64	-3.58
groEL	Chaperonin GroEL	-6.64	-6.64

Chapter 3: Exploring S. aureus Proteome During Skin Infection: Comparative Analysis of In Vivo and In Vitro Infection Models

Dina Nahhas[1,2*], Salvatore Pisanu[1], Priscila R. Guerra[3], John E. Olsen[3], Sergio Uzzau[2], Daniela Pagnozzi[1]

[1]Porto Conte Ricerche S.r.l, Tramariglio, Alghero (SS), Italy.
[2]Department of Biomedical Sciences, Università degli Studi di Sassari, Sassari, Italy.
[3]Department of Veterinary and Animal Sciences, University of Copenhagen, Copenhagen, Denmark.
nahhas@portocontericerche.it

Abstract

Methicillin-resistant *Staphylococcus aureus* (MRSA) is a significant pathogen in skin infections, known for its resistance and adaptability. In this study, we aimed to deepen our understanding of MRSA by investigating its proteomic profile. This exploration can potentially elucidate the mechanisms of virulence and adaptation, thereby offering new evidence and targets for novel treatments. To achieve this, we compared the proteomic profiles of two MRSA strains, JE2 and ST398, in an *in vivo* mouse model of human skin infection and an *in vitro* 3D skin model of human infection. We focused on exploring the dynamics and metabolic changes during the infection process.

MRSA strains were cultured and infected in tissues at 10^7 CFU/mL concentrations for the *in vivo* model and 10^8 CFU/mL for the *in vitro* model. The *in vivo* model involved BALB/c mice, while the *in vitro* model used a commercially available 3D skin model composed of human fibroblasts and keratinocytes. Proteins from infected tissues were extracted and analyzed using two proteomic approaches: an isobaric labeling strategy, tandem mass tag (TMT), for the *in vivo* infection model, and label-free quantification (LFQ) for the *in vitro* infection model. The proteomic analysis aimed to identify bacterial proteins and evaluate their expression variations linked to the infection model.

The comprehensive proteomic analysis revealed a complex MRSA proteomic profile, shedding new light on this pathogen's behavior. We observed an increase in proteins associated with the arginine biosynthesis pathway, underlining its essential role in MRSA survival and adaptation in both skin infection models. The betaine biosynthesis pathway also showed an increased activity, a significant finding due to its involvement in osmotic stress management across both models. Moreover, we identified numerous virulence proteins, including acid phosphatase (SapS), autolysin (Atl), leucocidin subunits (HlgA, HlgB), MAP protein, Immunoglobulin G-binding protein A (Spa), and ATP-dependent molecular chaperones (ClpB and ClpC). We also observed strain-specific responses, with certain proteins exclusively present in either the JE2 or ST398 strains, reflecting their specific adaptation strategies.

By elucidating the proteomic differences and adaptations of MRSA in skin infection models, this study contributes to providing evidence and knowledge that could be useful for the comprehension of MRSA infections and for the evaluation of new therapeutic approaches.

Keywords: Skin infection, MRSA, shotgun proteomics, *in vivo* model, 3D skin model.

1. Introduction

Staphylococcus aureus (*S. aureus*) is a ubiquitous, Gram-positive bacterium that colonizes the skin, nose, and mucous membranes of healthy individuals. It is a common pathogen isolated from skin and soft tissue infections (SSTI) and is associated with a wide range of diseases, including pneumonia, endocarditis, and bacteremia (Tong et al., 2015c). The emergence of methicillin-resistant *Staphylococcus aureus* (MRSA) strains has complicated treatment options, making it crucial to understand the complex dynamics of MRSA infections, including bacterial adaptations and host immune responses (Ali Alghamdi et al., 2023).

S. aureus can survive in environments with limited oxygen, iron, and nutrients, managing infection-induced stresses through high metabolic flexibility and different pathways (Minh Giao Bui, 2015). One form of bacterial adaptation to skin infection is adaptation to low pH. The skin is characterized by an acidic pH (4.1 - 5.8) due to the thin outer layer known as the 'acid mantle' (Ehrhardt Proksch, 2018), prompts *S. aureus* to adjust its metabolic pathways, such as purine biosynthesis and ammonia production, to adapt to this condition (Costa and Horswill, 2022). Additionally, SA accumulates fumarate hydratase (FumC) during skin infection (Wong Fok Lung and Prince, 2020).

Proteomics offers a powerful tool for exploring the molecular mechanisms underlying bacterial infections. A previous study characterizing the spatial proteome at the host-pathogen interface during *S. aureus* abscess formation identified 32 *S. aureus* proteins specifically associated with this condition, illustrating the potential of this approach (Guiberson et al., 2020). By employing mass spectrometry, researchers have begun to elucidate the proteome of *S. aureus*, identifying potential biomarkers of virulence and

targets for intervention strategies (Bruderer et al., 2017),(Zubarev and Makarov, 2013). However, the specific proteomic profiles of MRSA during skin infections remain underexplored.

In this study, we addressed this knowledge- by characterizing the proteome profiles of two MRSA strains: JE2, a community-associated strain prevalent in various human infections, and ST398, a livestock-associated strain that is also reported to cause skin infections in both humans and animals (Kennedy et al., 2008),(Guardabassi et al., 2009),(Bouiller et al., 2020). Using both an *in vivo* mouse infection and an *in vitro* 3D skin model, we compared the protein expression profiles of these strains during skin infection to elucidate their distinct virulence mechanisms and adaptation strategies. These models provide diverse insights into bacterial adaptation to skin infections, offering a comprehensive view of how MRSA interacts with host tissues. Our ultimate objective was to identify potential antimicrobial targets through proteomic analysis, paving the way for the development of targeted therapies to manage resistant bacterial infections.

2. Materials and Methods

2.1. Bacterial strains and culture

MRSA strains, ST398 (van Rijen et al., 2008), and JE2 (Fey et al., 2013b), were obtained from the Department of Veterinary and Animal Sciences at the University of Copenhagen, Denmark. Two to three colonies of each strain were inoculated into 7 mL of Tryptic Soy Broth (TSB) and incubated overnight with shaking at 125 rpm at 37°C. The following day, the bacteria were subcultured at a 1:66 ratio in a fresh TSB medium and grown to a mid-exponential phase, achieving an optical density at 600 nm (OD_{600} of 0.5-0.6). The cultures were then harvested by centrifugation at 12,000 rpm for 12 minutes at 4°C, followed by washing with cold PBS (phosphate buffer saline) to remove any residual medium and collecting the pellet. The bacterial suspension was adjusted with the desired volume of PBS based on CFU counting performed after serial dilutions to achieve concentrations of $1x10^7$ CFU/mL for the *in vivo* mice infection and $1x10^8$ CFU/mL for the *in vitro* skin infection model.

2.2. *In vivo mice model for human wound infection and bacterial clearance*

Mice infection experiments were conducted at the Faculty of Health Sciences at the University of Copenhagen in respect of the principles of the European Convention for the Protection of Vertebrate Animals guidelines (Council of Europe, ETS no. 123) and after obtaining a license from the Danish Animal Experimental Board (license number 2021-15-0201-00988). Thirty-six female BALB/c mice, aged 5 to 7 weeks, were divided into six groups (G) of six mice each as follows: G1 and G2 served as control groups, receiving sterile PBS and were sacrificed at 2- and 4- days post-infection (dpi), respectively. G3 and G4 were infected with the ST398 strain and sacrificed at 2 dpi and 4 dpi, respectively,

while G5 and G6 were infected with the JE2 strain and sacrificed at 2 dpi and 4 dpi, respectively. Before the experiment, mice were acclimatized for one week at ambient temperature and received a libitum standard rodent diet. The procedure was performed under anesthesia with 4% v/v isoflurane (Attane Vet, Denmark). The dorsal area of each mouse was shaved using electric clippers and disinfected with a gauze pad soaked in alcohol (Harslund et al., 2013). Once the area was dry, a 2 mm diameter wound was created using a Ø 7 mm dermal curette purchased from Stetoskop (Copenhagen, Denmark). The wounds were subsequently infected with the previously prepared $1x10^7$ CFU/mL of MRSA. Immediately after infection, 0.1 mg/kg buprenorphine was administered subcutaneously for analgesia. Post-infection, mice were monitored every 8 hours for lesion development using a lesion scoring system, and body weight was recorded to assess infection progression. At the designated endpoints, mice were sacrificed according to their assigned groups. The infected skin areas and underlying tissues were excised using sterile scissors and forceps. Tissue samples were homogenized in 1 mL PBS using a TissueLyser LT mechanical homogenizer (Qiagen, Hilden, Germany) with bead beating for three minutes to ensure bacterial liberation from the tissues (this step has served only for bacterial count). Bacterial counts were determined after serial dilutions in PBS-solutions which were plated overnight at 37 °C on Baird Parker agar supplemented with Rabbit Plasma Fibrinogen (RPF), which selectively promotes *Staphylococcus* growth. The remaining tissue samples were stored at -80°C for further analysis. The workflow is shown in **Figure 10.**

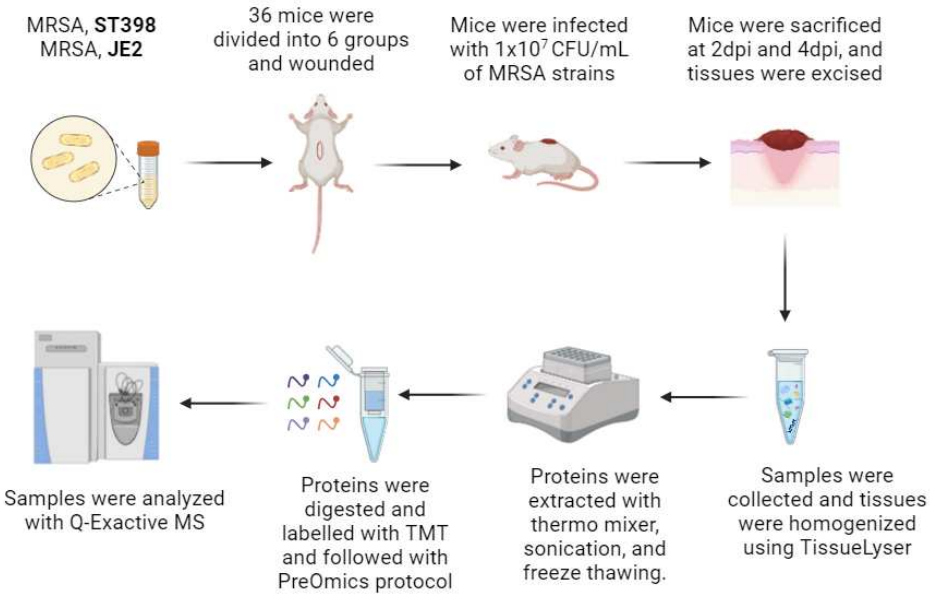

Figure 10. *Workflow of the in vivo infection experiments (https://www.biorender.com).*

2.3. Protein extraction

Protein extraction was done following an in-house method (Tanca et al., 2014) with some modifications. First, to separate bacterial proteins from mouse proteins, lysed samples were centrifuged at 18,000 x *g* for 15 min to segregate tissue and bacteria. This process resulted in a distinct pellet at the bottom, while PBS and lipids remnants from the tissues floated at the top. We removed the supernatant and proceeded with the formed pellet. The isolated pellet was suspended in a solution of 2% sodium dodecyl sulfate (SDS) with 10 mM dithiothreitol (DTT). Following this, the samples were frozen before the mechanical extraction of proteins using the TissueLyser. This cycle of freezing (-80 °C) and mechanical extraction was repeated three times to ensure thorough protein extraction (ten minutes each time). The proteins were then processed with TMT labeling as described below.

2.4. TMT10plex labeling for protein quantification

To change the buffer, it was necessary to carry out a precipitation step of the proteins as recommended by the manufacturer. Therefore, we added six volumes of pre-chilled (-20°C) acetone to the samples and left them overnight. The following day, we centrifuged the mixture at 8000 x g for 10 minutes at 4°C and discarded the acetone. Before proceeding with the labeling step, protein quantification of the samples was done using a BCA protein assay (Thermo Fisher Scientific). We then proceeded with 100 µg of proteins.

Next, we prepared the samples in accordance with the Tandem Mass Tags TMT10plex™ protocol (Thermo Fisher Scientific), and for the protein digestion, peptide labeling, and cleaning steps we used the PreOmics iST – NHS columns. We resuspended 100 µg of proteins in 100 µL of Tetraethylammonium bromide (TEAB) and performed trypsin digestion overnight at 37°C. Peptide labeling was achieved by adding 41 µL of TMT labeling reagents to the samples as follows: TMT-126 was added to equal portions of a bacterial culture grown in TSB *in vitro,* tissue samples from 2 dpi, and tissue samples from 4dpi. Samples from the bacterial culture *in vitro* were added to increase the probability of detecting bacterial proteins from the *in vivo* samples as recommended (Andersen et al., 2022). TMT-128C, TMT-129N, and TMT-129C tags were added to samples from 2 dpi (n=3), and TMT-130N, TMT-130C, and TMT-131C were added to samples from 4 dpi (n=3), for a total of 7-plex.

After incubation, we quenched the reaction by adding 8 µL of 5% hydroxylamine provided by the manufacturer. Following a recommendation by the PreOmics manufacturer, we added an extra step: the addition of 100 µL of their stop buffer. We then proceeded with

the purification step as advised by PreOmics. Afterward, we dried the samples using an Eppendorf Concentrator Plus (Hamburg, Germany). Samples were then suspended with formic acid, and peptide quantification was done using the Pierce Quantitative Colorimetric Peptide Assay (Thermo Fisher Scientific). Finally, we combined an equal amount of our 7 samples for each strain and analyzed them in MS.

2.5. *In vitro* 3D skin infection model

We used a commercially available skin model, EpiDerm Full Thickness (EpiDERM-FT™), a dermal-epidermal skin model with a fully developed basement membrane produced by MatTek Life Science (Bratislava, Slovakia). This model is metabolically active and reported to be fully representative of human skin composed of human fibroblasts and keratinocytes, mimicking the full thickness of human skin (Kim et al., 2011). Upon arrival, following the manufacturer's guidelines, the skin equivalents were immediately placed in six-well plates supplied with 2.5 mL of the culture medium (EFT-400 media provided by the manufacturer), followed by a 24-hour incubation at 37°C in an incubator set to 5% CO2 and the required relative humidity.

The next day we removed the media and replaced it with fresh media. Then, we inoculated the skin tissues with 10^8 CFU/mL MRSA strains (JE2 and ST398), conducting six replicates for each strain and six replicates of control (tissues inoculated with sterile PBS). The experiment was carried out for 48 hours. Afterward, the infected tissues were washed with the provided sterile PBS, and the washing liquid was collected and used to perform serial dilutions to check for bacterial counts on tryptic soy agar plates (TSA). The tissues underneath were harvested and subsequently homogenized in 1mL of PBS using

TissueLyser to carry out the bacterial counts. All samples were conserved at -80 °C for later use.

2.6. Protein extraction and quantification from 3D skin model

Protein extraction was performed following the in-house method described above in paragraph **2.3**. Subsequently, protein extracts were quantified with the Pierce BCA protein assay (Thermo Fisher Scientific). We proceeded with tryptic digestion of 100 µg of proteins using the S-Trap micro column (ProtiFi). We followed the instructions provided by the manufacturer with some adjustments. Specifically, the lysis buffer added was carefully controlled to ensure that the SDS concentration did not exceed the recommended levels. Then, samples were sonicated for 15 minutes, followed by protein denaturation, reduction, and alkylation steps. The proteins were then captured using S-Trap microcolumns with a binding/washing buffer and centrifugation at 4,000 x g for 30 seconds. This was succeeded by a series of three sequential washing steps to ensure thorough cleaning of the proteins. Subsequently, the proteins were incubated and digested with trypsin overnight at 37°C. Peptides were then eluted and collected using a collection buffer (20% acetonitrile and 1% formic acid), then they were dried using an Eppendorf Concentrator Plus (Hamburg, Germany). Finally, samples were dissolved in formic acid, and quantification was conducted using the Pierce Quantitative Colorimetric Peptide Assay (Thermo Fisher Scientific). We used a label-free quantification approach for these samples (LFQ).

2.7. Shotgun proteomics and statistical analysis

Peptide samples were prepared and analyzed using a Q-Exactive mass spectrometer coupled with an UltiMate 3000 RSLCnano system (Thermo Scientific, San Jose, CA, USA). Specifically, 4 µg of peptide mixtures per sample were first concentrated and desalted using a trap-column (Acclaim PepMap C18, 75 µm × 2 cm nanoViper, 3 µm, 100 Å, Thermo Fisher Scientific). These peptides were then separated on a C18 reversed-phase column (Acclaim PepMap RSLC C18, 75 µm × 50 cm nanoViper, 2 µm, 100 Å, Thermo Scientific) employing a 245-minute linear gradient from 5 to 37.5% solvent B (0.1% formic acid in 80% acetonitrile) in solvent A (0.1% formic acid) (Addis et al., 2022). Fragmentation spectra were acquired through Higher Energy Collisional Dissociation (HCD) using nitrogen as the collision gas. The raw data were analyzed using the Proteome Discoverer software (version 2.4, Thermo Scientific) with SEQUEST-HT as the search engine. Protein identification was based on the *Staphylococcus aureus* 1280 reference database from UniProt (release 2023_03), encompassing 108,516 protein entries.

The search parameters included a precursor mass tolerance of 10 ppm, an MS/MS tolerance of 0.02 Da, and allowed charge states of +2, +3, and +4. Trypsin or Trypsin/LysC was specified as the protease with up to two missed cleavages. Static modification was set to cysteine carbamidomethylation, while dynamic modifications included methionine oxidation, N-terminal acetylation, methionine loss, and combined methionine loss with acetylation. The false discovery rate (FDR) was kept below 1% using the Percolator algorithm for peptide validation and protein significance. Differential protein expression was assessed through a consensus workflow in Proteome Discoverer 2.4,

with experiments organized into two conditions of three samples each. Label-free quantification was based on precursor ion abundance, using peak area, and significance was determined via a t-test with Benjamini-Hochberg correction for multiple testing adjustments. Proteins were considered significantly differentially expressed with a log2-transformed abundance ratio (LogAR) of ≤−1.5 or ≥+1.5 and an adjusted p-value of ≤0.05 (Shah et al., 2019).

In the *in vitro* experiment, precursor abundance was based on intensity, normalization was based on all peptides and we used Minora as a processing node. In the TMT labeling experiment, these values were critical for the accurate identification and quantification of peptides labeled with different TMT tags across samples. We employed a workflow optimized for reporter ion-based quantification. The analysis focused on unique and razor peptides, with trypsin/LysC for complete digestion. We did some modifications in the processing step; in both the dynamic and static modifications, we added two steps: 1- Cysteine modification / +113.084 Da (C) 2- TMT6plex / +229.163 Da (K). Reporter ion intensity was performed with 20 ppm tolerance, and the most confident centroid was set as the integration method. Protein abundances were calculated as the summation of associated peptide group abundances. Quantification of peptide groups was based on their uniqueness (unique peptides) and following the principle of parsimony (razor peptides). No imputation of missing values was performed. In addition to, the evaluation of TMT labeling efficiency, TMT6plex modification was set as variable modification (peptide N-terminus, K residues).

To annotate the differentially expressed proteins with KEGG KO (orthology) information, and to know the cluster orthologous groups of the proteins (COG) we employed eggNOG-

mapper 2.1.12 (Cantalapiedra et al., 2021). Then, we mapped the proteins to KEGG pathways using the online tool (https://www.genome.jp/kegg/ko.html) (Kanehisa et al., 2016). Pathway comparison was done the Meta4P bioinformatics tool (Porcheddu et al., 2022), using normalized protein abundances as input. Meta4P bioinformatics tool has helped with aggregating the protein abundance data based on their KEGG pathway annotation, estimating the total abundance of each KEGG pathway per sample. The significance of differences in pathway abundance between the studied conditions was assessed using a t-test (performed via Microsoft Excel™) and adjusting the p-value by Benjamini-Hochberg correction using the False Discovery Calculator contained in Tools (https://tools.carbocation.com/about).

Graphs were created using GraphPad 8.3.0, and Venn diagrams were created using interactivenn tool (Interactive Venn Diagrams, https://www.interactivenn.net/) (Heberle et al., 2015).

3. Results

3.1. Mice infection model

3.1.2. Infection observation and development

Before the infection, the body weight of mice was on average 19.51±1.04 g per mouse. On day 2 of the experimental infection, the control group (G1) dropped by 0.5 to reach an average of 19.2±1.57 g, while G2 gained weight to reach an average of 19.2±0.90 g. G3 lost 0.4 g per mouse to reach an average of 19.16±1.37 g, while G4 almost remained the same with an average of 19.51±1.11 per mouse, and groups 5 and 6 gained 0.3 g reaching an average of 20±1.07 and 19.5±0.93 g at 48h, respectively. On day 4, the control group (G2) continued to gain weight to reach an average of 20.01±1.07 g and 19.58±0.93 g per mouse, respectively, whereas groups 4 and 6 experienced body loss at 4dpi compared to 2dpi to reach an average of 19.28±1.24 g and 19.16±0.88 g per mouse (**Figure 11).** However, weight change was never significant between the groups during infection time. After 24h, no lesions and slight redness were observed in the control groups (G1 and G2), and slight lesions to no lesions were present in mice of G3 and G4 (mice infected with ST398). Intermediate red lesions and a slight increase in the infected area were noticed in mice of G5 and G6 (mice infected with JE2 strain) with no pus seen at the infection site.

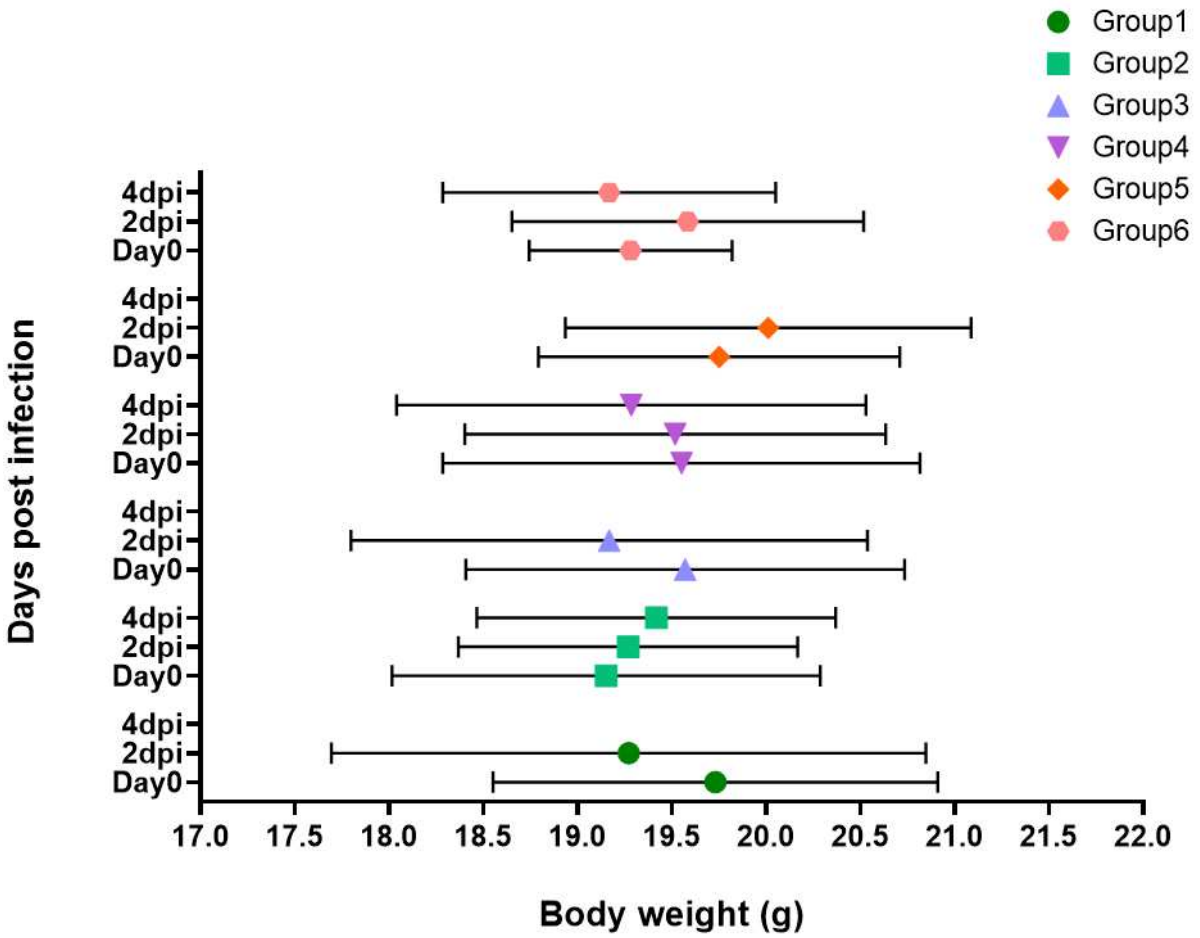

Figure 11. *Mean body weight of mice with standard deviation during the infection period. Each dot represents the average body weight, calculated from six biological replicates per group, expressed in grams (g) on days 0, 2, and 4.*

3.1.3. Bacterial clearance

Before analyzing the bacterial protein profiles, we first evaluated bacterial counts after the *in vivo* experiment, as depicted in **Figure 12A.** G1 and G2 (control groups) exhibited no bacterial growth, indicating no contamination or development of infection. In contrast, G3 and G4, infected with the ST398 strain, displayed $1x10^4$ CFU/mL and $2x10^3$ CFU/mL bacterial counts at 2 dpi and 4 dpi, respectively. Counts were below the detection level in one mouse per group. This was a significant decrease in the bacterial count for both groups compared to the initial bacterial load ($1x10^7$ CFU/mL) with a p-value of 3.4×10^{-24}

and a p-value of 1.8×10^{-34} for G3 and G4, respectively. Groups G5 and G6, infected with the JE2 strain, showed $8x10^6$ CFU/mL and $5x10^5$ CFU/mL bacterial counts at 2 dpi and 4 dpi, respectively. The drop in the bacterial count for G6 was significant with a p-value of 1.9×10^{-11}, while G5 was not significant compared to the significant decrease in G6 (p-value of 0.7).

Figure 12B. illustrates the bacterial count after the *in vitro* experiment. After 2 days of experimental infection, the control group inoculated with PBS showed no bacterial count, whereas groups infected with the ST398 and JE2 strains displayed bacterial counts of $1.2x10^9$ and $2.68x10^9$ CFU/mL, respectively. Both demonstrated a significant increase in the bacterial count by the end of the experiment (p-value of 3.54×10^{-4} for ST398 and 8.5×10^{-3} JE2).

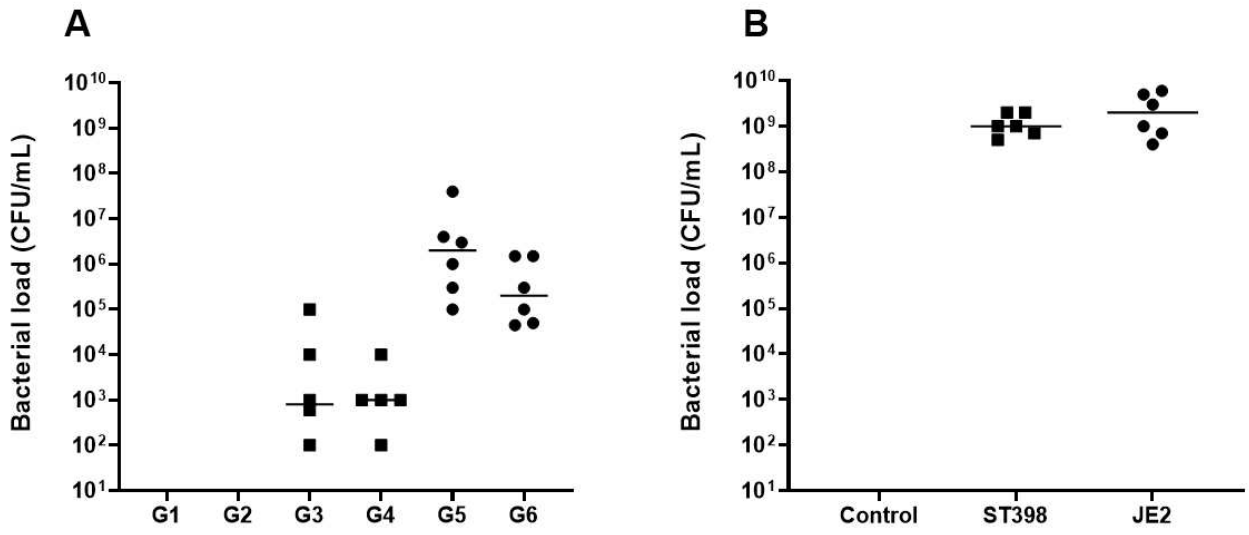

Figure 12. *Bacterial counts at the termination of experiments at day 2 (G1, G3, and G5) and day 4 (G2, G4, G6) from the in vivo infection model* ***(A)*** *and the in vitro infection model* ***(B).*** *The scatter plots display bacterial counts for each tissue and the vertical line indicates the mean CFU value.*

3.1.4. Protein expression and identification

The development in bacterial proteome during *in vivo* infection with ST398 and JE2 strains was monitored using TMT-based quantitative proteomics. A total of 307,847 (ST398) and 306,219 (JE2) spectra were obtained, of which 307,235 and 305,756 matched known spectra. Among these spectra, 341 and 938 bacterial peptides, and 182 and 277 bacterial proteins were identified for ST398 and JE2 strains, respectively. Among the identified proteins, 128 proteins were found to be common in both strains, as shown in **Figure 13A.** and with more details in **Table ST1** (Supplementary Data). The protein that showed the highest abundance in both strains was the glyceraldehyde-3-phosphate dehydrogenase (GapC), a glycolytic enzyme, followed by elongation factor (Tuf). Most of the identified proteins had a higher average normalized abundance in the JE2 strain compared to ST398. However, 9 of the 128 proteins that were shared between the strains showed higher abundances in ST398 compared to JE2, as shown in **Figure 13B**. These proteins were glycine cleavage system H protein (GcvH), DUF1292 domain-containing protein (GF572_08675), L-lactate dehydrogenase (Ldh2), large ribosomal subunit protein bL35 (RpmI), small ribosomal subunit protein bS20 (RpsT), thioredoxin (TrxA), DNA starvation/stationary phase protection protein (Dps), penicillin-binding protein 2a (MecA), and para-aminobenzoate synthetase component I (PabB_2).

In **Figure 13C**. we categorized the overall proteins identified in both strains from 2dpi and 4dpi within clusters of orthologous groups (COGs). Most of the identified proteins in both strains were involved in translation (J), energy production and conversion (C), proteins with unknown function (S), and carbohydrate metabolism and transport (G). However, category DNA processing and modification (A) was only detected in the JE2 strain and it

contained DNA binding protein (SAV0385). Then we looked at the average abundance of normalized proteins with significant differences between 2dpi and 4dpi**.** Only those in common between both strains are shown in **Figures 14A.** and **14B.** The figure shows that MecA, which encodes penicillin-binding protein (PBP), is the one with the highest abundance at 2dpi in both strains, followed by para-aminobenzoate synthetase component I (PabB_2), which is more abundant at day 4 post-infection. Small ribosomal subunit protein bS6 (RpsF) and 50S ribosomal protein L1 (RplA) were more expressed at 4dpi and showed lower abundance with the ST398 strain compared to the JE2 strain. We also have characterized the shared proteins during the infection according to biological functions. We found betaine aldehyde dehydrogenase (BetB) to be in common, besides, JE2 expressed choline dehydrogenase (BetA), both of which make part of glycine betaine biosynthesis (Feng et al., 2022b). Moreover, both strains expressed proteins involved in glycolysis such as glyceraldehyde-3-phosphate dehydrogenase (GapC), phosphoglycerate kinase (Pgk), enolase (Eno), pyruvate kinase (Pyk), 2,3-bisphosphoglycerate-dependent phosphoglycerate mutase (GpmA), and triosephosphate isomerase (TpiA). Alongside this, small and large ribosomal subunit proteins, which are essential for protein biosynthesis, were expressed in both strains. Moreover, proteins that are important for growth in broth and might be involved in biofilm persistence, such as ATP synthase subunit alpha (AtpA) and ATP synthase subunit beta (AtpD) (Bosch et al., 2020a). We also found UDP-N-acetyl muramyl-tripeptide--D-alanyl-D-alanine ligase (murF) which plays a role in cell wall biosynthesis as well (Sobral et al., 2006).

In addition, we found ATP-dependent protease subunits ClpP and ClpC that are associated with both virulence and oxidative stress response (Michel et al., 2006). Proteins involved in oxidative stress such as alkyl hydroperoxide reductase (AhpC) which detoxified low levels of H2O2 (Gaupp et al., 2012), thioredoxin (TrxA), and thioredoxin

reductase (TrxB) which also protect bacteria from oxidative stress. Additionally, manganese transport protein C (MntC), a surface ion scavenging protein (Salazar et al., 2014), was expressed. In addition, superoxide dismutase (SodA) was solely seen in the JE2 strain. We found other proteins that are involved in other processes and could be related to the infection, such as trigger factor (Tig), malate: quinone oxidoreductase (Mqo2), while fumarate hydratase (FumC), and serine-Aspartate Repeat-containing protein C (SdrC) were only seen in ST398 **(Table 5)**.

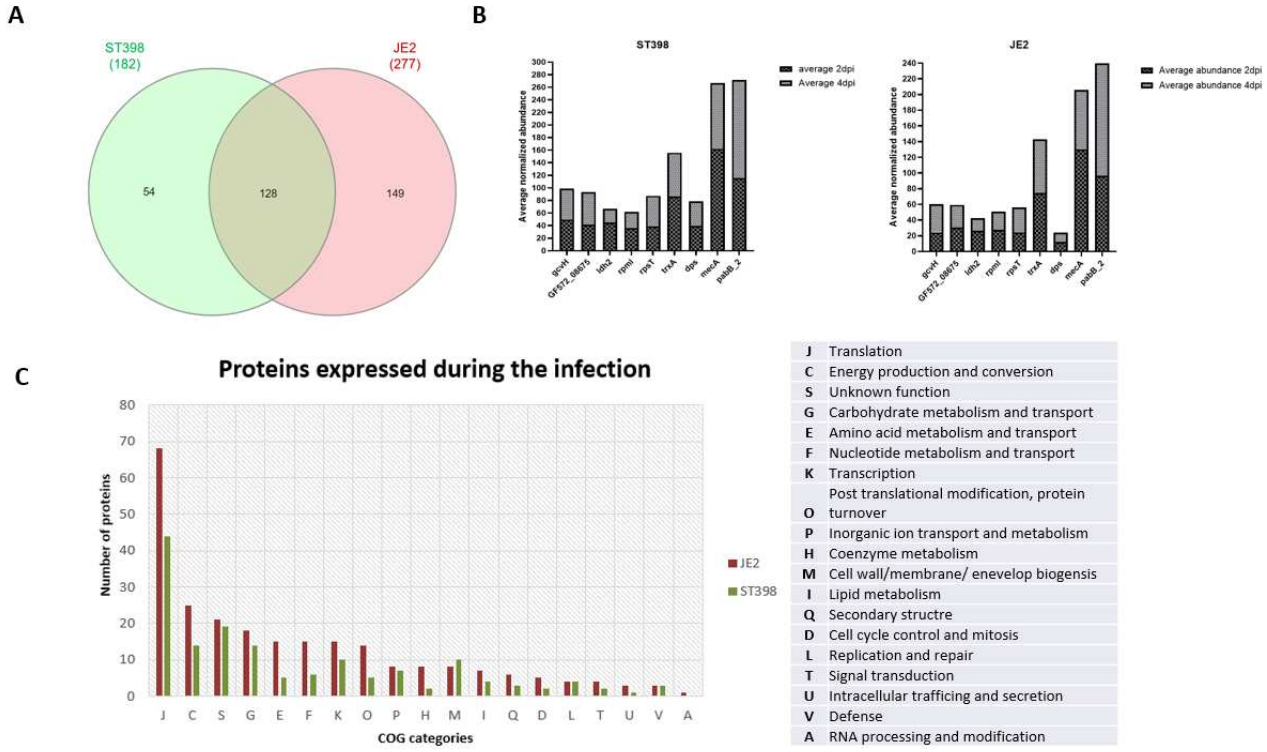

Figure 13. *The number of bacteria proteins shared and not shared between ST398 and JE2 during mice infection of the skin (A). The proteins with average normalized abundance showed higher expression in ST398 than in JE2 (B). Bar graphs showing the number of proteins according to COG categories during in vivo mice infections with ST398 and JE2 (C).*

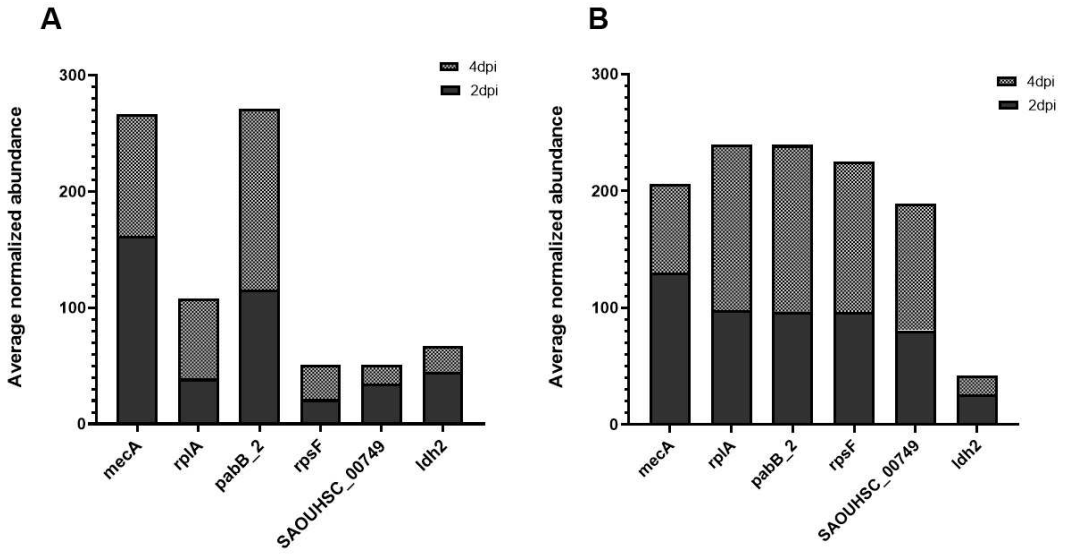

Figure 14. *Bar graphs showing the average normalized abundance of proteins with significant differences between 2dpi and 4dpi and expressed in both ST398 (A) and JE2 (B).*

Table 5. *Proteins detected in ST398 and JE2 strains during skin infection.*

Biological process	Gene name	Protein name	Strains
Glycine betaine biosynthesis	*betB*	**Betaine aldehyde dehydrogenase**	ST398 and JE2
	betA	**Choline dehydrogenase**	JE2
Glycolysis	*gapC*	**Glyceraldehyde-3-phosphate dehydrogenase**	ST398 and JE2
	pgk	**Phosphoglycerate kinase**	ST398 and JE2
	eno	**Enolase**	ST398 and JE2
	pyk	**Pyruvate kinase**	ST398 and JE2
	gpmA	**2,3-bisphosphoglycerate-dependent phosphoglycerate mutase**	ST398 and JE2
	tpiA	**Triosephosphate isomerase**	ST398 and JE2
Growth	*atpA*	**ATP synthase subunit alpha**	ST398 and JE2
	atpD	**ATP synthase subunit beta**	ST398 and JE2
	murF	**UDP-N-acetylmuramoyl-tripeptide--D-alanyl-D-alanine ligase**	ST398 and JE2
Virulence	*clpP*	**ATP-dependent protease subuit clpP**	ST398 and JE2
	clpC	**ATP-dependent protease subuit clpC**	ST398 and JE2
Oxidative stress	*ahpC*	**Alkyl hydroperoxide reductase**	ST398 and JE2
	trxA	**Thioredoxin**	ST398 and JE2
	trxB	**Thioredoxin reductase**	ST398 and JE2

Biological process	Gene name	Protein name	Strains
	mntC	**Manganese transport protein C**	ST398 and JE2
	sodA	**Superoxide dismutase**	JE2
Other processes	*tig*	**Trigger factor**	ST398 and JE2
	mqo2	**Malate:quinone oxidoreductase**	ST398 and JE2
	fumC	**Fumarate hydratase**	ST398
	sdrC	**Serine-Aspartate repeat-containing protein C**	ST398

3.2. *In vitro* skin model

3.2.2. Bacterial responses: Pathway analysis

We identified 2194 bacterial proteins from the *in vitro* model infection with ST398 and 2074 from JE2. Among those proteins, we found 374 and 259 proteins to increase during the infection in ST398 and JE2, respectively.

We clustered all the proteins during infection within cluster orthologous groups (COG) to achieve the prediction of protein sets obtained from the ST398 and JE2 strains (**Figure 15A).** This analysis clustered the proteins into 20 different COG categories for both strains. Although the majority of proteins were functionally included in a specific cluster, a percentage of 19.1% and 18.8% for ST398 and JE2 respectively were included in a common cluster defined as unknown function (S) due to lack of functional annotation. A total of 12 clusters showed a higher number of categorized proteins in JE2 infection than in ST398 infection. These clusters were involved in translation (J), transcription (K), energy production and conversion (C), cell wall envelop biogenesis (M), carbohydrate metabolism and transport (G), nucleotide metabolism and transport (F), replication and repair (L), coenzyme metabolism (H), lipid metabolism (I), signal transduction (T), defense (V), RNA processing and modification (A) and cytoskeleton (Z). In contrast, 7 clusters

were found to have a greater number of proteins expressed during infection with ST398 compared to JE2. The clusters involved were found to be the amino acids metabolism and transport (E), inorganic ion transport and metabolism (P), post-translational modification and protein turnover (O), cell cycle control and mitosis (D), secondary structure (Q), intracellular trafficking and secretion (U), and cell mobility (N).

Then, we aggregated the normalized abundances of these proteins within pathways using data retrieved from the KEGG database. For the ST398 strain, pathways that increased during infection included arginine biosynthesis and pyruvate metabolism. Additionally, there was a significant decrease in the abundance of proteins related to purine metabolism and valine, leucine, and isoleucine metabolism pathways, as shown in **Figure 15B.** Similar trends were observed in the JE2 strain, with an increase in proteins associated with arginine biosynthesis and pyruvate metabolism. However, we also found histidine metabolism (his) pathway to be non-significantly increasing. Conversely, purine metabolism (p-value: 0.0001) showed a decrease in protein abundance (**Figure 15C**).

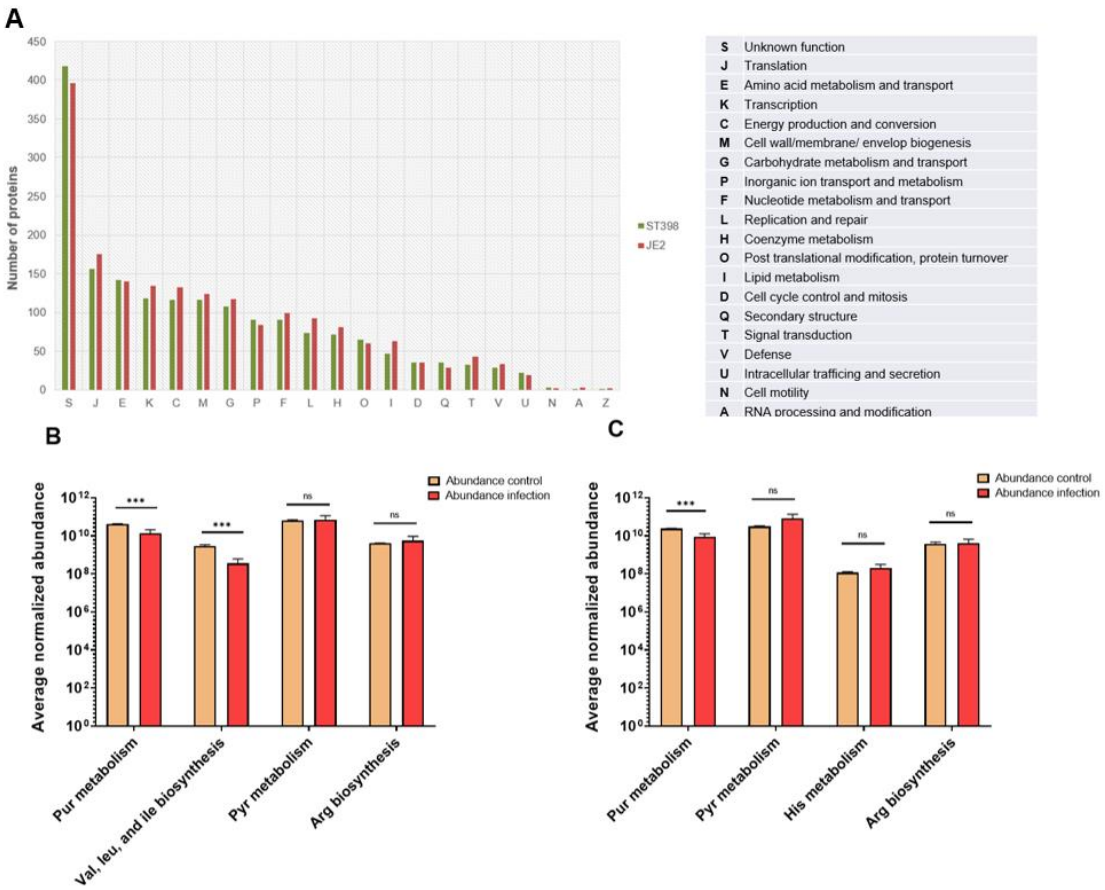

Figure 15. *Column chart showing the total proteins during the infection in ST398 (green) and JE2 (red) clustered into orthologous groups with their description on the right* ***(A).*** *Bar graph showing the total proteins involved in different pathways during skin infection in ST398* ***(B)*** *and JE2 in* ***(C).*** *The significance notation (*** p<0.001 and ns for non-significant). Pur for purine, Val, Leu, Ile for valine, leucine, and isoleucine, His for histidine, and Arg for arginine.*

3.2.3. Bacterial responses – Identification of Differentially Expressed Proteins (DEPs)

We investigated the differential bacterial proteome, which allowed us to identify the DEPs obtained from the experimental infection compared to the bacterial culture *in vitro* (control). DEPs were defined as those with a log2-transformed abundance ratio (LogAR) of ≤−1.5 or ≥+1.5 and an adjusted p-value of ≤0.05. 275 and 199 DEPs were identified in ST398 and JE2 infection, respectively. Of these DEPs, 99 and 98 exhibited increased expression during the infection, respectively, in ST398 and JE2 infection models, while 167 and 101 DEPs had decreased expression. Detailed information on DEPs in ST398

and JE2 are described in Tables ST7 and ST8, respectively (Supplementary Data). As shown in **Figure 16A**, 17 shared DEPs and 82 and 81 unique DEPs were highlighted in the infection with ST398 and JE2 respectively. The normalized abundances of the shared proteins were compared between the two strains by heat map (**Figure 16B**). Shared DEPs exhibited different abundances between the strains, with 10 proteins more abundant in ST398 and 7 proteins in JE2. Some of these identified DEPs were involved in bacterial development and adaptation during the infection, such as leukocidin F subunit (HlgA), leukocidin S subunit (HlgB), ATP-dependent molecular chaperone (ClpB), and autolysin (Atl). In particular, the latter DEPs are responsible for virulence mechanisms (Frees et al., 2004; Staali and Colin, 2021a; Zheng et al., 2022). Other DEPs, like MAP domain-containing protein (MAP), acid phosphatase (SapS), and formate acyltransferase (PflB) are mainly implicated in intracellular survival by inhibiting and modulating host defense mechanisms (Lee et al., 2002; Ahmad-Mansour et al., 2022),(Bertrand et al., 2022). In particular, PflB was the DEP with the highest abundance in both strains. In addition, we also found proteins involved in arginine biosynthesis, such as ornithine carbamoyltransferase (ArgF) and carbamate kinase (ArcC). Apart from shared proteins, 82 and 81 unique proteins were identified in ST398 and JE2, respectively. **Figure 16C** and **Figure 16D** show the sets of DEPs associated with infections from ST398 and JE2, respectively. Among the DEPs identified specifically in ST398, 10 DEPs were implicated in the infectious process **(Figure 16C)**, including three DEPs known to be involved in the virulence process, such as chitinase B (ChiB), coagulase (Coa), and immunoglobulin-binding protein (Sbi). We also found proteins that play a role in host immune evasion and cell protection like thermonuclease (Nuc), staphylococcal complement inhibitor (Scc), anti

holin-like protein (LrgB), ferritin (FtnA), and tagatose-6-phosphate kinase (LacC). Also, we found proteins involved in adherence to host tissues, such as Cna B-type domain-containing protein (Cna) and fibrinogen-binding protein (FnBP). Similarly, among the DEPs found to be unique to strain JE2, 7 DEPs were associated with diverse infection adaptation and virulence mechanisms (**Figure 16D**), including elastin binding protein (EbpS), trigger factor (Tig), LPXTG-anchored heme-scavenging protein (IsdA), EAR protein (Ear), MapN protein (MapN). The other DEPs in this strain were oxygen-dependent choline dehydrogenase (BetA) and clumping factor A (ClfA) involved in host immune evasion, and host adherence, respectively.

Furthermore, the analysis highlighted that 96 and 167 DEPs were decreased during the ST398 and JE2 infection respectively, and 17 of these DEPs were shared between the strains (**Figure 17A**). The decreased DEPs in common between both strains were (UPF0342 protein, acyl carrier protein, nitrogen fixation protein NifU, branched-chain amino acid transport system carrier protein, fibrinogen and keratin-10 binding surface anchored protein, virulence factor, LLM class flavin-dependent oxidoreductase, Na(+)/H(+) antiporter subunit F1, probable inorganic carbon transporter subunit, large ribosomal subunit protein uL3, thioredoxin domain-containing protein, UPF0741 protein, DUF420 domain-containing protein, RND multidrug efflux transporter Acriflavine resistance protein, DUF443 domain-containing protein, triosephosphate isomerase, and urease subunit gamma) (**Figure 17B**).

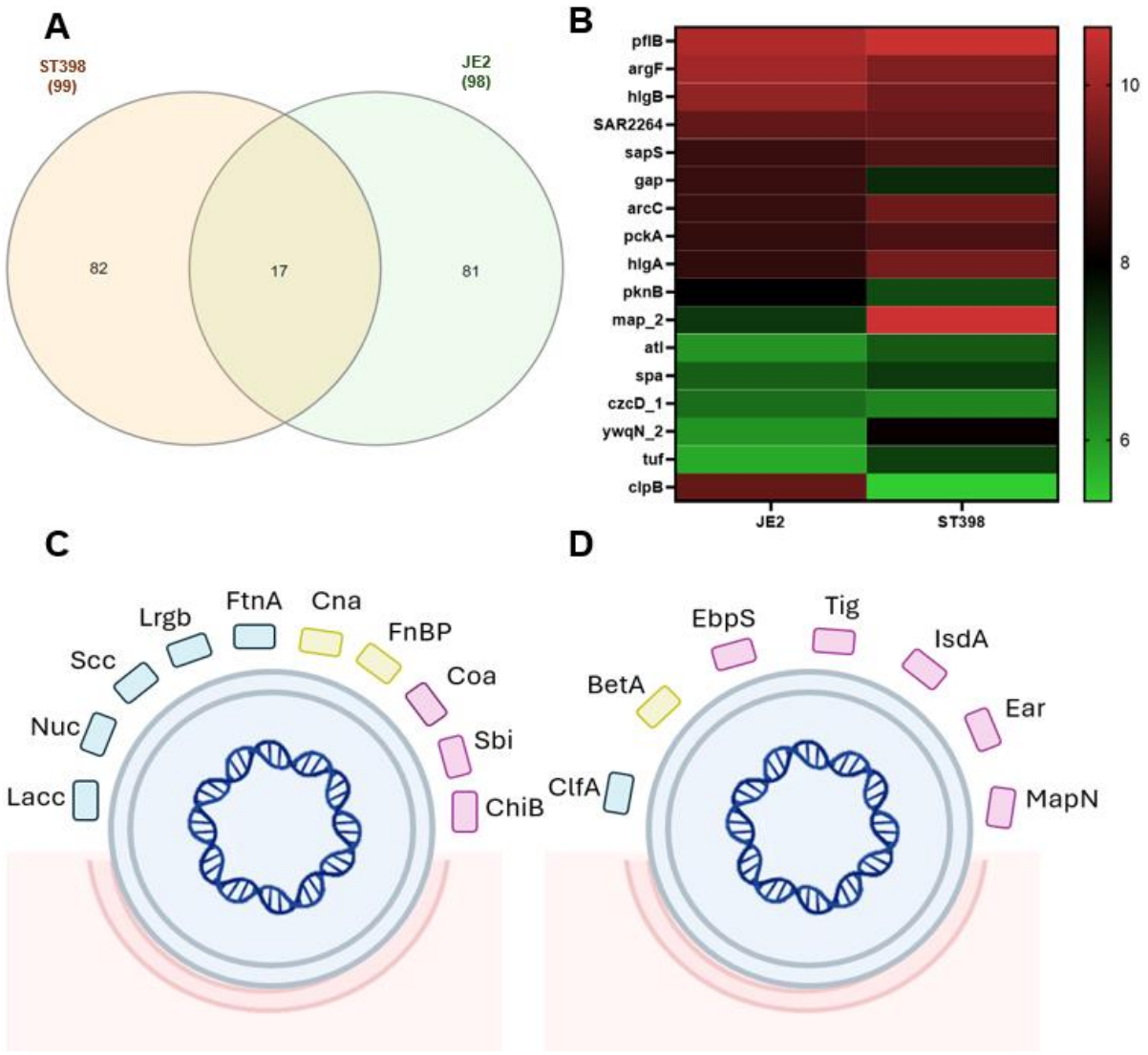

Figure 16. *Venn diagram shows the comparison of DEPs with increased expression during infection with ST398 and JE2 (A). Heat map reporting the normalized abundance of the shared DEPs, expressed as a scaling factor based on Log_{10} average normalized abundance between samples. The lower abundances are in green, and the highest abundances are in red (B). Characteristic proteins for the infection expressed by ST398 (C) and JE2 strain (D). The rectangles represent specific functions of the DEPs associated with virulence (pink), host adherence capability (yellow), and capable of immune evasion (blue).*

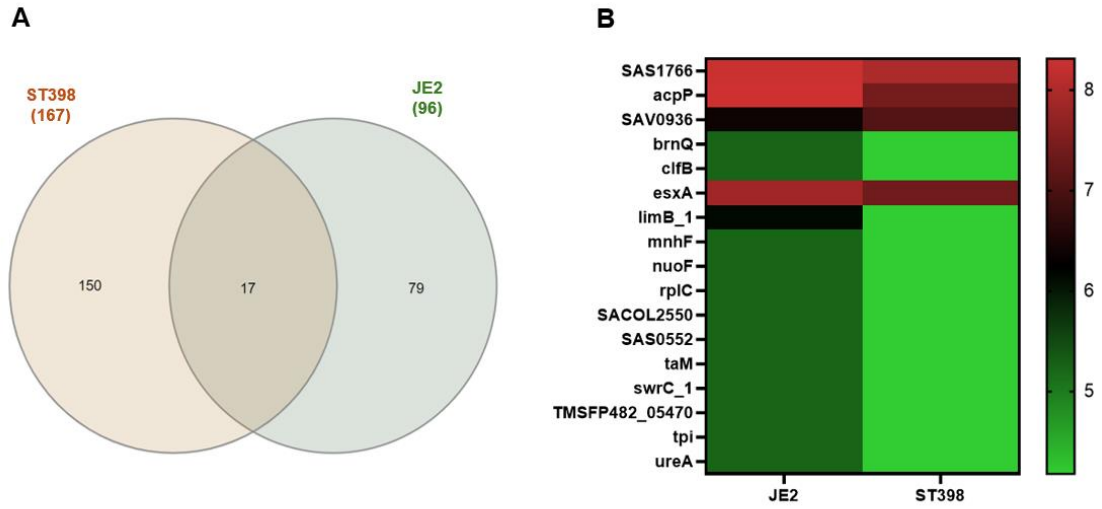

Figure 17. *Venn diagrams show the comparison of DEPs with decreased expression in the skin model infections with ST398 and JE2* ***(A)****. A Heat map of the shared DEPs demonstrated in Log10 average normalized abundance scaling from lower abundances (green) to highest abundances (red)* ***(B).***

4. Discussion and Conclusion

In this study, we aimed to characterize the variation in proteomic profiles of MRSA strains ST398 and JE2 during skin infection using two distinct infection models (*in vivo* and *in vitro*). By comparing the proteomes from the *in vivo* mouse model and the *in vitro* 3D skin model, we sought to elucidate strain-specific mechanisms of virulence and adaptations associated with skin infection. This comparative approach revealed differences and similarities in the proteomic profiles between the *S. aureus* strains and the infection models used.

Our first observation was that bacterial colonization was more efficient with JE2 strains at the end of the *in vivo* infection. There was a significant reduction in ST398 at 2dpi and 4dpi. Additionally, we observed a significant decrease in bacterial load in mice infected with the MRSA strain JE2, but only at 4 days post-infection (DPI), with the highest bacterial load observed at 2 dpi. The differences in infection development between the strains could be attributed to their different origins and virulence profiles. The low recovery of bacteria from the infected tissues has limited the proteomic analysis to the most abundant proteins in the *in vivo* model. In particular, this affected the number of bacterial proteins identified and quantified in the two-time points analyzed. For this reason, we also investigated the variation of *S. aureus* proteome in a skin model *in vitro*.

The *in vitro* model enabled the recovery of a higher load of colonizing bacteria and, in turn, allowed the investigation of a broader range of bacterial and host proteins during the infectious process. Further, some bacterial functions showed similar variation in both models, including proteins involved in arginine biosynthesis, validating the usefulness of the *in vitro* model.

In particular, we highlighted an increase in the abundance of ornithine carbamoyltransferase (ArgF) and carbamate kinase (ArcC) in both strains and infection models. The arginine-ornithine antiporter (ArcD) was also detected in the *in vitro* model for both strains, while arginine deiminase (ArcA) was uniquely identified in JE2. The increase in these proteins could be related to the activation of the arc operon, which is postulated to provide *S. aureus* with the necessary means to grow in the acidic milieu characteristic of skin infection sites (Thurlow et al., 2013). These data support an adaptation mechanism to the acidic environment during skin infections, suggesting that an increase in the arginine biosynthesis pathway is crucial for bacterial survival. This pathway appears to be vital for bacterial growth and virulence during infection. Among the adaptation mechanisms, we also found the betaine biosynthesis pathway that has a role in osmotic stress management during infection (Feng et al., 2022b). This pathway was associated with the increase of expression of choline dehydrogenase (BetA*)* in both *in vivo* and *in vitro* models for JE2. BetA was not detected in ST398, while, betaine-aldehyde dehydrogenase (BetB) was present in both strains in the *in vivo* model, highlighting the importance of this pathway in maintaining cellular integrity under osmotic stress. This pathway is believed to protect proteins and nucleic acid structure from salt stress and to increase osmotic homeostasis (Feng et al., 2022b). Hence, we confirm that the skin infection site is characterized by osmotic instability, making betaine biosynthesis a target to reduce bacterial adaptability to the infection environment, as previously suggested (Alreshidi et al., 2016). Apart from arginine and betaine pathways, we found DEPs associated with Panton-Valentine leukocidin (PVL) and cytotoxic exotoxins produced by *S. aureus* (SA), which causes leukocyte destruction and tissue necrosis, to be expressed. PVL is

predominantly associated with CA-MRSA strains (Adler et al., 2006). We identified the leukocidin S subunit (HlgA) and leukocidin F subunit (HlgB), which were found to increase in both strains in the *in vitro* model, and leukocidin LukS component (Fragment) (HlgC), which was exclusively increased in ST398. These proteins induce the opening of Ca2+ channels and form specific membrane pores, leading to cell death (Staali and Colin, 2021b), highlighting their contribution to *S. aureus* pathogenicity. Lipinska et al. describe how infecting rabbits' skin with PVL-positive MRSA isolates and PVL knockout strains led to a difference in extensive lesion development (Lipinska et al., 2011). Furthermore, other studies have highlighted that PVLs, regardless of their cytotoxic effects, can also play an important and positive immunomodulatory role during MRSA infections (Yoong and Pier, 2012). Therefore, we support the evidence that this system leads to the development of skin infections.

Other DEPs that were specifically induced during infection included the subunits of the ATP synthase complex: AtpA and AtpD in the *in vivo* model, and AtpE in JE2 in the *in vitro* model. The ATP synthase complex is the primary energy generator for cellular respiration, but it also appears to play an important role in influencing the host inflammatory response to biofilm infection (Bosch et al., 2020b). Other interesting DEPs shared by the two strains and, in some cases, between the two infection experiments included the trigger factor (Tig), detected in JE2 in both models and ST398 in the *in vitro* skin model. Tig is involved in biofilm formation and contributes to virulence. Indeed, a previous study investigated the role of tig in *S. aureus* infection, finding that a tig mutant has reduced biofilm formation *in vitro* (Keogh et al., 2021). Also, ClpL and ClpC, which make a part of the protease system. Experimental evidence showed that CLP proteases

contribute to the virulence of *S. aureus* and infection development (Illigmann et al., 2021). Indeed, mutants missing ClpP or ClpX were not able to develop abscesses in mice influencing also the biofilm formation (Frees et al., 2003).

The protein with the highest abundance in the *in vivo* model was glyceraldehyde-3-phosphate dehydrogenase-C (GapC). Before, this protein was found to adhere and internalize to mammalian epithelial cells, although its absence would not seem to prevent the adherence. However, it was proven to be essential for intra-mammary infection establishment (Kerro-Dego et al., 2012). Another essential protein identified is the *S. aureus* Map protein, an immunomodulator that interferes with T cell-mediated responses. The capacity of Map to alter T cell function was tested more specifically *in vitro* and *in vivo* using native and recombinant forms of Map. T cells or mice treated with recombinant Map had reduced T cell proliferative responses and a significantly reduced delayed-type hypersensitivity response to challenge antigen, respectively (Lee et al., 2002). These data suggest a role for Map as a possible immunomodulatory protein that may play a role in persistent SA infections by affecting protective cellular immunity. Moreover, we found that the protein fumarate hydratase (FumC) was expressed in ST398 in both infection models. FumC is an enzyme that degrades fumarate and is involved in glycolysis, thus, enhancing bacterial survival (Wong Fok Lung et al., 2019). Its increased levels have been highlighted in *S. aureus* clinical isolates from atopic dermatitis and cystic fibrosis, showing its importance for the infections of *S. aureus* (Acker et al., 2019; Gabryszewski et al., 2019).

In addition, the 3D skin infection model allowed us to identify thousands of proteins during the infection, thus highlighting the difference in behavior between both strains. In particular, it highlighted variations in amino acid metabolism, which was shown to

increase more in JE2 during the infection, such as histidine metabolism. We noticed a depletion in valine, leucine, and isoleucine pathway in ST938. Furthermore, we characterized skin infection fitness proteins necessary for infection in each strain by looking at proteins with significant expression. In ST398, we found proteins such as chitinase B (ChiB), which has been proven to be necessary for colonization in *Listeria monocytogenes* and was also shown to be an extracellular protein of *S. aureus* that could be related to virulence (Chaudhuri et al., 2010; Zhao et al., 2019). It may play an important role in *S. aureus* skin colonization, however, further studies are needed to determine this. Thermonuclear (Nuc) was reported in the literature to be necessary for escaping neutrophil extracellular traps (NETs) and can take part in biofilm formation (Mann et al., 2009; Berends et al., 2010). Another protein directly contributing to skin infection in this strain was cell wall anchored collagen adhesin (Cna). Cna is involved in the infection process of *S. aureus* and has been identified as a virulence factor in various animal models of staphylococcal infections, such as arthritis, keratitis, endocarditis, mastitis, and osteomyelitis (Hienz et al., 1996; Elasri et al., 2002). Complement inhibitor (Scc) protein plays a role in immune evasion (Jongerius et al., 2007). Another protein identified with JE2 strain infection was elastin binding protein (EbpS) which is mainly involved in mammalian tissue colonization (Downer et al., 2002).

However, despite the notable differences observed between the *in vivo* mouse model and the *in vitro* 3D skin model, both have provided valuable insights by revealing numerous proteins involved in skin infection. This comprehensive approach has offered a holistic view of bacterial adaptation to the infection site. Notably, in the *in vivo* model, the majority of proteins were implicated in translation, energy production, and carbohydrate

metabolism, suggesting a focus on fundamental cellular processes crucial for bacterial survival and proliferation within the host environment.

Conversely, proteins identified in the *in vitro* model predominantly contributed to energy production, cell wall biogenesis, and amino acid transport. This emphasis on cellular processes related to bacterial growth and adaptation underscores the relevance of the *in vitro* model in delineating strain-specific virulence profiles and identifying potential therapeutic targets.

Notably, the distinct protein profiles identified from the *in vitro* model have provided invaluable insights into the virulence mechanisms and adaptation strategies employed by the strains under study. On the other hand, the *in vivo* model, reflective of human skin infection dynamics, highlights proteins crucial for bacterial survival amidst the hostile immune response mounted by the host. These proteins are predominantly involved in survival mechanisms and protein biosynthesis, shedding light on the intricate interplay between bacterial pathogens and the host immune system during infection.

In conclusion, there were some challenges in this study, particularly the low bacterial protein abundances observed in the *in vivo* skin infection. Consequently, the proteins evaluated were descriptive of the entire proteome rather than the proteins with high abundance during the infection. This limitation might result in an imprecise description of the changes occurring during skin infection, reflecting general protein expression rather than specific responses to the infection.

Acknowledgment

This study has received funding from the European's Union Horizon 2020 research and innovation program under the Marie Skłodowska Curie grant agreement number 956154. We would like to thank the people who helped in the lab, especially Natasha the lab technician at the University of Copenhagen.

Credit authors

Dina Al Nahhas: Writing - Original Draft, investigation, formal analysis, data curation.
Salvatore Pisanu: Conceptualization, methodology, writing - review & Editing, and supervision.
Priscila Guerra: Conceptualization, resources, investigation, and methodology.
John Olsen: Conceptualization, methodology, supervision, writing – review & Editing.
Sergio Uzzau: Conceptualization, methodology, writing - review & Editing, and supervision.
Daniela Pagnozzi: Conceptualization, methodology, writing - review & Editing, and supervision.

Chapter 4: Screening of Compounds with Antimicrobial Activity Targeting Methicillin-Resistant Staphylococcus aureus

Dina Al Nahhas[1,2*], Salvatore Pisanu[1], Sandra M. Wellner[3], Margherita Sosio[4], Sonia I Maffioli[4], Stefano Donadio[4], Sergio Uzzau[2], Daniela Pagnozzi[1]

[1]Porto Conte Ricerche S.r.l, Tramariglio, Alghero (SS), Italy.
[2]Department of Biomedical Sciences, University of Sassari, Sassari, Italy.
[3]Department of Veterinary and Animal Sciences, University of Copenhagen, Copenhagen, Denmark.
[4]NAICONS laboratories, Milan, Italy.

Abstract

Methicillin-resistant *Staphylococcus aureus* (MRSA) continues to pose a significant threat to public health, necessitating urgent exploration of novel antimicrobial agents. In this study, we tested 75 compounds with known anti-microbial activity and screened 160 actinomycete-derived extracts, aiming to identify potential antimicrobial compounds against two MRSA strains, ST398 and JE2, representing diverse epidemiological contexts. Notably, our results revealed strain-specific variations in the inhibitory effects of the tested compounds, highlighting the significance of strain selection in antimicrobial screening protocols.

Among the compounds tested at 100 µg/ml, paramagnetoquinones exhibited the highest antimicrobial activity, inhibiting JE2 growth by 95.3% and ST398 growth by 88%. Furthermore, compounds NAI-107, Enduracyclinones, and NAI-414 demonstrated potent antimicrobial activity against both strains. By using extract screening and compound identification strategies, we identified two previously described molecules, elaiophylin, and nigericin, as promising antimicrobial agents against MRSA. Elaiophylin, known for its anticancer properties, has also been reported for its antimicrobial effect, primarily through the inhibition of the bacterial efflux pump mechanism. Nigericin is known to disrupt ATP

production and electron transport by acting as an ionophore, facilitating the exchange of potassium (K+) and hydrogen (H+) ions, thereby impeding bacterial growth.

Our findings highlight the potential of compound screening in targeting specific MRSA strains, offering insights into novel therapeutic strategies to combat MRSA infections. Our study helps to increase the variety of antimicrobial screening and emphasizes the importance of diverse approaches in identifying effective treatments. This contributes to ongoing efforts to reduce antimicrobial resistance and improve patient health outcomes.

Keywords: MRSA, antimicrobial activity, extracts, purification, antimicrobial resistance.

1. Introduction

Staphylococcus aureus, a gram-positive opportunistic pathogen, represents a significant challenge in hospital and community settings due to its ability to cause a wide array of infections. These range from relatively mild skin and soft tissue infections to life-threatening infections such as endocarditis, osteomyelitis, bacteremia, and severe pneumonia (Humphreys, 2012). After penicillin was discovered in 1940 (Klevens, 2007), infections were somewhat controlled with treatment until bacterial strains resistant to penicillin and beta-lactam antibiotics emerged. In particular, the presence of these resistant strains was much more frequent in hospital environments (hospital-acquired HA-MRSA) (RAYNER and MUNCKHOF, 2005). The resistance was developed by the bacterium's ability to hydrolyze the β-lactam bond by expressing beta-lactamases or by expressing penicillin-binding protein (BPP 2a) (Fuda et al., 2005). Later, in 1960, methicillin was discovered, which is an antibiotic designed to resist the enzymatic activity of beta-lactamases; in less than two years, methicillin-resistant *Staphylococcus aureus* (MRSA) first emerged (Barber, 1961). This resistance was attributed to acquiring the *mecA* gene, responsible for producing penicillin-binding protein 2a (PBP2a) (Hartman and Tomasz, 1984b). In 1990, the spread of MRSA was associated with new strains causing infections in non-hospitalized patients (community-acquired MRSA, CA-MRSA), becoming one of the most important pathogens associated with nosocomial infections (W. Hryniewicz, 1999). CA-MRSA strains differ genetically from HA-MRSA strains by different types of the staphylococcal cassette chromosome mec (SCCmec) and the production of toxins such as the Panton-Valentine leukocidin and cytotoxin (Asghar, 2014). Numerous studies in various countries identified similar cases (Styers et al., 2006; Falagas et al., 2013). Then

another variant was classified under the term livestock-associated MRSA (LA-MRSA), giving rise to a third category of MRSA strains recognized as a source of infection in livestock animals (Reischl et al., 2009). LA-MRSA poses a risk due to the transmission from animals to humans, especially to veterinarians and farmers. Nowadays, MRSA variants show resistance to numerous classes of antibiotics; this problem forces the scientific community to focus its skills and resources on the research of new antimicrobial molecules and the development of new pharmacological interventions (Shireen et al., 2013). In recent years, attention has turned toward new molecules extracted from natural products and synthetic compounds as potential sources of new antimicrobial agents (Zhao et al., 2022). The screening of such compounds for antimicrobial activity has become a pivotal step in the early stages of drug discovery. Additionally, advances in isolating and identifying bioactive molecules, including secondary metabolites, are crucial for developing new drugs (Kim et al., 2022).

In this study, we tested 75 compounds of known activity and 160 extracts from NAICONS laboratories. For the screening, we used two different strains of MRSA: JE2 (USA300 isolate), a community-associated methicillin-resistant *Staphylococcus aureus* (CA-MRSA) isolated from human infections that causes most invasive CA-MRSA diseases (Kennedy et al., 2008), and ST398, a livestock-associated methicillin-resistant *Staphylococcus aureus* (LA-MRSA) well-characterized strain isolated from pigs (Guardabassi et al., 2009), which has also been reported to cause skin and soft tissue infections in humans (Bouiller et al., 2020). We chose to compare the effect of compounds and extracts on these two strains as they originate from different environments and are known to have distinct virulence profiles. The potential for screening with different strains

was to transform the management of *S. aureus* infections. Emphasizing the need for continued research and innovation, we explore the prospects of these methodologies to screen compounds with antimicrobial activity to counteract and mitigate the global threat of antibiotic resistance.

2. Materials and Methods

2.1. Compound and Extract Acquisition

All screening materials were sourced from NAICONS Srl laboratories in Milan, Italy.

The extracts were obtained either from Streptomyces strains (Streptomyces extract plate) or other actinomycetes genera (rare extract plate). Full extracts were prepared from cultures (2 mL) by adding ethanol (4 mL) and shaking for 1 h at 30°C followed by centrifugation at 4000 rpm for 8 minutes. Fractionated extracts were obtained both from mycelium and cleared broth after centrifugation of 8 mL cultures at 4000 rpm for 8 minutes. Three mycelium extracts were obtained with 20%, 50%, and 100% ethanol. (4 mL each, 1h shaking at 30°C followed by centrifuge at 4000 rpm for 8 minutes). Cleared broth was treated with HP20 (0,8 mL, shaking for 1h at 30°C). After centrifugation (8000 rpm 1 minute) the resin was extracted with increasing concentration of ethanol (5%, 30%, and 80%, shaking for 15 minutes at 30°C followed by centrifugation at 8000 rpm for 1 minute). All the extracts were dried overnight at room temperature and stored at 4°C.

2.2. Strains and bacterial growth

Two different MRSA strains, ST398 and JE2, were obtained from the Faculty of Veterinary and Animal Sciences at the University of Copenhagen, Denmark. Initially, 2-3 colonies of each bacterium were inoculated into 7 mL of Tryptic Soy Broth (TSB) and incubated

overnight at 37 °C. The day after, 1 mL of the culture was added to 10 mL of Mueller Hinton Broth (CA-MHB) cation adjusted, mainly magnesium and calcium, until reaching an optical density (OD_{600} of 0.3-0.5), then adjusted to a 0.5 McFarland standard by adding 100 µL to 10 mL of CA-MHB.

2.3. Screening compounds of known activity

A plate containing 75 known compounds was prepared for experimentation, as shown in **Table 1**. Initially, each compound was dissolved in a suitable solvent to achieve a concentration of 100 µg/mL. Subsequently, 100 µL of each compound solution was aliquoted into separate wells of a 96-well plate. The compounds' solutions were then dried overnight at 40°C under vacuum. The plates were stored at +4°C until further use. Before experimentation, the dried compounds were resuspended by adding 100 µL of a 10% DMSO solution to each well. The compounds attained a final concentration of 100 µg/mL following resuspension. For screening, four biological replicates of each bacterial strain were prepared. Each well received 50 µL of MHB media and 40 µL of bacterial culture, followed by 10 µL of the compound solution. Control wells in columns 11 and 12 contained MHB with bacteria and MHB without bacteria, respectively. Plates were incubated overnight at 37 °C. OD_{600} was measured at 0, 19, and 24 hours. The inhibition percentage was calculated as follows:

$$\textbf{Inhibition \%} = 1 - \left(\frac{OD_{600}\ with\ compound}{OD_{600}\ without\ compound} \right) \times 100$$

Compounds were considered active if they achieved an inhibition percentage of ≥70

Table 6. Antibiotics and compounds used for drug screening, positions A1, F1, H1, G3, and E5 are empty.

	1	2	3	4	5	6	7	8	9	10
A	actinomycin	NAI-112	paramagnetoquinones	allopeptimycins	α-817 octacyclomycin	butenolide	Roxaticin	chrolactomycin	6-ammino penicillanic acid	Ramoplanin
B	D	purpuromycin	GE23077	NAI-107	streptolydigin	allocyclinones	Bafilomycin	amphotericin B	gentamycin	GE2270
C	luxomycin	thermorubin	vancomycin	tetracycline	viomycin	Cl-tetracycline	colistin	A40926	penicillinG	teicoplanin
D	Manumycin	nosiheptide	kirromycin	salinomycin	clindamycin	metronidazole	nystatin	Chloramphenicol	thiostrepton	monensin
E	fusidic acid	novobiocin	streptomycin	neomycin		gramicidin	spectinomycin	kasugamycin	tunicamycin	lincomycin
F		Gargantulide	gardimycin	NAI-857	erythromycin	rifampicin	NAI- 414	Enduracyclinones	Rifamycin O	Rifamycin S
G	apramycin	kanamycin		daptomycin	cycloheximide	cycloserin	ciprofloxacin	Corallomycin	polymixin	puromycin
H		PUM	levofloxacin	linezolid	nisin	nalidixic acid	phosphomycin	streptothricin	nocardamin (desferoxamine)	concanamycin

2.4. Screening extracts of unknown activity and molecules purification

We tested two different 96-well plates, each containing 80 full extracts: one plate was composed of extracts obtained from Streptomyces strains, while the other contained extracts prepared from other actinomycete strains. To each well 125 µL of 10% DMSO was added to dissolve the dried extracts. Subsequently, 10 µL of each extract was added to a well containing 40 µL bacterial solution and 50 µL of MHB. For each plate, we included two columns of controls: one with MHB and bacteria and the other with only MHB, as done previously when we tested the compounds. Optical density OD_{600} measurements were conducted at 0, 19, and 24 hours. Extracts exhibiting 70% or greater inhibition against MRSA were subjected to further verification, fractionation, and purification to identify the active compound (**Figure 18**). Upon activity confirmation, the six fractionated extracts (three from mycelium and three from the cleared broth) were also tested in serial dilutions. At first, the fractions are suspended in 125 µL of 10% DMSO, tested as done before for the full extracts. Active fractions were further sub-fractionated into 24 fractions using High-Performance Liquid Chromatography (HPLC). (One fraction per minute). We used a Shimadzu HPLC system LC 2010A-HT (Kyoto, Japan) equipped with a Merck LiChrospher RP-18 reverse-phase column (5 µm, I.D. x L 4.6 × 125 mm, Merck, Darmstadt, Germany) at 50°C. The mobile phases consisted of 0.05% formic acid (HCOOH) for phase A and acetonitrile (ACN) for phase B. The flow rate was set at 1 mL/min. Samples were fractionated using a linear gradient: ACN was increased from 10% to 95 in 18 minutes followed by 5 minutes at 95%. UV detection was carried out at 230 and 270 nm.

These 24 subfractions were dried using a speed vacuum concentrator overnight and resuspended later in 10% DMSO for further screening, as described previously. Upon activity confirmation, the active fraction was analyzed using high-resolution mass spectrometry (HRMS) to identify the specific compound responsible for the activity. For each active fraction detected, the adjacent inactive fractions (preceding and subsequent) were also analyzed to monitor the elution peak of the active fraction. The analysis was performed using a Vanquish UHPLC system connected to an Orbitrap Exploris 120 mass spectrometer, utilizing a YMC-Triart ODS column. The mobile phase included 0.1% formic acid in water (A), LCMS grade acetonitrile (B), and LCMS grade isopropyl alcohol (C), with a gradient flow program over a 23-minute cycle. The flow rate was set at 0.8 mL/min with a sample injection volume of 8 µL at 40°C. During the separation, 75% of the flow was directed to a Diode Array detector and 25% to the mass spectrometer, which was equipped with a heated electrospray ionization source operating in both positive and negative modes. Finally, MS/MS and UV-Vis spectra were analyzed and matched against both internal (Simone et al., 2013) and external databases (Blunt et al., 2012; Sorokina et al., 2021; Rutz et al., 2022; van Santen et al., 2022) to identify the active compounds.

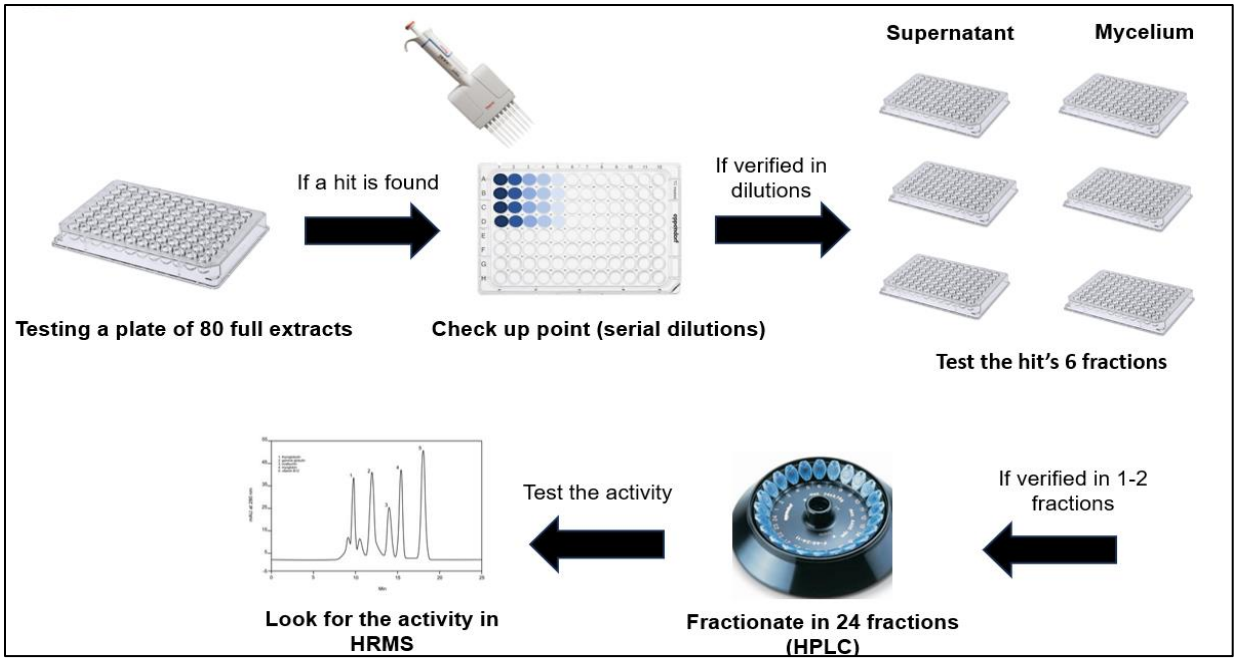

Figure 18. *Workflow followed for extract screening.*

3. Results

3.1. Evaluation of the inhibition percentage of the tested compounds

A total of 75 known compounds were tested to evaluate the percentage inhibition against two strains of *S. aureus* denominated ST398 and JE2, respectively. Screening of known compounds highlighted minimal variations of percentage inhibition dependent on the type of strain analyzed, as shown in **Figure 19.** Overall, most compounds demonstrated similar inhibition profiles for both strains, as detailed in **Table ST5** (Supplementary Data). In **Figure 19A**, the scatter plot shows that 33 out of the 75 compounds inhibited the growth of the ST398 strain by at least 70%, while **Figure 19B.** shows that 38 out of the 75 compounds inhibited the JE2 strain by 70%. Notably, the 33 compounds that effectively inhibited both strains, are highlighted in bold **Table ST5** (Supplementary Data). A total of 7 compounds highlighted a different trend between the two strains. The corallomycin (G8) showed a higher percentage of inhibition activity in ST398 (83%) than in JE2 (66.4%). Conversely, six other compounds exhibited greater antibacterial activity against the JE2 strain compared to ST398, specifically luxomycin (C1), A40926 (C8), levofloxacin (H3), penicillin G (C9), puromycin (G19), and nalidixic acid (H6).

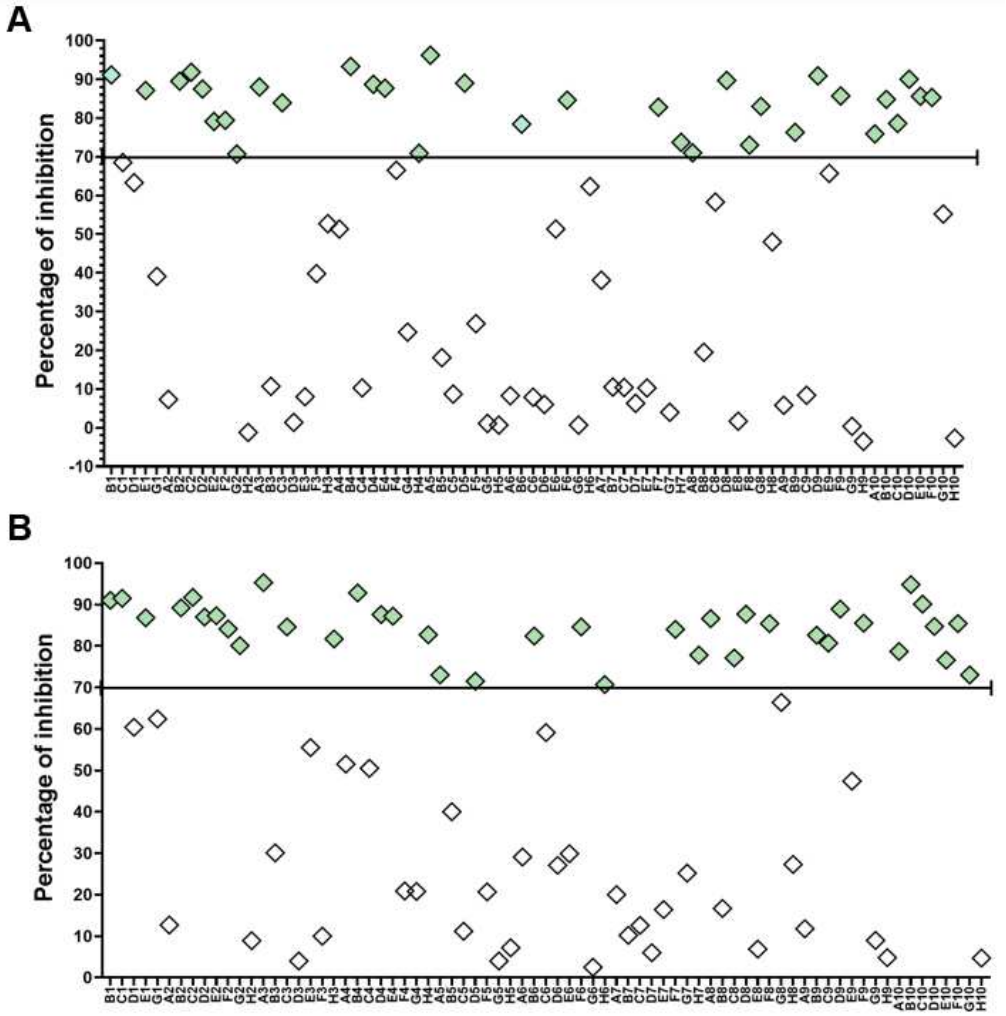

Figure 19. *Scatter plots showing the percentage inhibition of ST398 (**A**) and JE2 (**B**) strains obtained from the screening of known compounds. In green, compounds with an inhibitory activity equal to or greater than 70% are reported.*

3.2. Evaluation of the inhibition percentage of the extracts and molecule purification

After compound screening, we proceeded to screen the extracts. We tested a total of 80 full extracts obtained from Streptomyces against two strains, ST398 and JE2, as shown in **Figures 20A** and **20B**, respectively. **Figures 21A** and **21B** show the results of screening 80 extracts from rare actinomycetes against the same strains, ST398 and JE2. The analysis of Streptomyces extracts identified 11 common hits with inhibition percentages greater than 75% in both strains, accounting for approximately 14% of the

total extracts tested. The inhibition percentage of these 11 hits was further investigated using a serial dilution assay. We performed five serial dilutions, finding that only two hits, designated D6 and H6, consistently inhibited the growth of both strains with 100% efficacy in at least one or two dilutions **Table ST6** (Supplementary Data).

The second plate, which contained extracts from rare actinomycetes, revealed only four common hits between the strains, indicated with green color dots in the scatter plots in **Figure 22**. Other hits were identified only in ST398 and JE2 (orange color). A serial dilution assay confirmed the antimicrobial activity of only one hit, D8, in three successive dilutions against both strains **Table ST7** (Supplementary Data). Upon confirmation of activity from the serial dilution assay, we selected three extracts (two Streptomyces extracts, D6 and H6, and one rare extract, D8) for further investigation.

We tested the six fractionated extracts of each full extract (three obtained from the mycelium and three obtained from the cleared broth) to determine the presence of antimicrobial activity and the nature of the molecule responsible (hydrophilic or hydrophobic). The D6 extract showed promising activity in fraction 4 (supernatant) across four serial dilutions, while the H6 extract showed potential antimicrobial activity in fraction 5 (supernatant) against both strains. The D8 extract also highlighted strong activity in fraction 5 against both strains **Table ST8** (Supplementary Data).

Since one fraction with antimicrobial activity was identified for each extract, we proceeded with the fractionation of these fractions using an HPLC system. Each sub-fraction was then suspended in the appropriate volume, and their activity against MRSA was further tested. The results of screening the 72 sub-fractions are shown in **Figure 22A** for the ST398 strain and **Figure 22B** for the JE2 strain. D6 sub-fractions displayed some

antibacterial activity against the ST398 strain in subfraction 15, designated A1, inhibiting growth by 40%. The same subfraction inhibited JE2 growth by 10.4%. H6 showed antimicrobial activity in two sub-fractions, 14 and 22, designated B1 and B2, respectively. These subfractions inhibited the growth of the ST398 strain by 96%. For the JE2 strain, the same subfractions inhibited growth by 65% and 41%, respectively. Conversely, the D8 sub-fractions showed no promising antimicrobial activity against either strain.

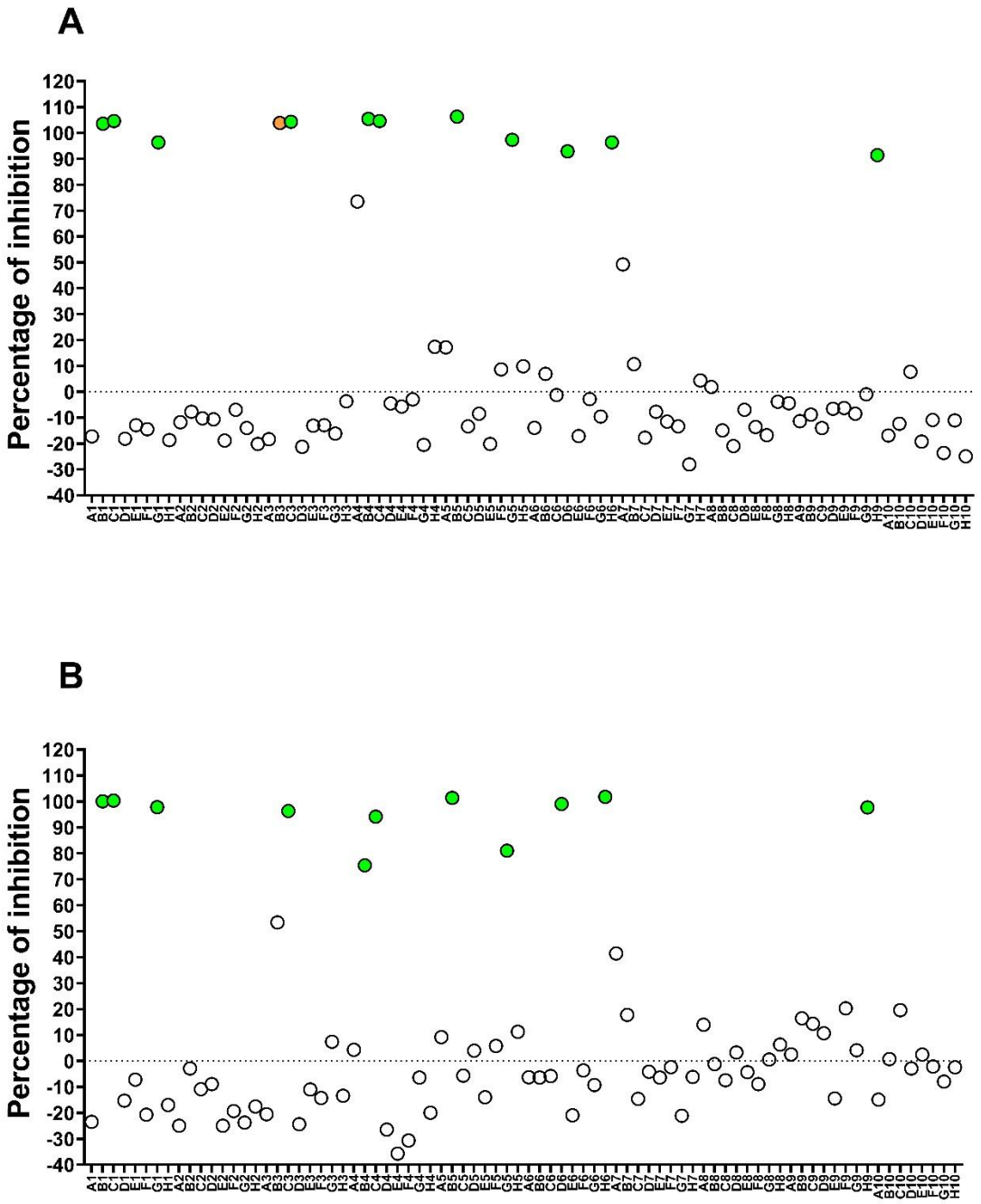

Figure 20. *Scatter plots showing the percentage inhibition of ST398 strain (**A**) and JE2 strain (**B**) obtained from the screening of extracts from Streptomyces. In green and orange dots, extracts with an inhibitory activity equal to or greater than 70% are reported. Specifically, green dots represent extracts with activity in common between the two strains, and orange dots, extracts with activity detected only on a single strain.*

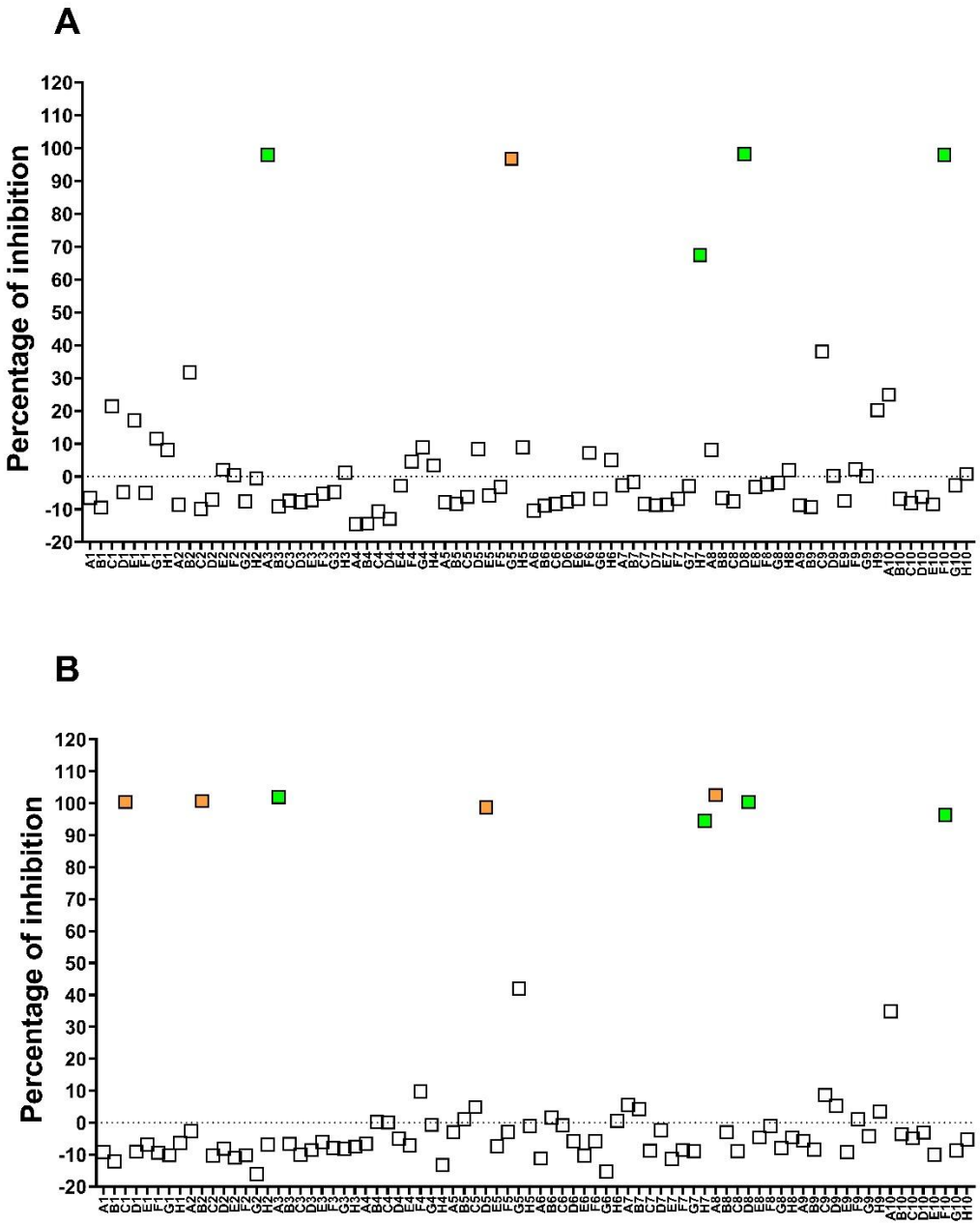

Figure 21. *Scatter plots showing the percentage inhibition of ST398 strain (**A**) and JE2 strain (**B**) obtained from the screening of extracts from rare actinomycetes. In green and orange dots, extracts with an inhibitory activity equal to or greater than 70% are reported. Specifically, green dots represent extracts with activity in common between the two strains, and orange dots, extracts with activity detected only in a single strain.*

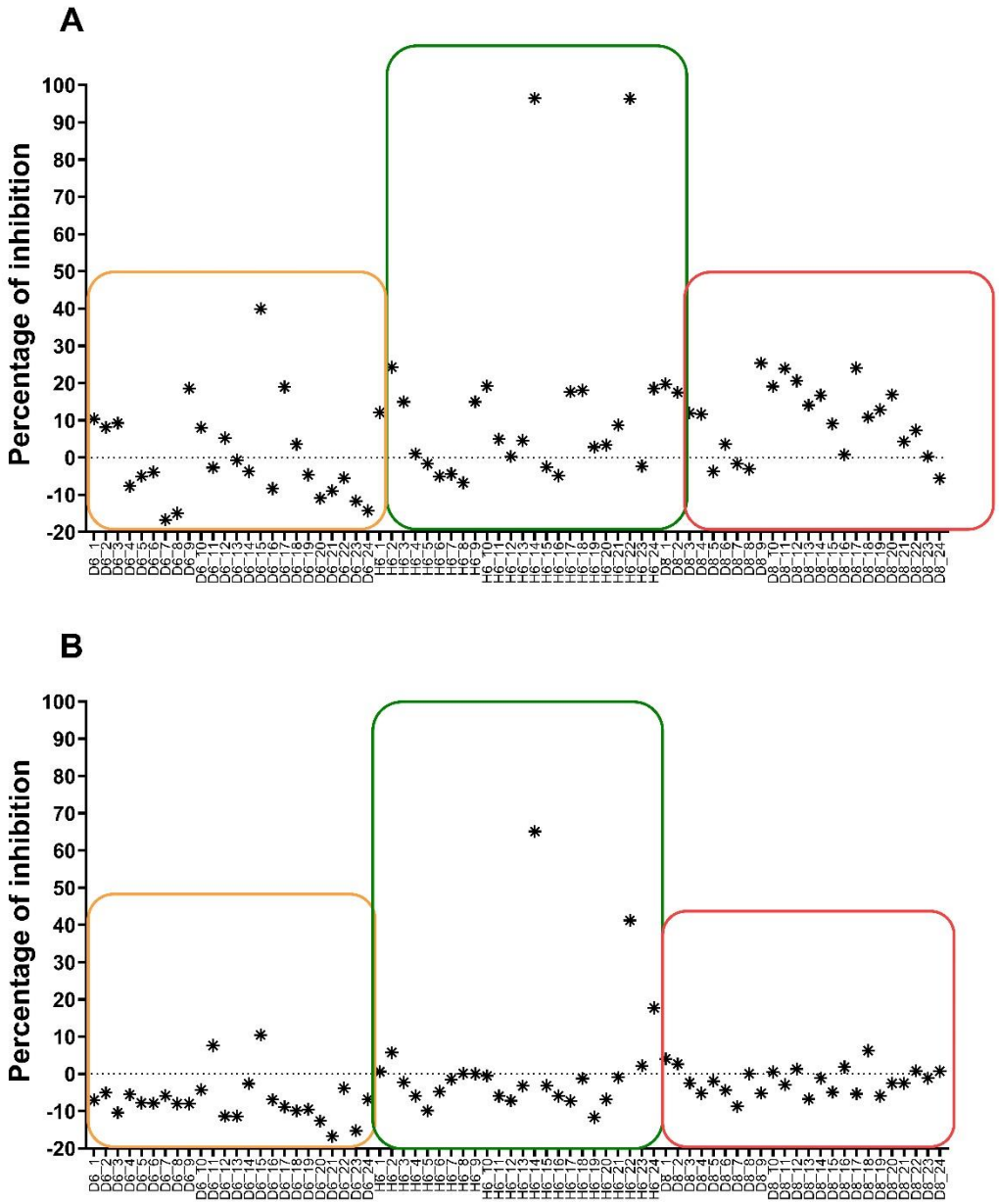

Figure 22. *Scatter plots showing the percentage inhibition of ST398 strain (**A**) and JE2 strain (**B**) of the subfractions obtained through fractionation in the HPLC system. D6 subfractions are shown in the orange box, H6 subfractions are in the green box, and D8 subfractions are in the red box.*

3.3. Identification of compounds by mass spectrometry analysis

After the identification of active fractions with antimicrobial activity, we proceeded with the identification of the molecules associated with the activity by mass spectrometry. For the first compound analyzed, denominated A1**,** the following signals were detected after fragmentation 446.3112 m/z and 444.2968 m/z in the positive and the negative ion modes, respectively, and with the two main signals 272.1855 and 106.0499 upon fragmentation. At the moment, it has not been possible to identify the compound because the MS signals detected did not match the MS signals present in the databases used. The MS/MS analysis of the second compound, B1 detected in the full scan as 742.5098 m/z and 747.4648 corresponding to $[M+NH_4]^+$ and $[M+Na]^+$ respectively**,** was characterized by signals reported in **Figure 23.** and matching with the molecule nigericin (Harvey et al., 2007). In the end, the third compound, **B2,** detected an ion of 1047.5850 m/z in full scan and two different ions of 729.3819 m/z and 411.1779 m/z after MS fragmentation (**Figure 24**). We confirm that those fragments belong to the elaiophylin molecule, as described by Boya et al. (Boya et al., 2017).

After confirming the activity of the molecules, by literature search, we found that both elaiophylin and nigericin are hexaene antibiotics produced by the microorganism Streptomyces hygroscopicus CH-7 (Ilic et al., 2016).

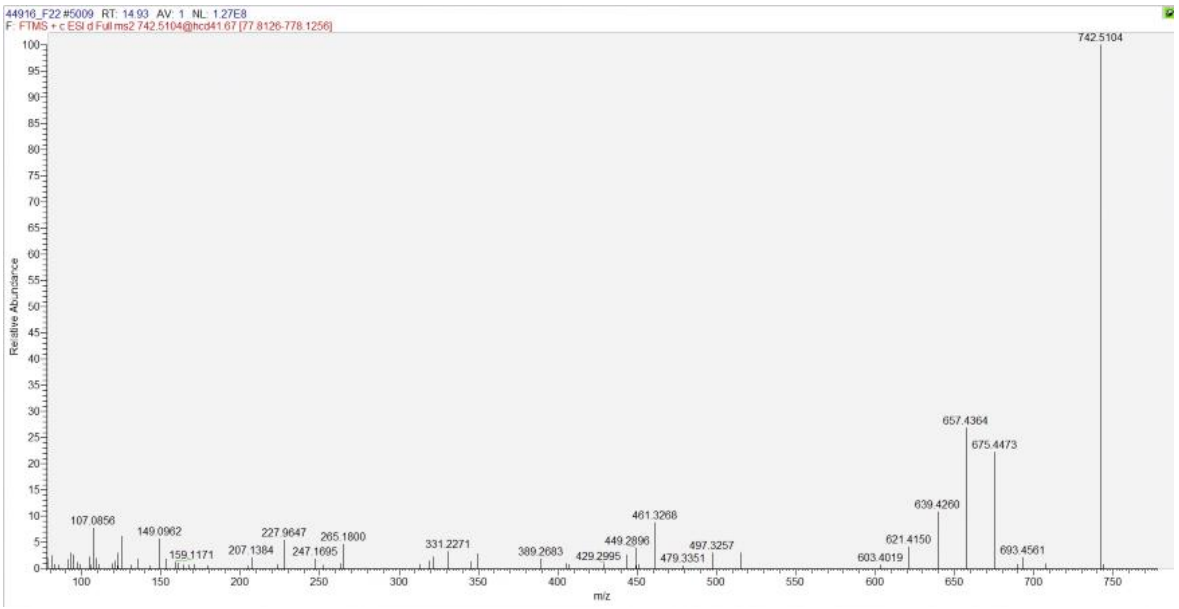

Figure 23. *Fragmentation mass spectrum of nigericin displayed by m/z ratio and relative abundance.*

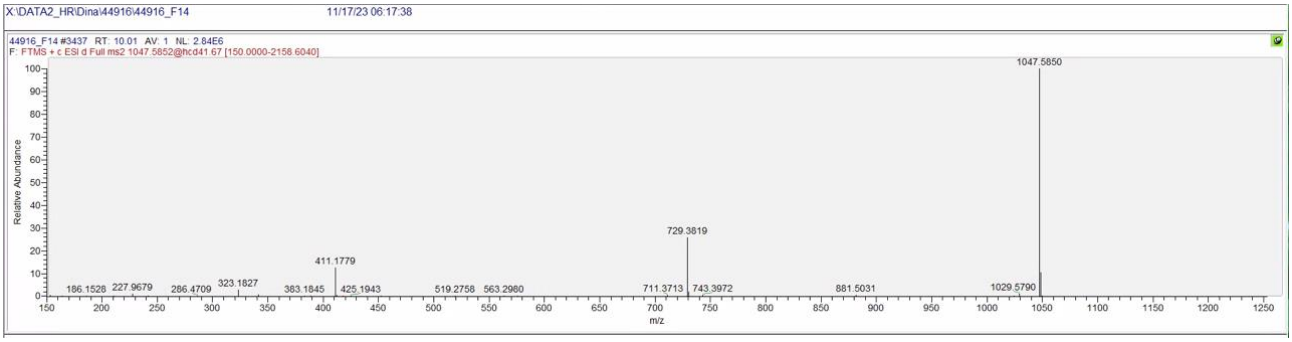

Figure 24. *Fragmentation mass spectrum of elaiophylin displayed by m/z ratio and relative abundance.*

4. Discussion and Conclusion

Methicillin-resistant *Staphylococcus aureus* is a constantly evolving pathogen in developing resistance to antibiotic treatment resulting in a wide variety of diseases. In recent years, some generations of antibiotics have been developed but despite this, there is an urgent need to discover new antibiotics and molecules to fight these pathogens (Pasberg-Gauhl, 2014). This study aimed to screen for compounds with known antimicrobial activity and extracts, generated by NAICONS laboratories and the identified molecules annotated in their platform Micro4All, against two different strains of MRSA, ST398 and the JE2 strain. These analyses also allowed the evaluation of strain differences in the antimicrobial activity of compounds and extracts as a function of strain. We observed that out of 75 compounds tested, 38 compounds inhibited the growth of JE2 strain with an inhibition percentage equal to or greater than 70%, while 33 of those inhibited the growth of ST398 strain. A total of 33 compounds were found to have a common antimicrobial activity against the two strains although different inhibition percentages depending on the strain were observed.

Among these compounds, it was worth noting that the paramagnetoquinones described by Iorio et al (Iorio et al., 2017) showed the highest percentage of inhibition against the JE2 strain (95.3%) and exhibited a percentage of inhibition of 88% against ST398. This compound was isolated from the actinomycete genus Actinoallomurus and showed very low minimum inhibitory concentration (MIC) values of 0.015 µg/mL against Gram-positive pathogens, including antibiotic-resistant strains. However, it was not tested before against ST398 and JE2, so we confirmed the activity of these molecules against our strains as well. Another known compound that was extremely active against ST398 and JE2 was

NAI-107. This compound inhibited both strains with an inhibition percentage equal to 94%, highlighting a strong antimicrobial activity against both strains. NAI-107 is a lantibiotic active against Gram-positive bacteria, including vancomycin-resistant *Staphylococcus aureus* (VRSA). Its antibacterial activity consists of disrupting some steps of cell wall formation, leading to the accumulation of the soluble peptidoglycan precursor UDP-N-acetylmuramic acid-pentapeptide (UDP-MurNAc-pentapeptide) within the cytoplasm (Münch et al., 2014). The analysis of known compounds also highlighted two other compounds, enduracyclinones, and NAI-414, with potential antibacterial activity against ST398 and JE2. Enduracyclinones, inhibiting the growth of ST398 and JE2 by 73% and 85.4%, respectively active against Gram-positive pathogens (especially *Staphylococcus* spp), including drug-resistant strains, with MIC in the range of 0.0005 to 4 µg/mL and streptococci. Studies have suggested a dual mechanism of action by inhibiting both DNA and peptidoglycan biosynthesis (Monciardini et al., 2019). Finally, the NAI-414 compound highlighted a good percentage of inhibition, approximately 83%, for the growth of both strains. It was confirmed to belong to the spirotetronate class exhibiting anti-staphylococcal activity and anti-tumor activity against microvascular endothelial cells (Mazzetti et al., 2012).

Regarding the active molecules obtained upon the screening and the characterization from the extracts, two compounds, elaiophylin, and nigericin, were identified out of a total of three purified compounds.

Elaiophylin, is a well-known molecule for its antimicrobial activity against Gram-positive bacteria, especially *S. aureus.* It is a macrodiolide, and its principal mechanism of action is based on inhibiting the efflux pump mechanism (NorA efflux protein), which appears to

be overexpressed in *S. aureus* during biofilm growth (Gui et al., 2019). This mechanism causes a reduction and/or inhibition of bacterial growth. Currently, another mechanism of action has also been suggested to inhibit bacterial growth, which involves the creation of pores in the lipid bilayer of the membrane, as by Grigoriev et al. (Grigoriev et al., 2001). Elaiophylin also possesses anti-cancer activities with moderate toxicity cells, autophagy inhibitory effect, and antiangiogenic activity besides immunosuppressive and anti-inflammatory effects (Gui et al., 2019). Numerous studies have also confirmed that it is a drug to combine with other antibiotics, such as norfloxacin and ethidium bromide, to enhance the effect of pharmacological treatments (Rodrigues dos Santos Barbosa et al., 2021). The second molecule purified responsible for the antibacterial activity, nigericin, is involved in the reduction of ATP production and electron transport chain. This compound exhibits antibacterial activity against Gram-positive bacteria and no activity against Gram-negative bacteria (Zhu et al., 2022). During the purification steps, both elaiophylin and nigericin showed a reduction in antimicrobial activity compared to the starting extracts. This could be associated with various aspects that were not considered during the study, such as the stability of the molecules during the drying and resuspension processes, their degradation, and even the combination of their antibacterial activity with other compounds present in the extract. Therefore, considering these aspects, it will be necessary to carry out other studies in the future to investigate and understand these fundamental aspects for the characterization of an antibacterial compound. The evaluation of the already-known compounds and those purified from the analyzed extracts allowed us to show the potential of at least 7 compounds in counteracting the growth of MRSA strains. Of these compounds, the antibacterial activity of 6 molecules is already known, in particular, these

are able to counteract the growth of Gram-positive bacteria such as *Staphylococcus* spp., as well as being active on other bacterial strains. Therefore, the study, in addition to confirming the potential of these molecules, provided new evidence of their antibacterial activity against specific MRSA strains, such as ST398 and JE2.

This study's contribution lays the foundation for future studies focused on the research, purification, identification, and therapeutic exploitation of known and unknown bioactive compounds that may provide new potential tools to combat antibiotic resistance.

Acknowledgments

This study has received funding from the European's Union Horizon 2020 research and innovation program under the Marie Skłodowska Curie grant agreement number 956154. We would like to thank Marianna Iorio and Matteo Simone at NAICONS laboratories for their help with the identification of the molecules. Christina and Stephania for their help in the lab and John E Olsen from the University of Copenhagen for providing the bacterial strains.

Conflict of interest

The author declares no conflict of interest.

5. Supplementary Data_3

ST 5. Average inhibition percentage of known compounds on MRSA strains ST398 and JE2 (4 biological replicates).

Compound	percentage of inhibition_ST398	percentage of inhibition_JE2
α-817 octacyclomycin	**96.2**	**73.0**
NAI-107	**93.3**	**92.8**
thermorubin	**91.8**	**91.7**
actinomycin D	**91.1**	**91.0**
thiostrepton	**90.9**	**88.9**
monensin	**90.0**	**84.7**
Cloramphenicol	**89.7**	**87.7**
purpuromycin	**89.5**	**89.2**
clindamycin	**89.0**	**71.5**
salinomycin	**88.7**	**87.6**
NAI-113	**88.0**	**95.3**
neomycin	**87.7**	**87.2**
nosiheptide	**87.5**	**87.0**
fusidic acid	**87.1**	**86.8**
Rifamycin O	**85.7**	**85.5**
lincomycin	**85.6**	**76.6**
Rifamycin S	**85.3**	**85.4**
GE2270	**84.8**	**94.8**
rifampicin	**84.6**	**84.6**
vancomycin	**83.9**	**84.6**
Corallomycin	**83.0**	66.4
NAI- 414	**82.8**	**84.0**
Gargantulide	**79.4**	**84.1**
novobiocin	**79.1**	**87.3**
teicoplanin	**78.6**	**90.1**
α-698 (p5+6)	**78.4**	**82.4**

gentamycin	**76.3**	**82.6**
Ramoplanin	**75.9**	**78.7**
phosphomycin	**73.7**	**77.8**
NAI-491	**73.0**	**85.4**
chrolactomycin	**71.0**	**86.6**
linezolid	**70.9**	**82.7**
kanamycin	**70.7**	**80.1**
luxomycin	68.5	**91.5**
NAI-857	66.5	20.9
tunicamycin	65.7	47.4
Manumycin	63.3	60.4
nalidixic acid	62.3	**70.7**
A40926	58.3	**77.1**
puromycin	55.2	**73.0**
levofloxacin	52.7	**81.7**
gramicidin	51.3	29.9
NAI-808	51.3	51.5
streptothricin	48.0	27.3
gardimycin	39.8	10.0
apramycin	39.1	62.4
Roxaticin	38.1	20.0
erythromycin	26.9	20.7
daptomycin	24.7	20.8
amphotericin B	19.5	16.7
streptolydigin	18.1	40.0
GE23077	10.7	30.1
Bafilomycin	10.5	10.2
colistin	10.4	12.6
spectinomycin	10.3	16.4
tetracycline	10.3	50.5

viomycin	8.7	11.2
penicillinG	8.4	**80.7**
butenolide	8.3	29.1
streptomycin	8.0	55.5
Cl-tetracycline	7.9	59.1
NAI-112	7.3	12.7
nystatin	6.3	6.0
metronidazole	6.0	27.1
6-ammino penicillanic acid	5.8	11.8
ciprofloxacin	4.0	25.2
kasugamycin	1.7	6.9
kirromycin	1.4	4.0
cycloheximide	1.1	4.0
cycloserin	0.7	2.5
nisin	0.7	7.2
polymixin	0.4	9.0
PUM	-1.2	8.9
concanamycin	-2.7	4.7
nocardamin (desferoxamine)	-3.5	4.8

ST 6. *Serial dilutions (checkup points) of the 11 hits from the streptomyces plate, initially identified for inhibiting both ST398 and JE2 strains, represented by the full extract and its serial dilutions.*

ST398		1/2	1/4	1/8	1/16	1/32	JE2		1/2	1/4	1/8	1/16	1/32
A7	63.2	-24.5	-27.2	-26.9	-26.2	-24.4	A7	9.7	-3.1	-8.0	-6.4	-11.7	-8.6
B1	97.6	13.7	-11.3	-17.4	-24.3	-23.9	B1	97.6	94.9	5.8	10.2	0.2	-7.8
B3	97.5	44.9	-26.2	-27.2	-24.8	-28.4	B3	98.7	14.5	-4.4	-11.0	-15.4	-16.1
B4	92.1	6.0	-20.5	-15.8	-19.3	-21.7	B4	-2.9	8.8	-16.5	-10.9	-7.3	-9.8
B5	92.9	18.8	-16.5	-19.1	-22.0	-18.8	B5	46.2	-5.9	-13.9	-8.4	-13.1	-16.6
C1	89.4	37.5	-9.1	-9.2	-4.2	-9.6	C1	11.7	1.8	-11.6	-12.2	-10.4	-18.1
C3	89.3	89.5	88.9	76.4	16.6	-9.4	C3	92.8	38.4	53.4	5.1	-9.6	-9.3
C4	86.2	88.8	88.0	71.5	46.0	20.8	C4	92.8	5.1	-2.6	-12.8	-11.5	-14.6
D6	78.1	67.7	68.9	83.2	84.3	61.8	D6	99.9	100.6	-9.5	-15.4	-6.5	-7.2
G1	95.8	95.9	76.3	75.7	79.6	51.5	G1	96.6	26.8	-13.2	2.0	-8.4	-14.9
G5	97.4	37.0	30.6	40.7	54.5	34.6	G5	61.6	1.2	-28.3	-20.4	-18.0	-24.9
H6	91.3	91.8	90.9	93.3	32.1	10.6	H6	94.0	93.7	96.0	0.2	-11.4	-16.8
H7	-15.7	-21.0	-20.4	-17.3	-11.4	-11.9	H7	-25.2	-30.1	-31.3	-29.3	-30.7	-28.3
H9	-27.9	-1.3	-11.0	-13.0	-6.9	-13.0	H9	91.4	-25.5	-26.0	-23.2	-25.2	-24.9

ST 7. *Serial dilutions (checkup points) of the 8 hits from the rare actinomycetes plate, initially identified for inhibiting both ST398 and JE2 strains, represented by the full extract and its serial dilutions.*

ST398		1/2	1/4	1/8	1/16	JE2		1/2	1/4	1/8	1/16
A3	85.4	41.8	30.1	27.5	24.5	A3	58	27	14	-26	-33
B2	64.7	49.2	38.9	35.6	23.4	B2	57	37	24	20	5
C1	100.0	34.8	14.2	1.7	10.6	C1	101	19	-7	-23	-12
D8	97.0	95.7	97.7	42.0	20.9	D8	98	96	41	28	-43
E10	11.3	-1.0	-0.6	-0.7	-2.5	E10	100	-26	-26	-26	-28
F10	95.9	9.4	11.8	9.8	17.5	F10	96	97	-10	-13	-3
G5	96.4	14.3	14.3	18.3	14.4	G5	97	-7	-7	-2	-7
H7	97.9	36.0	33.1	31.2	34.4	H7	99	21	17	14	18

ST 8. *Serial dilutions (checkup points) of the six fractions from each active selected extract, were tested against both ST398 and JE2 strains.*

ST398	H6	1/2	1/4	1/8	1/16	D6	1/2	1/4	1/8	1/16
P1	-13.0	-4.2	-0.2	5.5	3.9	-10.8	0.2	4.4	4.8	7.2
P2	-7.2	-1.4	0.8	8.0	4.2	-3.2	0.4	2.0	3.4	7.1
P3	76.2	33.5	20.6	15.4	9.1	107.4	-6.7	-5.1	-0.9	2.3
P4	106.0	106.1	106.2	100.0	97.1	106.5	106.4	107.1	107.3	107.1
P5	94.8	90.6	100.8	103.3	-5.3	-10.4	-5.8	-4.8	-0.9	-3.0
P6	108.5	56.9	27.5	19.5	-2.1	-8.6	-4.9	-2.8	1.8	-2.4

JE2	H67	1/2	1/4	1/8	1/16	D6	1/2	1/4	1/8	1/12
P1	-15.3	-10.1	-6.5	-5.1	-5.4	-14.7	-2.3	1.1	2.9	6.0
P2	-11.4	-8.1	-6.3	0.5	-5.0	-6.4	-4.4	-2.1	-5.2	1.0
P3	48.4	22.9	6.9	4.7	-4.5	69.8	-8.9	-10.7	-4.9	-2.7
P4	95.9	95.2	92.9	87.0	58.9	81.0	96.1	97.0	95.2	97.1
P5	89.3	84.8	94.6	94.0	88.9	78.8	97.0	96.6	96.6	97.4
P6	94.4	51.1	23.6	9.8	10.4	-6.9	-10.1	-10.4	-3.3	-1.6

ST398	D8	1/2	1/4	1/8	1/16
P1	-8.1	-2.8	0.5	0.5	1.7
P2	-0.1	3.7	5.6	10.4	2.5
P3	32.8	20.5	-2.4	5.1	5.1
P4	97.2	96.9	16.4	5.0	-3.1
P5	100.0	99.5	100.4	101.3	101.4
P6	-10.1	-5.7	-1.3	-0.8	5.8

JE2	D82	1/2	1/4	1/8	1/16
P1	-7.2	-3.3	-8.1	-1.9	-3.9
P2	-5.2	-0.3	-11.2	5.2	-1.8
P3	2.0	1.2	-9.6	-3.0	-6.6
P4	88.8	93.1	2.5	-1.3	0.8
P5	94.6	4.6	96.1	-13.6	-5.1
P6	-13.0	-10.1	-9.2	-8.0	-7.0

Chapter 5: Discussion, Conclusions, and Future Perspectives

The research presented in the previous chapters provides insights into MRSA's stress response to environmental stressors such as lowered pH, temperature, and increased salinity. These conditions simulate the stress encountered at wound sites, offering potentially crucial knowledge to understand bacterial responses during skin infection models: both an *in vitro* 3D skin model and an *in vivo* mouse model. Additionally, we tested compounds with known antimicrobial activity and extracts from various species with unknown activity, providing valuable insights into the potential and direction for using antimicrobials to develop new treatments.

The first study, "Comparative Proteomic Profiling of Methicillin-Resistant *Staphylococcus aureus* Under Varied Experimental Conditions," allowed us to characterize and study the differentially expressed proteins (DEPs) during the stress response to evaluate and understand how the bacterium shifts its metabolism in such situations. We found that decreased pH and temperature led to reduced bacterial growth, which was explained by a reduction in purine metabolism for the *de novo* synthesis of IMP. IMP serves as the substrate for inosine 5'-monophosphate dehydrogenase (IMPDH), a growth rate-limiting enzyme crucial for expanding the cellular guanine nucleotide pool, making IMPDH an intriguing target for novel antimicrobial drugs (Juvale et al., 2019). This was further highlighted in EC3 with added NaCl, demonstrating the bacterial metabolic shift response. Moreover, in both conditions and strains, we observed significant decreases in DEPs involved in sulfur metabolism, including cysteine synthase (CysK), known for its role in oxidative stress defense (Tikhomirova et al., 2024). Both strains compensated for the downregulation of cysteine by significantly increasing the expression of catalase protein

(katA) and aldo/keto reductases, primary scavengers for H2O2 and detoxification, respectively (Mandell, 1975; Lapthorn et al., 2013). We also noted a significant increase in DEPs associated with arginine biosynthesis in both strains. Arginine plays a role in producing ammonia (NH3), which raises levels of ammonium ions (NH4+), serving as a buffer to regulate pH levels inside and outside of cells under acidic conditions (Cotter and Hill, 2003). Apart from these similarities, we also noted differences in amino acid metabolism responses. The JE2 strain showed increased expression of DEPs involved in histidine and lysine metabolism besides arginine, while the ST398 strain downregulated DEPs involved in valine, leucine, and isoleucine metabolism, indicating differences in their stress management and adaptation strategies.

These observations were further highlighted in the skin infection models examined in the second study, "Exploring *S. aureus* Proteome During Skin Infection: Comparative Analysis of *In Vivo* and *In Vitro* Infection Models." We confirmed that arginine is essential for bacterial growth, adaptation, and enhanced virulence during infection. We identified proteins involved in arginine biosynthesis, such as carbamoyl transferase (ArgF) and carbamate kinase (ArcC), in both strains and infection models, confirming our findings from the first study. Furthermore, we found proteins involved in betaine biosynthesis, such as BetA, which converts choline to betaine aldehyde (Rosenstein et al., 1999). This protein was found in both strains and models and increased in EC3 in the first study. Betaine is required for maintaining cellular integrity under osmotic stress, protecting proteins and nucleic acids from salt stress, and maintaining osmotic homeostasis (Feng et al., 2022b). This further confirms our findings, as there was previously insufficient evidence about the osmotic characteristics of human skin infection sites. These similarities in protein

expression served to validate our work. Additionally, we detected several proteins from the *in vivo* model involved in different biological processes contributing to skin infection development, including biofilm formation, oxidative stress, and other adaptive processes. One such protein is FumC in the ST398 strain, validated to be involved in skin infection and previously seen in patients with AD and cystic fibrosis (Howden et al., 2023), indicating its potential as a target.

We also characterized the increasing DEPs from the *in vitro* skin infection, identifying several interesting proteins that could contribute to skin infection. One of them is acid phosphatase (SapS), found only in ST398. This protein decreased in EC2 and EC3 in the first study, indicating it wasn't needed during stress but increased during the infection. Mansour et al. described SapS as a novel virulence factor (Ahmad-Mansour et al., 2022), and our findings support this, suggesting it as a potential target. We further compared findings from the *in vitro* and *in vivo* models, identifying proteins expressed in the *in vivo* model with significantly increased abundance in the *in vitro* infection model. Several proteins involved in pyruvate metabolism were found in both models. Pyruvate regulates the virulence of *S. aureus* by enhancing PVL production, necessary for infection (Harper et al., 2018). Targeting pyruvate kinase (Pyk) and pyruvate fermentation (PflB) could disrupt pyruvate biosynthesis and attenuate bacterial virulence.

This study provides a comprehensive approach to tackling MRSA skin infections, whether through a complex system (mouse immune response) or an easily manipulated skin infection model resembling human skin infection but with greater feasibility for focusing on the bacterium (3D skin model). The final chapter, focusing on antimicrobial screening, provided insights into screening methods and purifying molecules exhibiting anti-

microbial activity against MRSA. We found that paramagnetoquinones and enduracyclinones are very effective against MRSA. The purification of elaiophylin and nigericin highlights the potential of bacterial extracts.

This research has significantly advanced our understanding of MRSA stress adaptation, protein expression during skin infection, and potential antimicrobial molecules for treating different strains with varying epidemiological contexts.

The work presented in this thesis has great potential for further investigation and testing in future studies. However, it also has some limitations that should be considered. For instance, including more than two MRSA strains would be valuable, given that the two studied MRSA strains are from different origins and exhibit different proteomic and genomic profiles. Therefore, validating our studies on additional MRSA strains might reveal similarities of targets across different strains. Another limitation is the investigation of solely the intracellular proteome of the bacterium. A complementary study including the extracellular proteome of the bacteria could provide a complete overview of the secreted proteins and the changes in the bacterium's proteome and pathogenesis as well. Therefore, we encourage future research to include more strains, perform full proteomics analysis, and focus on using this data in a Genome-Scale Model (GSM) of *S. aureus* to understand protein essentiality and redundancy for skin infection. This should be followed by knock-out experiments of the identified potential proteins using the 3D skin model to validate these targets. Additionally, testing the identified antimicrobial compounds' MIC and their safety on skin infection, followed by studying the proteome to understand protein expression differences in that context, could enhance the development of targeted

antimicrobial therapies and improve our ability to manage MRSA skin infections effectively.

References

1. Abreu, R., Rodríguez-Álvarez, C., Lecuona, M., Castro, B., González, J. C., Aguirre-Jaime, A., et al. (2019). Increased Antimicrobial Resistance of MRSA Strains Isolated from Pigs in Spain between 2009 and 2018. *Vet Sci* 6, 38. doi: 10.3390/vetsci6020038

2. Acker, K. P., Wong Fok Lung, T., West, E., Craft, J., Narechania, A., Smith, H., et al. (2019). Strains of Staphylococcus aureus that Colonize and Infect Skin Harbor Mutations in Metabolic Genes. *iScience* 19, 281–290. doi: 10.1016/j.isci.2019.07.037

3. Addis, M. F., Pisanu, S., Monistero, V., Gazzola, A., Penati, M., Filipe, J., et al. (2022). Comparative secretome analysis of Staphylococcus aureus strains with different within-herd intramammary infection prevalence. *Virulence* 13, 174–190. doi: 10.1080/21505594.2021.2024014

4. Adler, A., Temper, V., Block, C., Abramson, N., and Moses, A. (2006). Panton-Valentine Leukocidin–producing *Staphylococcus aureus*. *Emerg Infect Dis* 12, 1789–1790. doi: 10.3201/eid1211.060726

5. Ahmad-Mansour, N., Elhawy, M. I., Huc-Brandt, S., Youssouf, N., Pätzold, L., Martin, M., et al. (2022). Characterization of the Secreted Acid Phosphatase SapS Reveals a Novel Virulence Factor of Staphylococcus aureus That Contributes to Survival and Virulence in Mice. *Int J Mol Sci* 23, 14031. doi: 10.3390/ijms232214031

6. Akhtar, A. A., and Turner, D. P. (2022a). The role of bacterial ATP-binding cassette (ABC) transporters in pathogenesis and virulence: Therapeutic and vaccine potential. *Microb Pathog* 171. doi: 10.1016/j.micpath.2022.105734

7. Akhtar, A. A., and Turner, D. P. (2022b). The role of bacterial ATP-binding cassette (ABC) transporters in pathogenesis and virulence: Therapeutic and vaccine potential. *Microb Pathog* 171. doi: 10.1016/j.micpath.2022.105734

8. Ali Alghamdi, B., Al-Johani, I., Al-Shamrani, J. M., Musamed Alshamrani, H., Al-Otaibi, B. G., Almazmomi, K., et al. (2023). Antimicrobial resistance in methicillin-resistant staphylococcus aureus. *Saudi J Biol Sci* 30, 103604. doi: 10.1016/j.sjbs.2023.103604

9. Alifano, P., Fani, R., Lio`, P., Lio`, L., Lazcano, A., Bazzicalupo, M., et al. (1996). Histidine Biosynthetic Pathway and Genes: Structure, Regulation, and Evolution.

10. Alreshidi, M. M., Dunstan, R. H., Gottfries, J., Macdonald, M. M., Crompton, M. J., Ang, C. S., et al. (2016). Changes in the cytoplasmic composition of amino acids and proteins observed in Staphylococcus aureus during growth under variable growth conditions representative of the human wound site. *PLoS One* 11. doi: 10.1371/journal.pone.0159662

11. Aminov, R. I. (2010). A Brief History of the Antibiotic Era: Lessons Learned and Challenges for the Future. *Front Microbiol* 1. doi: 10.3389/fmicb.2010.00134

12. Amiri-Dashatan, N., Koushki, M., Abbaszadeh, H.-A., Rostami-Nejad, M., and Rezaei-Tavirani, M. (2018). Proteomics Applications in Health: Biomarker and Drug Discovery and Food Industry. *Iran J Pharm Res* 17, 1523–1536.

13. Andersen, S., Nawrocki, A., Johansen, A. E., Herrero-Fresno, A., Menéndez, V. G., Møller-Jensen, J., et al. (2022). Proteomes of Uropathogenic Escherichia coli Growing in Human Urine and in J82 Urinary Bladder Cells. *Proteomes* 10. doi: 10.3390/proteomes10020015

14. Arthur, M., Reynolds, P., and Courvalin, P. (1996). Glycopeptide resistance in enterococci.

15. Asghar, A. H. (2014). Molecular characterization of methicillin-resistant Staphylococcus aureus isolated from Makkah hospitals. *Pak J Med Sci* 30. doi: 10.12669/pjms.304.4946

16. Audretsch, C., Gratani, F., Wolz, C., and Dandekar, T. (2021). Modeling of stringent-response reflects nutrient stress induced growth impairment and essential amino acids in different Staphylococcus aureus mutants. *Sci Rep* 11. doi: 10.1038/s41598-021-88646-1

17. Bäckhed, F., Fraser, C. M., Ringel, Y., Sanders, M. E., Sartor, R. B., Sherman, P. M., et al. (2012). Defining a healthy human gut microbiome: Current concepts, future directions, and clinical applications. *Cell Host Microbe* 12, 611–622. doi: 10.1016/j.chom.2012.10.012

18. Barber, M. (1961). Methicillin-resistant staphylococci. *J Clin Pathol* 14, 385–393. doi: 10.1136/jcp.14.4.385

19. Barber, M., and Rozwadowska-Dowzenko, M. (1948). INFECTION BY PENICILLIN-RESISTANT STAPHYLOCOCCI. *The Lancet* 252, 641–644. doi: 10.1016/S0140-6736(48)92166-7

20. Benedict, F. G., Miles, W. R., and Johnson, A. (1919). The Temperature of the Human Skin. *Proceedings of the National Academy of Sciences* 5, 218–222. doi: 10.1073/pnas.5.6.218

21. Berends, E. T. M., Horswill, A. R., Haste, N. M., Monestier, M., Nizet, V., and Von Köckritz-Blickwede, M. (2010). Nuclease expression by Staphylococcus aureus facilitates escape from neutrophil extracellular traps. *J Innate Immun* 2, 576–586. doi: 10.1159/000319909

22. Bertrand, B. P., Heim, C. E., West, S. C., Chaudhari, S. S., Ali, H., Thomas, V. C., et al. (2022). Role of Staphylococcus aureus Formate Metabolism during Prosthetic Joint Infection. *Infect Immun* 90. doi: 10.1128/iai.00428-22

23. Blair, J. E., and Carr, M. (1960). Distribution of Phage Groups of *Staphylococcus aureus* in the Years 1927 through 1947. *Science (1979)* 132, 1247–1248. doi: 10.1126/science.132.3435.1247

24. Blunt, J., Munro, M., and Upjohn, M. (2012). "The Role of Databases in Marine Natural Products Research," in *Handbook of Marine Natural Products*, (Dordrecht: Springer Netherlands), 389–421. doi: 10.1007/978-90-481-3834-0_6

25. Bo Peng, Hui Li, and Xuanxian Peng (2019). Proteomics approach to understand bacterial antibiotic resistance strategies.

26. Bore, E., Langsrud, S., Langsrud, Ø., Rode, T. M., and Holck, A. (2007). Acid-shock responses in Staphylococcus aureus investigated by global gene expression analysis. *Microbiology (N Y)* 153, 2289–2303. doi: 10.1099/mic.0.2007/005942-0

27. Bosch, M. E., Bertrand, B. P., Heim, C. E., Alqarzaee, A. A., Chaudhari, S. S., Aldrich, A. L., et al. (2020a). Staphylococcus aureus ATP Synthase Promotes Biofilm Persistence by Influencing Innate Immunity. *mBio* 11. doi: 10.1128/mBio.01581-20

28. Bosch, M. E., Bertrand, B. P., Heim, C. E., Alqarzaee, A. A., Chaudhari, S. S., Aldrich, A. L., et al. (2020b). Staphylococcus aureus ATP Synthase Promotes Biofilm Persistence by Influencing Innate Immunity. *mBio* 11. doi: 10.1128/mBio.01581-20

29. Bouiller, K., Bertrand, X., Hocquet, D., and Chirouze, C. (2020). Human Infection of Methicillin-Susceptible Staphylococcus aureus CC398: A Review. *Microorganisms* 8, 1737. doi: 10.3390/microorganisms8111737

30. Boya, C. A., Fernández-Marín, H., Mejiá, L. C., Spadafora, C., Dorrestein, P. C., and Gutiérrez, M. (2017). Imaging mass spectrometry and MS/MS molecular networking reveals chemical interactions among cuticular bacteria and pathogenic fungi associated with fungus-growing ants. *Sci Rep* 7. doi: 10.1038/s41598-017-05515-6

31. Bruderer, R., Bernhardt, O. M., Gandhi, T., Xuan, Y., Sondermann, J., Schmidt, M., et al. (2017). Optimization of experimental parameters in data-independent mass spectrometry significantly increases depth and reproducibility of results. *Molecular and Cellular Proteomics* 16, 2296–2309. doi: 10.1074/mcp.RA117.000314

32. Caballero Cerbon, D. A., Gebhard, L., Dokuyucu, R., Ertl, T., Härtl, S., Mazhar, A., et al. (2024). Challenges and Advances in the Bioproduction of L-Cysteine. *Molecules* 29, 486. doi: 10.3390/molecules29020486

33. Calderón-Rivera, N., Múnera-Jaramillo, J., Jaramillo-Berrio, S., Suesca, E., Manrique-Moreno, M., and Leidy, C. (2023). Cardiolipin Strongly Inhibits the Leakage Activity of the Short Antimicrobial Peptide ATRA-1 in Comparison to LL-37, in Model Membranes Mimicking the Lipid Composition of Staphylococcus aureus. *Membranes (Basel)* 13. doi: 10.3390/membranes13030304

34. CALVORI, C., FRONTALI, L., LEONI, L., and TECCE, G. (1965). Effect of Rifamycin on Protein Synthesis. *Nature* 207, 417–418. doi: 10.1038/207417a0

35. Cantalapiedra, C. P., Herņandez-Plaza, A., Letunic, I., Bork, P., and Huerta-Cepas, J. (2021). eggNOG-mapper v2: Functional Annotation, Orthology Assignments, and Domain Prediction at the Metagenomic Scale. *Mol Biol Evol* 38, 5825–5829. doi: 10.1093/molbev/msab293

36. “Celbenin” - resistant Staphylococci (n.d.).

37. Chambers, H. F., and DeLeo, F. R. (2009). Waves of resistance: Staphylococcus aureus in the antibiotic era. *Nat Rev Microbiol* 7, 629–641. doi: 10.1038/nrmicro2200

38. Chaudhuri, S., Bruno, J. C., Alonzo, F., Xayarath, B., Cianciotto, N. P., and Freitag, N. E. (2010). Contribution of Chitinases to *Listeria monocytogenes* Pathogenesis. *Appl Environ Microbiol* 76, 7302–7305. doi: 10.1128/AEM.01338-10

39. Cheng, K., Chui, H., Domish, L., Hernandez, D., and Wang, G. (2016). Recent development of mass spectrometry and proteomics applications in identification and typing of bacteria. *Proteomics Clin Appl* 10, 346–357. doi: 10.1002/prca.201500086

40. Choueiry, F., Xu, R., and Zhu, J. (2022). Adaptive Metabolism of Staphylococcus aureus Revealed by Untargeted Metabolomics. *J Proteome Res* 21, 470–481. doi: 10.1021/acs.jproteome.1c00797

41. Classics in infectious diseases. “On abscesses”. Alexander Ogston (1844-1929). (1984). *Rev Infect Dis* 6, 122–8.

42. Cornaglia, G., and Rossolini, G. M. (2009). Forthcoming therapeutic perspectives for infections due to multidrug-resistant Gram-positive pathogens. *Clinical Microbiology and Infection* 15, 218–223. doi: 10.1111/j.1469-0691.2009.02740.x

43. Cosgrove, K., Coutts, G., Jonsson, I.-M., Tarkowski, A., Kokai-Kun, J. F., Mond, J. J., et al. (2007). Catalase (KatA) and Alkyl Hydroperoxide Reductase (AhpC) Have Compensatory Roles in Peroxide Stress Resistance and Are Required for Survival, Persistence, and Nasal Colonization in *Staphylococcus aureus*. *J Bacteriol* 189, 1025–1035. doi: 10.1128/JB.01524-06

44. Costa, F. G., and Horswill, A. R. (2022). Overcoming pH defenses on the skin to establish infections. *PLoS Pathog* 18. doi: 10.1371/journal.ppat.1010512

45. Cotter, P. D., and Hill, C. (2003). Surviving the Acid Test: Responses of Gram-Positive Bacteria to Low pH. *Microbiology and Molecular Biology Reviews* 67, 429–453. doi: 10.1128/mmbr.67.3.429-453.2003

46. Cranston D, and Sidebottom E (2016). *Penicillin and the Legacy of Norman Heatley - Hardcover*.

47. Crossley, K., Landesman, B., and Zaske, D. (1979). An Outbreak of Infections Caused by Strains of Staphylococcus aureus Resistant to Methicillin and Aminoglycosides. II. Epidemiologic Studies. *Journal of Infectious Diseases* 139, 280–287. doi: 10.1093/infdis/139.3.280

48. Cuny, C., Wieler, L., and Witte, W. (2015). Livestock-Associated MRSA: The Impact on Humans. *Antibiotics* 4, 521–543. doi: 10.3390/antibiotics4040521

49. David, M. Z., Taylor, A., Lynfield, R., Boxrud, D. J., Short, G., Zychowski, D., et al. (2013). Comparing pulsed-field gel electrophoresis with multilocus sequence typing, spa typing, staphylococcal cassette chromosome mec (SCCmec) typing, and PCR for panton-valentine leukocidin, arcA, and opp3 in methicillin-resistant Staphylococcus aureus isolates at a U.S. Medical Center. *J Clin Microbiol* 51, 814–9. doi: 10.1128/JCM.02429-12

50. Domon, B., and Aebersold, R. (2010). Options and considerations when selecting a quantitative proteomics strategy. *Nat Biotechnol* 28, 710–721. doi: 10.1038/nbt.1661

51. Downer, R., Roche, F., Park, P. W., Mecham, R. P., and Foster, T. J. (2002). The Elastin-binding Protein of Staphylococcus aureus(EbpS) Is Expressed at the Cell Surface as an Integral Membrane Protein and Not as a Cell Wall-associated Protein. *Journal of Biological Chemistry* 277, 243–250. doi: 10.1074/jbc.M107621200

52. Drlica, K. (1999). Mechanism of fluoroquinolone action. *Curr Opin Microbiol* 2, 504–508. doi: 10.1016/S1369-5274(99)00008-9

53. Ehrhardt Proksch (2018). pH in nature, humans and skin. *J Dermatol*.

54. Elasri, M. O., Thomas, J. R., Skinner, R. A., Blevins, J. S., Beenken, K. E., Nelson, C. L., et al. (2002). Staphylococcus aureus collagen adhesin contributes to the pathogenesis of osteomyelitis. *Bone* 30, 275–280. doi: 10.1016/S8756-3282(01)00632-9

55. Ellis, E. M. (2002). Microbial aldo-keto reductases. *FEMS Microbiol Lett* 216, 123–131. doi: 10.1111/j.1574-6968.2002.tb11425.x

56. ELLIS SIMONSEN, S. M., VAN ORMAN, E. R., HATCH, B. E., JONES, S. S., GREN, L. H., HEGMANN, K. T., et al. (2006). Cellulitis incidence in a defined population. *Epidemiol Infect* 134, 293–299. doi: 10.1017/S095026880500484X

57. ERIKSEN, K. R., and ERICHSEN, I. (1964). RESISTANCE TO METHICILLIN, ISOXAZOLYL PENICILLINS, AND CEPHALOTHIN IN *STAPHYLOCOCCUS AUREUS*. *Acta Pathologica Microbiologica Scandinavica* 62, 255–275. doi: 10.1111/apm.1964.62.2.255

58. Falagas, M. E., Karageorgopoulos, D. E., Leptidis, J., and Korbila, I. P. (2013). MRSA in Africa: Filling the Global Map of Antimicrobial Resistance. *PLoS One* 8, e68024. doi: 10.1371/journal.pone.0068024

59. Faoagali, J. L., Thong, M. L., and Grant, D. (1992). Ten years' experience with methicillin-resistant Staphylococcus aureus in a large Australian hospital. *Journal of Hospital Infection* 20, 113–119. doi: 10.1016/0195-6701(92)90113-Z

60. Feng, Y., Ming, T., Zhou, J., Lu, C., Wang, R., and Su, X. (2022b). The Response and Survival Mechanisms of Staphylococcus aureus under High Salinity Stress in Salted Foods. *Foods* 11. doi: 10.3390/foods11101503

61. Fey, P. D., Endres, J. L., Yajjala, V. K., Widhelm, T. J., Boissy, R. J., Bose, J. L., et al. (2013a). A genetic resource for rapid and comprehensive phenotype screening of nonessential Staphylococcus aureus genes. *mBio* 4. doi: 10.1128/mBio.00537-12

62. Fey, P. D., Endres, J. L., Yajjala, V. K., Widhelm, T. J., Boissy, R. J., Bose, J. L., et al. (2013b). A Genetic Resource for Rapid and Comprehensive Phenotype Screening of Nonessential Staphylococcus aureus Genes. *mBio* 4. doi: 10.1128/mBio.00537-12

63. Fischbach, M. A., and Walsh, C. T. (2009). Antibiotics for Emerging Pathogens. *Science (1979)* 325, 1089–1093. doi: 10.1126/science.1176667

64. Françoise Van Bambeke (2015). Lipoglycopeptide Antibacterial Agents in Gram-Positive Infections: A Comparative Review. *Drugs* 75, 2073–2095.

65. Franklin D. Lowy (1998). Staphylococcus aureus Infections. *N Engl J Med*.

66. Frazee, B. W., Lynn, J., Charlebois, E. D., Lambert, L., Lowery, D., and Perdreau-Remington, F. (2005). High prevalence of methicillin-resistant Staphylococcus aureus in emergency department skin and soft tissue infections. *Ann Emerg Med* 45, 311–320. doi: 10.1016/j.annemergmed.2004.10.011

67. Frees, D., Chastanet, A., Qazi, S., Sørensen, K., Hill, P., Msadek, T., et al. (2004). Clp ATPases are required for stress tolerance, intracellular replication and biofilm formation in *Staphylococcus aureus*. *Mol Microbiol* 54, 1445–1462. doi: 10.1111/j.1365-2958.2004.04368.x

68. Frees, D., Qazi, S. N. A., Hill, P. J., and Ingmer, H. (2003). Alternative roles of ClpX and ClpP in *Staphylococcus aureus* stress tolerance and virulence. *Mol Microbiol* 48, 1565–1578. doi: 10.1046/j.1365-2958.2003.03524.x

69. Fridkin, S. K., Hageman, J. C., Morrison, M., Sanza, L. T., Como-Sabetti, K., Jernigan, J. A., et al. (2005). Methicillin-Resistant *Staphylococcus aureus* Disease in Three Communities. *New England Journal of Medicine* 352, 1436–1444. doi: 10.1056/NEJMoa043252

70. Fuda, C. C. S., Fisher, J. F., and Mobashery, S. (2005). β-Lactam resistance in Staphylococcus aureus: the adaptive resistance of a plastic genome. *Cellular and Molecular Life Sciences* 62, 2617–2633. doi: 10.1007/s00018-005-5148-6

71. Gabryszewski, S. J., Wong Fok Lung, T., Annavajhala, M. K., Tomlinson, K. L., Riquelme, S. A., Khan, I. N., et al. (2019). Metabolic Adaptation in Methicillin-Resistant *Staphylococcus aureus* Pneumonia. *Am J Respir Cell Mol Biol* 61, 185–197. doi: 10.1165/rcmb.2018-0389OC

72. Gaupp, R., Ledala, N., and Somerville, G. A. (2012). Staphylococcal response to oxidative stress. *Front Cell Infect Microbiol* 2, 33. doi: 10.3389/fcimb.2012.00033

73. Gehrke, A.-K. E., Giai, C., and Gómez, M. I. (2023). Staphylococcus aureus Adaptation to the Skin in Health and Persistent/Recurrent Infections. *Antibiotics* 12, 1520. doi: 10.3390/antibiotics12101520

74. Georgiou, G., and Segatori, L. (2005). Preparative expression of secreted proteins in bacteria: Status report and future prospects. *Curr Opin Biotechnol* 16, 538–545. doi: 10.1016/j.copbio.2005.07.008

75. Goerge, T., Lorenz, M. B., van Alen, S., Hübner, N.-O., Becker, K., and Köck, R. (2017). MRSA colonization and infection among persons with occupational livestock exposure in Europe: Prevalence, preventive options and evidence. *Vet Microbiol* 200, 6–12. doi: 10.1016/j.vetmic.2015.10.027

76. Golubchik, T., Batty, E. M., Miller, R. R., Farr, H., Young, B. C., Larner-Svensson, H., et al. (2013). Within-Host Evolution of Staphylococcus aureus during Asymptomatic Carriage. *PLoS One* 8, e61319. doi: 10.1371/journal.pone.0061319

77. Gries, C. M., Sadykov, M. R., Bulock, L. L., Chaudhari, S. S., Thomas, V. C., Bose, J. L., et al. (2016). Potassium Uptake Modulates Staphylococcus aureus Metabolism. *mSphere* 1. doi: 10.1128/msphere.00125-16

78. Grigoriev, P. A., Schlegel, R., and Gräfe, U. (2001). Cation selective ion channels formed by macrodiolide antibiotic elaiophylin in lipid bilayer membranes. *Bioelectrochemistry* 54, 11–15. doi: 10.1016/S0302-4598(01)00102-7

79. Guan, N., and Liu, L. (2020). Microbial response to acid stress: mechanisms and applications. *Appl Microbiol Biotechnol* 104, 51–65. doi: 10.1007/s00253-019-10226-1

80. Guardabassi, L., O'Donoghue, M., Moodley, A., Ho, J., and Boost, M. (2009). Novel lineage of methicillin-resistant Staphylococcus aureus, Hong Kong. *Emerg Infect Dis* 15, 1998–2000. doi: 10.3201/eid1512.090378

81. Guérillot, R., Kostoulias, X., Donovan, L., Li, L., Carter, G. P., Hachani, A., et al. (2019). Unstable chromosome rearrangements in *Staphylococcus aureus* cause phenotype switching associated with persistent infections. *Proceedings of the National Academy of Sciences* 116, 20135–20140. doi: 10.1073/pnas.1904861116

82. Gui, M., Zhang, M., Wu, W., and Sun, P. (2019). Natural Occurrence, Bioactivity and Biosynthesis of Elaiophylin Analogues. *Molecules* 24, 3840. doi: 10.3390/molecules24213840

83. Guiberson, E. R., Weiss, A., Ryan, D. J., Monteith, A. J., Sharman, K., Gutierrez, B., et al. (2020). Spatially-targeted proteomics of the host-pathogen interface during staphylococcal abscess 11 12. *ACS Infect Dis*. doi: 10.1101/2020.09.01.267773

84. Hajdamowicz, N. H., Hull, R. C., Foster, S. J., and Condliffe, A. M. (2019). The impact of hypoxia on the host-pathogen interaction between neutrophils and staphylococcus aureus. *Int J Mol Sci* 20. doi: 10.3390/ijms20225561

85. Halsey, C. R., Lei, S., Wax, J. K., Lehman, M. K., Nuxoll, A. S., Steinke, L., et al. (2017). Amino acid catabolism in Staphylococcus aureus and the function of carbon catabolite repression. *mBio* 8. doi: 10.1128/mBio.01434-16

86. Harper, L., Balasubramanian, D., Ohneck, E. A., Sause, W. E., Chapman, J., Mejia-Sosa, B., et al. (2018). *Staphylococcus aureus* Responds to the Central Metabolite Pyruvate To Regulate Virulence. *mBio* 9. doi: 10.1128/mBio.02272-17

87. Harslund, J., Frees, D., Leifsson, P. S., Offenberg, H., Rømer, M. U., Brünner, N., et al. (2013). The role of Serpine-1 and tissue inhibitor of metalloproteinase type-1 in early host responses to Staphylococcus aureus intracutaneous infection of mice. *Pathog Dis* 68, 96–104. doi: 10.1111/2049-632X.12055

88. Hartman, B. J., and Tomasz, A. (1984a). Low-affinity penicillin-binding protein associated with beta-lactam resistance in Staphylococcus aureus. *J Bacteriol* 158, 513–516. doi: 10.1128/jb.158.2.513-516.1984

89. Hartman, B. J., and Tomasz, A. (1984b). Low-affinity penicillin-binding protein associated with beta-lactam resistance in Staphylococcus aureus. *J Bacteriol* 158, 513–516. doi: 10.1128/jb.158.2.513-516.1984

90. Harvey, B. M., Mironenko, T., Sun, Y., Hong, H., Deng, Z., Leadlay, P. F., et al. (2007). Insights into Polyether Biosynthesis from Analysis of the Nigericin Biosynthetic Gene Cluster in Streptomyces sp. DSM4137. *Chem Biol* 14, 703–714. doi: 10.1016/j.chembiol.2007.05.011

91. Heberle, H., Meirelles, G. V., da Silva, F. R., Telles, G. P., and Minghim, R. (2015). InteractiVenn: a web-based tool for the analysis of sets through Venn diagrams. *BMC Bioinformatics* 16, 169. doi: 10.1186/s12859-015-0611-3

92. Hienz, S. A., Schennings, T., Heimdahl, A., and Flock, J.-I. (1996). Collagen Binding of Staphylococcus aureus Is a Virulence Factor in Experimental Endocarditis. *Journal of Infectious Diseases* 174, 83–88. doi: 10.1093/infdis/174.1.83

93. Hitchings, G. H. (1973). Mechanism of Action of Trimethoprim-Sulfamethoxazole--I. *Journal of Infectious Diseases* 128, S433–S436. doi: 10.1093/infdis/128.Supplement_3.S433

94. Holman, J. D., Dasari, S., and Tabb, D. L. (2013). "Informatics of Protein and Posttranslational Modification Detection via Shotgun Proteomics," 167–179. doi: 10.1007/978-1-62703-360-2_14

95. Horsburgh, M. J., Ingham, E., and Foster, S. J. (2001). In Staphylococcus aureus, Fur is an interactive regulator with PerR, contributes to virulence, and is necessary for oxidative stress resistance through positive regulation of catalase and iron homeostasis. *J Bacteriol* 183, 468–475. doi: 10.1128/JB.183.2.468-475.2001

96. Howden, B. P., Giulieri, S. G., Wong Fok Lung, T., Baines, S. L., Sharkey, L. K., Lee, J. Y. H., et al. (2023). Staphylococcus aureus host interactions and adaptation. *Nat Rev Microbiol* 21, 380–395. doi: 10.1038/s41579-023-00852-y

97. Humphreys, H. (2012). Staphylococcus aureus: The enduring pathogen in surgery. *The Surgeon* 10, 357–360. doi: 10.1016/j.surge.2012.05.003

98. Ilic, S., Konstantinovic, S., Ciric, J., Savic, D., Gojgic-Cvijovic, G., and Veljkovic, V. (2016). Crude glycerol and whey as carbon and nitrogen sources for the production of antibiotics. *Advanced technologies* 5, 5–9. doi: 10.5937/savteh1601005I

99. Illigmann, A., Thoma, Y., Pan, S., Reinhardt, L., and Brötz-Oesterhelt, H. (2021). Contribution of the clp protease to bacterial survival and mitochondrial homoeostasis. *Microb Physiol* 31, 260–279. doi: 10.1159/000517718

100. Iorio, M., Cruz, J., Simone, M., Bernasconi, A., Brunati, C., Sosio, M., et al. (2017). Antibacterial Paramagnetic Quinones from *Actinoallomurus*. *J Nat Prod* 80, 819–827. doi: 10.1021/acs.jnatprod.6b00654

101. J. C. J. Barna, and D. H. Williams (1984). THE STRUCTURE AND MODE OF ACTION OF GLYCOPEPTIDE ANTIBIOTICS OF THE VANCOMYCIN GROUP. *microbiol* 38.

102. Jeong, B., Shah, M. A., Roh, E., Kim, K., Park, I., and Bae, T. (2022). Staphylococcus aureus Does Not Synthesize Arginine from Proline under Physiological Conditions. *J Bacteriol* 204. doi: 10.1128/jb.00018-22

103. Jongerius, I., Köhl, J., Pandey, M. K., Ruyken, M., van Kessel, K. P. M., van Strijp, J. A. G., et al. (2007). Staphylococcal complement evasion by various convertase-blocking molecules. *J Exp Med* 204, 2461–71. doi: 10.1084/jem.20070818

104. Joshi, G. S., Spontak, J. S., Klapper, D. G., and Richardson, A. R. (2011). Arginine catabolic mobile element encoded speG abrogates the unique hypersensitivity of Staphylococcus aureus to exogenous polyamines. *Mol Microbiol* 82, 9–20. doi: 10.1111/j.1365-2958.2011.07809.x

105. Julia M Ross, N. I., and Marten, M. R. (2015). Proteome Analyses of Staphylococcus aureus Biofilm at Elevated Levels of NaCl. *Clinical Microbiology: Open Access* 04. doi: 10.4172/2327-5073.1000219

106. Juvale, K., Shaik, A., and Kirubakaran, S. (2019). Inhibitors of inosine 5′-monophosphate dehydrogenase as emerging new generation antimicrobial agents. *Medchemcomm* 10, 1290–1301. doi: 10.1039/C9MD00179D

107. Kadlec, K., Feßler, A. T., Hauschild, T., and Schwarz, S. (2012). Novel and uncommon antimicrobial resistance genes in livestock-associated methicillin-resistant Staphylococcus aureus. *Clinical Microbiology and Infection* 18, 745–755. doi: 10.1111/j.1469-0691.2012.03842.x

108. Kalra, H., Adda, C. G., Liem, M., Ang, C., Mechler, A., Simpson, R. J., et al. (2013). Comparative proteomics evaluation of plasma exosome isolation techniques and assessment of the stability of exosomes in normal human blood plasma. *Proteomics* 13, 3354–3364. doi: 10.1002/pmic.201300282

109. Kandil, A., Hanora, A., Azab, M., and Enany, S. (2020). Proteomic analysis of bacterial communities associated with atopic dermatitis. *J Proteomics* 229. doi: 10.1016/j.jprot.2020.103944

110. Kanehisa, M., Sato, Y., Kawashima, M., Furumichi, M., and Tanabe, M. (2016). KEGG as a reference resource for gene and protein annotation. *Nucleic Acids Res* 44, D457–D462. doi: 10.1093/nar/gkv1070

111. Katayama, Y., Ito, T., and Hiramatsu, K. (2000). A New Class of Genetic Element, Staphylococcus Cassette Chromosome *mec* , Encodes Methicillin Resistance in *Staphylococcus aureus*. *Antimicrob Agents Chemother* 44, 1549–1555. doi: 10.1128/AAC.44.6.1549-1555.2000

112. Kennedy, A. D., Otto, M., Braughton, K. R., Whitney, A. R., Chen, L., Mathema, B., et al. (2008). Epidemic community-associated methicillin-resistant Staphylococcus aureus: Recent clonal expansion and diversification. Available at: www.pnas.org/cgi/content/full/

113. Keogh, R. A., Zapf, R. L., Frey, A., Marino, E. C., Null, G. G., Wiemels, R. E., et al. (2021). Staphylococcus aureus Trigger Factor Is Involved in Biofilm Formation and Cooperates with the Chaperone PpiB. *J Bacteriol* 203. doi: 10.1128/JB.00681-20

114. Kerro-Dego, O., Prysliak, T., Perez-Casal, J., and Potter, A. A. (2012). Role of GapC in the pathogenesis of Staphylococcus aureus. *Vet Microbiol* 156, 443–447. doi: 10.1016/j.vetmic.2011.11.018

115. Kim, P. Y., Kim, Y. S., Koo, I. G., Jung, J. C., Kim, G. J., Choi, M. Y., et al. (2011). Bacterial inactivation of wound infection in a human skin model by liquid-phase discharge plasma. *PLoS One* 6. doi: 10.1371/journal.pone.0024104

116. Kim, S., Lim, S.-W., and Choi, J. (2022). Drug discovery inspired by bioactive small molecules from nature. *Anim Cells Syst (Seoul)* 26, 254–265. doi: 10.1080/19768354.2022.2157480

117. Kimhi, Y., and Magasanik, B. (1970). Genetic basis of histidine degradation in Bacillus subtilis. *Journal of Biological Chemistry* 245, 3545–3548. doi: 10.1016/s0021-9258(18)62960-6

118. King, M. D., Humphrey, B. J., Wang, Y. F., Kourbatova, E. V, Ray, S. M., and Blumberg, H. M. (2006a). Emergence of community-acquired methicillin-resistant Staphylococcus aureus USA 300 clone as the predominant cause of skin and soft-tissue infections. *Ann Intern Med* 144, 309–17. doi: 10.7326/0003-4819-144-5-200603070-00005

119. King, M. D., Humphrey, B. J., Wang, Y. F., Kourbatova, E. V., Ray, S. M., and Blumberg, H. M. (2006b). Emergence of Community-Acquired Methicillin-Resistant *Staphylococcus aureus* USA 300 Clone as the Predominant Cause of Skin and Soft-Tissue Infections. *Ann Intern Med* 144, 309. doi: 10.7326/0003-4819-144-5-200603070-00005

120. kiran-et-al-2018-opuc-an-abc-transporter-that-is-associated-with-staphylococcus-aureus-pathogenesis (n.d.).

121. Kito, K., and Ito, T. (2008). Mass Spectrometry-Based Approaches Toward Absolute Quantitative Proteomics. *Curr Genomics* 9, 263–274. doi: 10.2174/138920208784533647

122. Klevens, R. M. (2007). Invasive Methicillin-Resistant <EMPH TYPE="ITAL">Staphylococcus aureus</EMPH> Infections in the United States. *JAMA* 298, 1763. doi: 10.1001/jama.298.15.1763

123. Kloos, W. E., and Bannerman, T. L. (1994). Update on clinical significance of coagulase-negative staphylococci. *Clin Microbiol Rev* 7, 117–140. doi: 10.1128/CMR.7.1.117

124. Klose, J., Nock, C., Herrmann, M., Stühler, K., Marcus, K., Blüggel, M., et al. (2002). Genetic analysis of the mouse brain proteome. *Nat Genet* 30, 385–393. doi: 10.1038/ng861

125. Kotra, L. P., Haddad, J., and Mobashery, S. (2000). Aminoglycosides: Perspectives on Mechanisms of Action and Resistance and Strategies to Counter Resistance. Available at: https://journals.asm.org/journal/aac

126. Ku, J. W., and Gan, Y. H. (2019). Modulation of bacterial virulence and fitness by host glutathione. *Curr Opin Microbiol* 47, 8–13. doi: 10.1016/j.mib.2018.10.004

127. Lapthorn, A. J., Zhu, X., and Ellis, E. M. (2013). The diversity of microbial aldo/keto reductases from Escherichia coli K12. *Chem Biol Interact* 202, 168–177. doi: 10.1016/j.cbi.2012.10.008

128. Larsen, J., Raisen, C. L., Ba, X., Sadgrove, N. J., Padilla-González, G. F., Simmonds, M. S. J., et al. (2022). Emergence of methicillin resistance predates the clinical use of antibiotics. *Nature* 602, 135–141. doi: 10.1038/s41586-021-04265-w

129. Leach, K. L., Swaney, S. M., Colca, J. R., McDonald, W. G., Blinn, J. R., Thomasco, L. M. M., et al. (2007). The Site of Action of Oxazolidinone Antibiotics in Living Bacteria and in Human Mitochondria. *Mol Cell* 26, 393–402. doi: 10.1016/j.molcel.2007.04.005

130. Lee, B. Y., Singh, A., David, M. Z., Bartsch, S. M., Slayton, R. B., Huang, S. S., et al. (2013). The economic burden of community-associated methicillin-resistant Staphylococcus aureus (CA-MRSA). *Clin Microbiol Infect* 19, 528–36. doi: 10.1111/j.1469-0691.2012.03914.x

131. Lee, L. Y., Miyamoto, Y. J., McIntyre, B. W., Höök, M., McCrea, K. W., McDevitt, D., et al. (2002). The Staphylococcus aureus Map protein is an immunomodulator that interferes with T cell–mediated responses. *Journal of Clinical Investigation* 110, 1461–1471. doi: 10.1172/JCI16318

132. Lenhardt, R., and Sessler, D. I. (2006a). Estimation of Mean Body Temperature from Mean Skin and Core Temperature. Available at: http://pubs.asahq.org/anesthesiology/article-pdf/105/6/1117/362811/0000542-200612000-00011.pdf

133. Lenhardt, R., and Sessler, D. I. (2006b). Estimation of Mean Body Temperature from Mean Skin and Core Temperature. Available at: http://pubs.asahq.org/anesthesiology/article-pdf/105/6/1117/362811/0000542-200612000-00011.pdf

134. Lessa, F. C., Mu, Y., Ray, S. M., Dumyati, G., Bulens, S., Gorwitz, R. J., et al. (2012). Impact of USA300 Methicillin-Resistant Staphylococcus aureus on Clinical Outcomes of Patients With Pneumonia or Central Line-Associated Bloodstream Infections. *Clinical Infectious Diseases* 55, 232–241. doi: 10.1093/cid/cis408

135. Levine, D. P. (n.d.). Vancomycin: A History. Available at: https://academic.oup.com/cid/article/42/Supplement_1/S5/275962

136. Li, H., and Auwerx, J. (2020). Mouse Systems Genetics as a Prelude to Precision Medicine. *Trends in Genetics* 36, 259–272. doi: 10.1016/j.tig.2020.01.004

137. Link, A. J., Eng, J., Schieltz, D. M., Carmack, E., Mize, G. J., Morris, D. R., et al. (1999). Direct analysis of protein complexes using mass spectrometry. *Nat Biotechnol* 17, 676–682. doi: 10.1038/10890

138. Lipinska, U., Hermans, K., Meulemans, L., Dumitrescu, O., Badiou, C., Duchateau, L., et al. (2011). Panton-Valentine leukocidin does play a role in the early stage of Staphylococcus aureus skin infections: A rabbit model. *PLoS One* 6. doi: 10.1371/journal.pone.0022864

139. Liu, G. Y. (2009). Molecular Pathogenesis of Staphylococcus aureus Infection. *Pediatr Res* 65, 71R-77R. doi: 10.1203/PDR.0b013e31819dc44d

140. Liu, X., Pai, P. J., Zhang, W., Hu, Y., Dong, X., Qian, P. Y., et al. (2016). Proteomic response of methicillin-resistant S. aureus to a synergistic antibacterial drug combination: A novel erythromycin derivative and oxacillin. *Sci Rep* 6. doi: 10.1038/srep19841

141. Livermore, D. M. (2000). Antibiotic resistance in staphylococci. Available at: www.ischemo.org

142. Lluis Masip, and George Georgiou (2006). The Many Faces of Glutathione in Bacteria.

143. Locatelli, C., Cremonesi, P., Caprioli, A., Carfora, V., Ianzano, A., Barberio, A., et al. (2017). Occurrence of methicillin-resistant Staphylococcus aureus in dairy cattle herds, related swine farms, and humans in contact with herds. *J Dairy Sci* 100, 608–619. doi: 10.3168/jds.2016-11797

144. Loi, V. Van, Busche, T., Kuropka, B., Müller, S., Methling, K., Lalk, M., et al. (2023). Staphylococcus aureus adapts to the immunometabolite itaconic acid by inducing acid and oxidative stress responses including S-bacillithiolations and S-itaconations. *Free Radic Biol Med* 208, 859–876. doi: 10.1016/j.freeradbiomed.2023.09.031

145. Lund, P., Tramonti, A., and De Biase, D. (2014). Coping with low pH: molecular strategies in neutralophilic bacteria. *FEMS Microbiol Rev* 38, 1091–1125. doi: 10.1111/1574-6976.12076

146. Lushchak, V. I. (2012). Glutathione Homeostasis and Functions: Potential Targets for Medical Interventions. *J Amino Acids* 2012, 1–26. doi: 10.1155/2012/736837

147. Makhlin, J., Kofman, T., Borovok, I., Kohler, C., Engelmann, S., Cohen, G., et al. (2007). Staphylococcus aureus ArcR controls expression of the arginine deiminase operon. *J Bacteriol* 189, 5976–5986. doi: 10.1128/JB.00592-07

148. Mandell, G. L. (1975). Catalase, superoxide dismutase, and virulence of Staphylococcus aureus. In vitro and in vivo studies with emphasis on staphylococcal--leukocyte interaction. *Journal of Clinical Investigation* 55, 561–566. doi: 10.1172/JCI107963

149. Mann, E. E., Rice, K. C., Boles, B. R., Endres, J. L., Ranjit, D., Chandramohan, L., et al. (2009). Modulation of eDNA release and degradation affects Staphylococcus aureus biofilm maturation. *PLoS One* 4. doi: 10.1371/journal.pone.0005822

150. Martins Costa, A. R., William Da Fonseca Batistão, D., Ribas, R. M., and Sousa, A. M. (2013). Staphylococcus aureus virulence factors and disease. Available at: https://www.researchgate.net/publication/304146404

151. Matthews, P., and Tomasz, A. (1990). Insertional inactivation of the mec gene in a transposon mutant of a methicillin-resistant clinical isolate of Staphylococcus aureus. *Antimicrob Agents Chemother* 34, 1777–1779. doi: 10.1128/AAC.34.9.1777

152. Mazzetti, C., Ornaghi, M., Gaspari, E., Parapini, S., Maffioli, S., Sosio, M., et al. (2012). Halogenated spirotetronates from Actinoallomurus. *J Nat Prod* 75, 1044–1050. doi: 10.1021/np300003n

153. Mendes, R. E., Deshpande, L. M., and Jones, R. N. (2014). Linezolid update: Stable in vitro activity following more than a decade of clinical use and summary of associated resistance mechanisms. *Drug Resistance Updates* 17, 1–12. doi: 10.1016/j.drup.2014.04.002

154. Michel, A., Agerer, F., Hauck, C. R., Herrmann, M., Ullrich, J., Hacker, J., et al. (2006). Global Regulatory Impact of ClpP Protease of *Staphylococcus aureus* on Regulons Involved in Virulence, Oxidative Stress Response, Autolysis, and DNA Repair. *J Bacteriol* 188, 5783–5796. doi: 10.1128/JB.00074-06

155. Minh Giao Bui, L. (2015). Staphylococcus aureus: stress response and its roles in pathogenesis.

156. Monciardini, P., Bernasconi, A., Iorio, M., Brunati, C., Sosio, M., Campochiaro, L., et al. (2019). Antibacterial Aromatic Polyketides Incorporating the Unusual Amino Acid Enduracididine. *J Nat Prod* 82, 35–44. doi: 10.1021/acs.jnatprod.8b00354

157. Münch, D., Müller, A., Schneider, T., Kohl, B., Wenzel, M., Bandow, J. E., et al. (2014). The Lantibiotic NAI-107 Binds to Bactoprenol-bound Cell Wall Precursors and Impairs Membrane Functions. *Journal of Biological Chemistry* 289, 12063–12076. doi: 10.1074/jbc.M113.537449

158. MUNCH-PETERSEN, E., and BOUNDY, C. (1962). Yearly incidence of penicillin-resistant staphylococci in man since 1942. *Bull World Health Organ* 26, 241–52.

159. Myles, I. A., and Datta, S. K. (2012). Staphylococcus aureus: an introduction. *Semin Immunopathol* 34, 181–184. doi: 10.1007/s00281-011-0301-9

160. Normal Heatley, and Norman George (2004). *Penicillin and luck : good fortune in the development of the "miracle drug" / Norman Heatley*.

161. Ong, S.-E., Blagoev, B., Kratchmarova, I., Kristensen, D. B., Steen, H., Pandey, A., et al. (2002). Stable Isotope Labeling by Amino Acids in Cell Culture, SILAC, as a Simple and Accurate Approach to Expression Proteomics. *Molecular & Cellular Proteomics* 1, 376–386. doi: 10.1074/mcp.M200025-MCP200

162. Otto, M. (2010). *Staphylococcus* colonization of the skin and antimicrobial peptides. *Expert Rev Dermatol* 5, 183–195. doi: 10.1586/edm.10.6

163. Pal, M., Berhanu, G., Megersa, L., Kandi, V., Kerorsa, G. B., and Marami, L. M. (2020). Distinguished researcher gate View project Inter-professional Health Care View project Epidemiology, Pathogenicity, Animal Infections, Antibiotic Resistance, Public Health Significance, and Economic Impact of Staphylococcus Aureus: A Comprehensive Review. *Am J Public Health Res* 8, 14–21. doi: 10.12691/ajphr-8-1-3

164. Pankow, S., Martínez-Bartolomé, S., Bamberger, C., and Yates, J. R. (2019). Understanding molecular mechanisms of disease through spatial proteomics. *Curr Opin Chem Biol* 48, 19–25. doi: 10.1016/j.cbpa.2018.09.016

165. Pasberg-Gauhl, C. (2014). A need for new generation antibiotics against MRSA resistant bacteria. *Drug Discov Today Technol* 11, 109–116. doi: 10.1016/j.ddtec.2014.04.001

166. Pérez-Llarena, F. J., and Bou, G. (2016). Proteomics as a tool for studying bacterial virulence and antimicrobial resistance. *Front Microbiol* 7. doi: 10.3389/fmicb.2016.00410

167. Pete Kinross1, A. P. 6, R. S. E. V. H. A. P. F. L. A. V. J. K. M. J. S. O. H. D. L. M. the E. human L.-M. study group[8] (2017). Livestock-associated meticillin-resistant Staphylococcus aureus (MRSA) among human MRSA isolates, European Union/European Economic Area countries, 2013.

168. Philip Nikolic (2023). Untargeted proteomic differences between clinical strains of methicillin-sensitive and methicillin-resistant Staphylococcus aureus. *Microb Pathog* 179.

169. Pinilla, C. M. B., Stincone, P., and Brandelli, A. (2021). Proteomic analysis reveals differential responses of Listeria monocytogenes to free and nanoencapsulated nisin. *Int J Food Microbiol* 346. doi: 10.1016/j.ijfoodmicro.2021.109170

170. Pisanu, S., Cubeddu, T., Pagnozzi, D., Rocca, S., Cacciotto, C., Alberti, A., et al. (2015). Neutrophil extracellular traps in sheep mastitis. *Vet Res* 46. doi: 10.1186/s13567-015-0196-x

171. Poole, L. B. (2005). Bacterial defenses against oxidants: mechanistic features of cysteine-based peroxidases and their flavoprotein reductases. *Arch Biochem Biophys* 433, 240–254. doi: 10.1016/j.abb.2004.09.006

172. Porcheddu, M., Abbondio, M., De Diego, L., Uzzau, S., and Tanca, A. (2022). Meta4P: A User-Friendly Tool to Parse Label-Free Quantitative Metaproteomic Data and Taxonomic/Functional Annotations. *J Proteome Res*. doi: 10.1021/acs.jproteome.2c00803

173. Proctor, R. A., Christman, G., and Mosher, D. F. (1984). Fibronectin-induced agglutination of Staphylococcus aureus correlates with invasiveness. *J Lab Clin Med* 104, 455–69.

174. Proksch, E. (2018). <scp>pH</scp> in nature, humans and skin. *J Dermatol* 45, 1044–1052. doi: 10.1111/1346-8138.14489

175. Randall, M. J., Jüngel, A., Rimann, M., and Wuertz-Kozak, K. (2018). Advances in the biofabrication of 3D skin in vitro: Healthy and pathological models. *Front Bioeng Biotechnol* 6. doi: 10.3389/fbioe.2018.00154

176. RAYNER, C., and MUNCKHOF, W. J. (2005). Antibiotics currently used in the treatment of infections caused by *Staphylococcus aureus*. *Intern Med J* 35. doi: 10.1111/j.1444-0903.2005.00976.x

177. Reischl, U., Frick, J., Hoermansdorfer, S., Melzl, H., Bollwein, M., Linde, H. J., et al. (2009). Single-nucleotide polymorphism in the SCCmec-orfX junction distinguishes between livestock-associated MRSA CC398 and human epidemic MRSA strains. *Euro Surveill* 14.

178. Reiß, S., Pané-Farré, J., Fuchs, S., François, P., Liebeke, M., Schrenzel, J., et al. (2012). Global Analysis of the Staphylococcus aureus Response to Mupirocin. *Antimicrob Agents Chemother* 56, 787–804. doi: 10.1128/AAC.05363-11

179. Ren, Z., Yu, J., Du, J., Zhang, Y., Hamushan, M., Jiang, F., et al. (2022). A General Map of Transcriptional Expression of Virulence, Metabolism, and Biofilm Formation Adaptive Changes of Staphylococcus aureus When Exposed to Different Antimicrobials. *Front Microbiol* 13. doi: 10.3389/fmicb.2022.825041

180. Rismondo, J., Percy, M. G., and Gründling, A. (2018). Discovery of genes required for lipoteichoic acid glycosylation predicts two distinct mechanisms for wall teichoic acid glycosylation. *Journal of Biological Chemistry* 293, 3293–3306. doi: 10.1074/jbc.RA117.001614

181. Rode, T. M., Møretrø, T., Langsrud, S., Langsrud, Ø., Vogt, G., and Holck, A. (2010a). Responses of *Staphylococcus aureus* exposed to HCl and organic acid stress. *Can J Microbiol* 56, 777–792. doi: 10.1139/W10-057

182. Rode, T. M., Møretrø, T., Langsrud, S., Langsrud, Ø., Vogt, G., and Holck, A. (2010b). Responses of Staphylococcus aureus exposed to HCL and organic acid stress. *Can J Microbiol* 56, 777–792. doi: 10.1139/W10-057

183. Rodrigues dos Santos Barbosa, C., Feitosa Muniz, D., Silvino Pereira, P., Maria de Arruda Lima, S., Datiane de Morais Oliveira Tintino, C., Cintia Alexandrino de Souza, V., et al. (2021). Evaluation of Elaiophylin extracted from Streptomyces hygroscopicus as a potential inhibitor of the NorA efflux protein in Staphylococcus aureus: An in vitro and in silico approach. *Bioorg Med Chem Lett* 50, 128334. doi: 10.1016/j.bmcl.2021.128334

184. Rosenstein, R., Futter-Bryniok, D., and Götz, F. (1999). The Choline-Converting Pathway in *Staphylococcus xylosus* C2A: Genetic and Physiological Characterization. *J Bacteriol* 181, 2273–2278. doi: 10.1128/JB.181.7.2273-2278.1999

185. Ross, P. L., Huang, Y. N., Marchese, J. N., Williamson, B., Parker, K., Hattan, S., et al. (2004). Multiplexed Protein Quantitation in Saccharomyces cerevisiae Using Amine-reactive Isobaric Tagging Reagents. *Molecular & Cellular Proteomics* 3, 1154–1169. doi: 10.1074/mcp.M400129-MCP200

186. Rutz, A., Sorokina, M., Galgonek, J., Mietchen, D., Willighagen, E., Gaudry, A., et al. (2022). The LOTUS initiative for open knowledge management in natural products research. *Elife* 11. doi: 10.7554/eLife.70780

187. Salazar, N., Castiblanco-Valencia, M. M., Silva, L. B. da, Castro, Í. A. de, Monaris, D., Masuda, H. P., et al. (2014). Staphylococcus aureus Manganese Transport Protein C (MntC) Is an Extracellular Matrix- and Plasminogen-Binding Protein. *PLoS One* 9, e112730. doi: 10.1371/journal.pone.0112730

188. Schilcher, K., and Horswill, A. R. (2020). Staphylococcal Biofilm Development: Structure, Regulation, and Treatment Strategies. *Microbiology and Molecular Biology Reviews* 84. doi: 10.1128/MMBR.00026-19

189. Schneider, L. A., Korber, A., Grabbe, S., and Dissemond, J. (2007). Influence of pH on wound-healing: A new perspective for wound-therapy? *Arch Dermatol Res* 298, 413–420. doi: 10.1007/s00403-006-0713-x

190. Shah, A. D., Goode, R. J. A., Huang, C., Powell, D. R., and Schittenhelm, R. B. (2019). Lfq-Analyst: An easy-To-use interactive web platform to analyze and visualize label-free proteomics data preprocessed with maxquant. *J Proteome Res*, 204–211. doi: 10.1021/acs.jproteome.9b00496

191. Shireen, T., Singh, M., Das, T., and Mukhopadhyay, K. (2013). Differential Adaptive Responses of Staphylococcus aureus to *In Vitro* Selection with Different Antimicrobial Peptides. *Antimicrob Agents Chemother* 57, 5134–5137. doi: 10.1128/AAC.00780-13

192. Shoaib, M., Aqib, A. I., Muzammil, I., Majeed, N., Bhutta, Z. A., Kulyar, M. F.-A., et al. (2023). MRSA compendium of epidemiology, transmission, pathophysiology, treatment, and prevention within one health framework. *Front Microbiol* 13. doi: 10.3389/fmicb.2022.1067284

193. Simone, M., Monciardini, P., Gaspari, E., Donadio, S., and Maffioli, S. I. (2013). Isolation and characterization of NAI-802, a new lantibiotic produced by two different Actinoplanes strains. *J Antibiot (Tokyo)* 66, 73–78. doi: 10.1038/ja.2012.92

194. Sivapragasam, S., and Grove, A. (2019). The link between purine metabolism and production of antibiotics in streptomyces. *Antibiotics* 8. doi: 10.3390/antibiotics8020076

195. Sobral, R. G., Ludovice, A. M., de Lencastre, H., and Tomasz, A. (2006). Role of murF in cell wall biosynthesis: isolation and characterization of a murF conditional mutant of Staphylococcus aureus. *J Bacteriol* 188, 2543–53. doi: 10.1128/JB.188.7.2543-2553.2006

196. Sorokina, M., Merseburger, P., Rajan, K., Yirik, M. A., and Steinbeck, C. (2021). COCONUT online: Collection of Open Natural Products database. *J Cheminform* 13. doi: 10.1186/s13321-020-00478-9

197. Speziale, P., and Pietrocola, G. (2021). Staphylococcus aureus induces neutrophil extracellular traps (NETs) and neutralizes their bactericidal potential. *Comput Struct Biotechnol J* 19, 3451–3457. doi: 10.1016/j.csbj.2021.06.012

198. Staali, L., and Colin, D. A. (2021a). Bi-component HlgC/HlgB and HlgA/HlgB γ-hemolysins from S. aureus: Modulation of Ca2+ channels activity through a differential mechanism. *Toxicon* 201, 74–85. doi: 10.1016/j.toxicon.2021.08.007

199. Staali, L., and Colin, D. A. (2021b). Bi-component HlgC/HlgB and HlgA/HlgB γ-hemolysins from S. aureus: Modulation of Ca2+ channels activity through a differential mechanism. *Toxicon* 201, 74–85. doi: 10.1016/j.toxicon.2021.08.007

200. Styers, D., Sheehan, D. J., Hogan, P., and Sahm, D. F. (2006). Laboratory-based surveillance of current antimicrobial resistance patterns and trends among Staphylococcus aureus: 2005 status in the United States. *Ann Clin Microbiol Antimicrob* 5, 2. doi: 10.1186/1476-0711-5-2

201. Swann, J. P. (1983). The Search for Synthetic Penicillin during World War II. *The British Journal for the History of Science* 16, 154–190. doi: 10.1017/S0007087400026789

202. Tanca, A., Palomba, A., Pisanu, S., Deligios, M., Fraumene, C., Manghina, V., et al. (2014). A straightforward and efficient analytical pipeline for metaproteome characterization. *Microbiome* 2. doi: 10.1186/s40168-014-0049-2

203. Tenover, F. C., McDougal, L. K., Goering, R. V, Killgore, G., Projan, S. J., Patel, J. B., et al. (2006). Characterization of a strain of community-associated methicillin-resistant Staphylococcus aureus widely disseminated in the United States. *J Clin Microbiol* 44, 108–18. doi: 10.1128/JCM.44.1.108-118.2006

204. Thompson, A., Schäfer, J., Kuhn, K., Kienle, S., Schwarz, J., Schmidt, G., et al. (2003a). Tandem Mass Tags: A Novel Quantification Strategy for Comparative Analysis of Complex Protein Mixtures by MS/MS. *Anal Chem* 75, 1895–1904. doi: 10.1021/ac0262560

205. Thompson, A., Schäfer, J., Kuhn, K., Kienle, S., Schwarz, J., Schmidt, G., et al. (2003b). Tandem Mass Tags: A Novel Quantification Strategy for Comparative Analysis of Complex Protein Mixtures by MS/MS. *Anal Chem* 75, 1895–1904. doi: 10.1021/ac0262560

206. Thurlow, L. R., Joshi, G. S., Clark, J. R., Spontak, J. S., Neely, C. J., Maile, R., et al. (2013). Functional Modularity of the Arginine Catabolic Mobile Element Contributes to the Success of USA300 Methicillin-Resistant Staphylococcus aureus. *Cell Host Microbe* 13, 100–107. doi: 10.1016/j.chom.2012.11.012

207. Tikhomirova, A., Rahman, M. M., Kidd, S. P., Ferrero, R. L., and Roujeinikova, A. (2024). Cysteine and resistance to oxidative stress: implications for virulence and antibiotic resistance. *Trends Microbiol* 32, 93–104. doi: 10.1016/j.tim.2023.06.010

208. Tong, S. Y. C., Davis, J. S., Eichenberger, E., Holland, T. L., and Fowler, V. G. (2015a). Staphylococcus aureus Infections: Epidemiology, Pathophysiology, Clinical Manifestations, and Management. *Clin Microbiol Rev* 28, 603–661. doi: 10.1128/CMR.00134-14

209. Tong, S. Y. C., Davis, J. S., Eichenberger, E., Holland, T. L., and Fowler, V. G. (2015b). Staphylococcus aureus infections: Epidemiology, pathophysiology, clinical manifestations, and management. *Clin Microbiol Rev* 28, 603–661. doi: 10.1128/CMR.00134-14

210. Tong, S. Y. C., Davis, J. S., Eichenberger, E., Holland, T. L., and Fowler, V. G. (2015c). Staphylococcus aureus Infections: Epidemiology, Pathophysiology, Clinical Manifestations, and Management. *Clin Microbiol Rev* 28, 603–661. doi: 10.1128/CMR.00134-14

211. Tsai, M., Ohniwa, R. L., Kato, Y., Takeshita, S. L., Ohta, T., Saito, S., et al. (2011). Staphylococcus aureus requires cardiolipin for survival under conditions of high salinity. *BMC Microbiol* 11. doi: 10.1186/1471-2180-11-13

212. Tsakou, F., Jersie-Christensen, R., Jenssen, H., and Mojsoska, B. (2020). The role of proteomics in bacterial response to antibiotics. *Pharmaceuticals* 13, 1–27. doi: 10.3390/ph13090214

213. Tuchscherr, L., Löffler, B., and Proctor, R. A. (2020). Persistence of Staphylococcus aureus: Multiple Metabolic Pathways Impact the Expression of Virulence Factors in Small-Colony Variants (SCVs). *Front Microbiol* 11. doi: 10.3389/fmicb.2020.01028

214. van Rijen, M. M. L., Van Keulen, P. H., and Kluytmans, J. A. (2008). Increase in a Dutch Hospital of Methicillin-Resistant Staphylococcus aureus Related to Animal Farming. *Clinical Infectious Diseases* 46, 261–263. doi: 10.1086/524672

215. van Santen, J. A., Poynton, E. F., Iskakova, D., McMann, E., Alsup, T. A., Clark, T. N., et al. (2022). The Natural Products Atlas 2.0: a database of microbially-derived natural products. *Nucleic Acids Res* 50, D1317–D1323. doi: 10.1093/nar/gkab941

216. Vercauteren, F. G. G., Bergeron, J. J. M., Vandesande, F., Arckens, L., and Quirion, R. (2004). Proteomic approaches in brain research and neuropharmacology. *Eur J Pharmacol* 500, 385–398. doi: 10.1016/j.ejphar.2004.07.039

217. von Eiff, C., Becker, K., Metze, D., Lubritz, G., Hockmann, J., Schwarz, T., et al. (2001). Intracellular Persistence of Staphylococcus aureus Small-Colony Variants within Keratinocytes: A Cause for Antibiotic Treatment Failure in a Patient with Darier's Disease. *Clinical Infectious Diseases* 32, 1643–1647. doi: 10.1086/320519

218. Voss, A., Loeffen, F., Bakker, J., Klaassen, C., and Wulf, M. (2005). Methicillin-resistant *Staphylococcus aureus* in Pig Farming. *Emerg Infect Dis* 11, 1965–1966. doi: 10.3201/eid1112.050428

219. W. Hryniewicz (1999). Epidemiology of MRSA. 27.

220. Walker, K. A., and Miller, V. L. (2020). The intersection of capsule gene expression, hypermucoviscosity and hypervirulence in Klebsiella pneumoniae. *Curr Opin Microbiol* 54, 95–102. doi: 10.1016/j.mib.2020.01.006

221. Washburn, M. P., Wolters, D., and Yates, J. R. (2001). Large-scale analysis of the yeast proteome by multidimensional protein identification technology. *Nat Biotechnol* 19, 242–247. doi: 10.1038/85686

222. Wilkins, M. R., Sanchez, J.-C., Gooley, A. A., Appel, R. D., Humphery-Smith, I., Hochstrasser, D. F., et al. (1996). Progress with Proteome Projects: Why all Proteins Expressed by a Genome Should be Identified and How To Do It. *Biotechnol Genet Eng Rev* 13, 19–50. doi: 10.1080/02648725.1996.10647923

223. Wolters, D. A., Washburn, M. P., and Yates, J. R. (2001). An Automated Multidimensional Protein Identification Technology for Shotgun Proteomics. *Anal Chem* 73, 5683–5690. doi: 10.1021/ac010617e

224. Wong Fok Lung, T., Monk, I. R., Acker, K. P., Mu, A., Wang, N., Riquelme, S. A., et al. (2019). Staphylococcus aureus small colony variants impair host immunity by activating host cell glycolysis and inducing necroptosis. *Nat Microbiol* 5, 141–153. doi: 10.1038/s41564-019-0597-0

225. Wong Fok Lung, T., and Prince, A. (2020). Consequences of Metabolic Interactions during Staphylococcus aureus Infection. *Toxins (Basel)* 12, 581. doi: 10.3390/toxins12090581

226. Wood, T. K., Knabel, S. J., and Kwan, B. W. (2013). Bacterial persister cell formation and dormancy. *Appl Environ Microbiol* 79, 7116–7121. doi: 10.1128/AEM.02636-13

227. Xu, Y., Zhang, B., Wang, L., Jing, T., Chen, J., Xu, X., et al. (2020). Unusual features and molecular pathways of Staphylococcus aureus L-form bacteria. *Microb Pathog* 140, 103970. doi: 10.1016/j.micpath.2020.103970

228. Yang, Y., Chen, Y., Zhang, G., Sun, J., Guo, L., Jiang, M., et al. (2020). Transcriptomic Analysis of Staphylococcus aureus Under the Stress Condition Caused by Litsea cubeba L. Essential Oil via RNA Sequencing. *Front Microbiol* 11. doi: 10.3389/fmicb.2020.01693

229. YASMINE BELKAID, and JULIA A. SEGRE (2014). Dialogue between skin microbiota and immunity. *Science (1979)*.

230. Yoithapprabhunath, T., Nirmal, R., Santhadevy, A., Anusushanth, A., Charanya, D., Rojiluke, et al. (2015). Role of proteomics in physiologic and pathologic conditions of dentistry: Overview. *J Pharm Bioallied Sci* 7, 344. doi: 10.4103/0975-7406.163448

231. Yoong, P., and Pier, G. B. (2012). Immune-Activating Properties of Panton-Valentine Leukocidin Improve the Outcome in a Model of Methicillin-Resistant Staphylococcus aureus Pneumonia. *Infect Immun* 80, 2894–2904. doi: 10.1128/IAI.06360-11

232. Zak, O., and O'Reilly, T. (1991). Animal models in the evaluation of antimicrobial agents. *Antimicrob Agents Chemother* 35, 1527–1531. doi: 10.1128/AAC.35.8.1527

233. Zhao, X., Palma Medina, L. M., Stobernack, T., Glasner, C., de Jong, A., Utari, P., et al. (2019). Exoproteome Heterogeneity among Closely Related *Staphylococcus aureus* t437 Isolates and Possible Implications for Virulence. *J Proteome Res* 18, 2859–2874. doi: 10.1021/acs.jproteome.9b00179

234. Zhao, Y., Wei, J., Li, C., Ahmed, A. F., Liu, Z., and Ma, C. (2022). A comprehensive review on mechanism of natural products against Staphylococcus aureus. *Journal of Future Foods* 2, 25–33. doi: 10.1016/j.jfutfo.2022.03.014

235. Zheng, X., Ma, S. X., St. John, A., and Torres, V. J. (2022). The Major Autolysin Atl Regulates the Virulence of Staphylococcus aureus by Controlling the Sorting of LukAB. *Infect Immun* 90. doi: 10.1128/iai.00056-22

236. Zhou, C., Bhinderwala, F., Lehman, M. K., Thomas, V. C., Chaudhari, S. S., Yamada, K. J., et al. (2019a). Urease is an essential component of the acid response network of Staphylococcus aureus and is required for a persistent murine kidney infection. *PLoS Pathog* 15, e1007538. doi: 10.1371/journal.ppat.1007538

237. Zhou, C., Bhinderwala, F., Lehman, M. K., Thomas, V. C., Chaudhari, S. S., Yamada, K. J., et al. (2019b). Urease is an essential component of the acid response network of Staphylococcus aureus and is required for a persistent murine kidney infection. *PLoS Pathog* 15. doi: 10.1371/journal.ppat.1007538

238. Zhu, X., Hong, A., Sun, X., Wang, W., He, G., Luo, H., et al. (2022). Nigericin is effective against multidrug resistant gram-positive bacteria, persisters, and biofilms. *Front Cell Infect Microbiol* 12. doi: 10.3389/fcimb.2022.1055929

239. Zubarev, R. A., and Makarov, A. (2013). Orbitrap mass spectrometry. *Anal Chem* 85, 5288–5296. doi: 10.1021/ac4001223